Regulation of autoimmune neuroinflammation by Hv1 proton channels

Dissertation

zur Erlangung der Würde des Doktors der Naturwissenschaften
des Fachbereichs Biologie, der Fakultät für Mathematik, Informatik
und Naturwissenschaften der Universität Hamburg

vorgelegt von

Britta Kristin Eggert
aus Celle

Hamburg 2016

Gutachter: Prof. Dr. Manuel Friese
Prof. Dr. Christian Lohr

Datum der Disputation: 13. Januar 2017
Vorsitzende der Prüfungskommission: Prof. Dr. Susanne Dobler

Content

List of Figures

List of Tables

1 Introduction

The immune system has evolved elaborate mechanisms to balance a highly efficient defense against pathogens and tumors to sustain tolerance against self. Hence, the nature and timing of immune responses are tightly regulated. If the underlying mechanisms of control are nevertheless overruled, inappropriate immune cell activation ensues which may go along with a loss of self-tolerance and the development of autoimmune disease.

In different autoimmune conditions including multiple sclerosis (MS) dysregulated activation of plasmacytoid dendritic cells (pDC) has been implicated. In this context, the work presented in this thesis demonstrates that pDCs require the presence of the voltage-gated proton channel Hv1 for activation. With the aim to gain insight into how dysregulation of pDCs in the absence of Hv1 might contribute to autoimmune pathogenesis in a mouse model of MS, further data is collected that proves the relevance of Hv1 proton channels for the maintenance of immune homeostasis. The following introduction therefore provides an overview on the etiology and pathophysiology of MS, on pDC function in health and disease as well as on the structure and function of Hv1 proton channels.

1.1 Multiple Sclerosis

MS was characterized as a disease entity as early as 1868 by the French pathologist Jean-Martin Charcot who was the first to describe the examination of sclerotic CNS lesions in patients with neurological malfunction in his lecture “Histologie de la sclérose en plaques”[1]. These plaques, which are a result of autoimmune inflammatory processes, demyelination and neurodegeneration in the central nervous system (CNS), are the pathological hallmark of MS. Plaque formation may generally occur in grey and white matter of both the brain and the spinal cord, preferentially, however, in the optic nerves, periventricular and spinal cord white matter as well as brain stem and cerebellum. This accounts for the heterogeneity of MS symptoms in individual patients. Most commonly, patients initially present with sensory or visual disturbances, but MS symptomology also includes severe impairment of motor function as well as fatigue, depression and mild cognitive impairment[2].

MS affects approximately 2.5 million patients worldwide being twice more common in women than in men. Although disease may be diagnosed at all ages including in children, the mean age of onset is at 30 years[3]. In 85% of patients, MS initially presents as a relapsing-remitting disease (relapsing-remitting MS, RRMS) having a disease course characterized by intermittent episodes of disease exacerbations followed by phases of remission[4]. Accordingly, the diagnosis of MS requires the formation of plaques that are disseminated in

location and time[2]. However, the extent of remission in-between relapses becomes less efficient with ongoing disease. Indeed, 80% of patients initially presenting with RRMS develop a progressive form of MS over time in which phases of remission are absent (secondary progressive MS, SPMS). Disease that is primary progressive, on the other hand, is only observed in 10% of patients at disease onset[3].

Similar to other autoimmune diseases, the overall risk of developing MS is determined by a combination of various environmental and genetic factors. Strikingly, the prevalence of MS strongly varies with latitude. While only around 2 cases per 100,000 persons occur in sub-Saharan Africa and southeast Asia, the prevalence in northern Europe is well above 100 patients per 100,000 individuals[3]. The precise environmental factors underlying this observation are still under debate, but might include differences in vitamin D levels[5] or infections. Indeed, the most significant association of an environmental factor to MS has been demonstrated for infection with Epstein Barr virus (EBV). Development of infectious mononucleosis as a consequence of EBV infection in young adulthood[6] and seropositivity for antibodies against EBV nuclear antigen confer an increased risk[7].

Consistent with a prominent role of inflammatory processes in disease pathogenesis, most genetic risk factors implied in the development of MS include genes related to immune cell function. The strongest association in genome wide association studies has been shown for the human leukocyte antigen (HLA) locus. HLA-DRB1*15:01 is the main risk factor for the development of MS while HLA-A*02:01 confers protection[8]. Other genetic risk factors are associated with cytokine signaling including variants in the genes encoding the alpha chains of the receptors for interleukin 2 (IL-2) and IL-7, both of which are involved in the establishment of appropriate T cell responses[9–11].

Pathophysiology of MS

Most of what is known about the pathogenesis of MS derives from observations in its mouse model experimental autoimmune encephalomyelitis (EAE) during which myelin specific T cell responses are experimentally induced in the periphery leading to neuroinflammation and neuronal degeneration associated with ascending paralysis[12]. Although it deserves to be noted that EAE is distinct from human MS in several aspects, peripheral activation of autoreactive T cells has also been proposed as a critical step of disease initiation in the latter. The precise circumstances that allow autoreactive T cells to become activated despite the tight control of immune activation against self remain elusive, but might involve bystander activation or molecular mimicry to viral or bacterial antigen which is one possible explanation for the aforementioned strong association of MS risk with EBV infection[13,14]. Similarly, the exact nature of autoantigens targeted in MS remains unknown although components of the

myelin sheath have been proposed[15]. As shown in mouse models, peripheral activation endows T cells with the ability to enter the CNS via the blood-brain or blood-cerebrospinal fluid (CSF) barrier which under healthy conditions restricts immune cell entry to the brain. In the subarachnoid space, T cells get reactivated by antigen-presenting cells, most likely macrophages or dendritic cells (DCs) which goes along with the secretion of proinflammatory cytokines. Consequently, more innate and adaptive immune cells are attracted while the activation of vascular endothelial cells further facilitates their entry into the CNS thereby advancing the initiation of inflammatory foci in the brain parenchyma. Demyelination occurs as a consequence of local inflammation and accompanying cytokine responses as well as direct attack by immune cells[16]. In this context, monocyte-derived macrophages have been shown to contribute to the onset of demyelination[17]. Loss of the myelin sheath predisposes neurons to degeneration for several reasons including loss of trophic support, impaired axonal conduction that is partially compensated for by redistribution of ion channels as well as impaired axonal transport[18,19]. Resident microglia become activated over the course of MS which might significantly contribute to the clearance of debris at least during initial phases of the disease[17]. EAE is undoubtedly driven by $CD4^+$ T cell responses and a prominent role for Th1 and Th17 polarized $CD4^+$ T cells has also been proposed in human disease in agreement with the strong genetic association of MS risk with HLA class II alleles[20]. Nonetheless, numbers of $CD8^+$ T cells exceed those of $CD4^+$ T cells in CNS lesions and the frequency of $CD8^+$ T cells correlates with axonal damage[21,22]. Although regulatory T cells accumulate in the CNS during MS, they fail to suppress autoimmune inflammation in EAE, either due to intrinsic functional impairment or as a result of reduced responsiveness of effector T cells[23]. In addition to T lymphocytes, B cells are thought to migrate to the CNS after they have been activated in draining lymph nodes[24] and oligoclonal antibodies are detectable in the CSF of MS patients[25]. Indeed, binding of autoantibodies to the myelin sheath is followed by activation of the complement system and lysis of oligodendrocytes[26]. Finally, pDCs, a cell type mostly implicated in the defense against viral infection, are present in white matter lesions and the CSF of MS patients[27,28]. Although precise mechanisms are still unclear, observations in mouse models suggest that they might modulate immune pathogenesis by secretion of type I interferon or antigen presentation, as will be discussed in more detail in the next chapter.

1.2 Plasmacytoid dendritic cells

The importance of interferon alpha (IFNα) in the defense against viral infections has been long known as well as the existence of a population of cells specialized in its secretion. Although the nature of these previously called natural interferon producing cells remained enigmatic for years, they are known today as plasmacytoid dendritic cells (pDCs)[29–32]. pDCs are defined as $CD11c^-$ $HLA\text{-}DR^+$ $CD123^+$ $CD303^+$ $CD304^+$ in humans and $CD11c^+$ major histocompatibility complex class II $(MHCII)^{lo}$ $B220^+$ Siglech H^+ $CD317^+$ cells in mice[33]. They are relatively rare, constituting only 0.5% of human peripheral blood mononuclear cells and mouse splenocytes. Upon recognition of viral nucleic acids, pDCs are uniquely equipped to very rapidly secrete massive amounts of type I IFN, mainly IFNα, which by various mechanisms induces an antiviral immune response of both innate and adaptive immunity and helps non-immune cells to set up a defense against viral infection. Accordingly, the attribute “plasmacytoid” derives from their secretory morphology in which they differ from the stellate appearing classical or conventional dendritic cells (cDCs)[34]. cDCs essentially contribute to the initiation and orchestration of immune responses due to their superior antigen presentation skills[35]. While the hallmark function of pDCs is the ability to produce massive amounts of IFNα, pDCs may indeed acquire an alternative activation state that is characterized by secretion of proinflammatory cytokines and the ability to present antigen. However, these sometimes called mature pDCs are rather feeble antigen-presenting cells and the physiological relevance of antigen presentation by pDCs is assumed to be different from cDCs[36]. In fact, due to intensive research on pDC function in recent years, their physiological role is assumed to be complex including pro- as well as anti-inflammatory functions depending on the circumstances and timing of their activation.

1.2.1 Ontogeny and differentiation of pDCs

Despite their obvious functional and morphological differences, both pDCs and cDCs develop from a common dendritic cell progenitor (CDP) in the bone marrow. CDPs stain negative for lineage markers but express the receptors macrophage-colony stimulating factor receptor, FMS-related tyrosine kinase 3 (Flt3) as well as low levels of CD117 (c-kit)[37,38] . Flt3-ligand (Flt3L) strongly expands cDCs and pDCs *in vivo* as well as in murine bone marrow cultures *in vitro* and its deficiency in mice is associated with significantly decreased numbers of DCs[37,39,40]. Although the ontogeny of pDCs is not yet understood in every detail, the existence of different intermediate progenitors downstream of CDPs has been proposed[41,42]. From a certain point in their development on, pDC progenitors express the transcription factor E2-2 which is essential for pDC development as well as maintenance of mature pDCs[43]. E2-2 belongs to the family of E proteins which is broadly involved in the regulation of

lymphocyte development together with their antagonists, the inhibitor of DNA-binding (ID) proteins[44]. Accordingly, upregulation of E2-2 in pDCs goes along with a reduced expression of its antagonist ID2[45]. Several findings confirm the importance of E2-2 expression for pDC development and homeostasis. First, E2-2 deficiency completely blocks the generation of pDCs in mice. Moreover, in patients suffering from Pitt-Hopkins syndrome, which is caused by E2-2 haploinsufficiency, pDCs are both decreased in numbers as well as functionally impaired[43]. Consistently, E2-2 regulates a number of pDC-characteristic transcription factors implicated in the later steps of development and genes implicated in pDC effector functions[43,46,47].

pDCs leave the bone marrow after complete maturation and circulate in the blood[46,48,49]. They can then also invade tissues and enter lymph nodes, the latter remarkably similar to T cells via high endothelial venules[50,51]. Although pDCs may also contribute to the defense against bacteria[52,53], their classical role is the defense against viruses which has been shown in the context of viral infections of skin and mucosa as well as the presence of viruses in the blood stream [54,55].

1.2.2 Activation of pDCs by nucleic acids in early and late endosomes

Since pDCs are essential for the defense against viral infection their classical activating stimulus is the detection of viral nucleic acids. Although some exceptions exits, most viruses elicit equal IFN responses in pDCs regardless whether they are active or heat- or UV-inactivated[56,57] indicating that pDCs do not need to be infected themselves for a solid IFN response but are instead capable to efficiently sense the presence of viruses in their vicinity. Accordingly, recognition of pathogen-derived RNA and DNA mainly occurs in the endosomal compartment by toll-like receptors (TLR) 7 and 9. TLR7 recognizes ssRNA[56,58,59] while TLR9 binds ssDNA containing unmethylated CpG-rich sequences[60]. Delivery of viral DNA or RNA to the endolysosomal compartment follows, for example, uptake of viral particles during direct cell to cell contact as well as after uptake of exosomes containing viral RNA from neighboring infected cells[61,62].

Ligand binding to TLR9 induces a conformational change in the receptor[63], interaction with the adaptor molecule myeloid-differentiation primary response gene 88 (MyD88) and subsequent recruitment of other signaling proteins like interleukin 1 receptor associated kinase 4 (IRAK4)[64,65], TNF receptor associated factor 6 (TRAF6)[66–68] and Bruton's tyrosine kinase (BTK)[69,70] into a multiprotein signaling complex. Depending on the nature of the TLR9-activating stimulus, different downstream targets are subsequently activated. As noted above, pDCs respond to activating stimuli by secretion of type I IFN, but may alternatively

also upregulate surface molecules needed for antigen presentation (**figure 1.1**). The latter activation state goes along with secretion of proinflammatory cytokines like interleukin 6 (IL-6) and tumor necrosis factor α (TNFα), but only negligible production of type I IFN. Whether pDCs are activated to become IFN-secreting or antigen-presenting cells is mainly dependent on the nature of the DNA oligonucleotide and the endolysosomal compartment in which it is sensed[71,72].

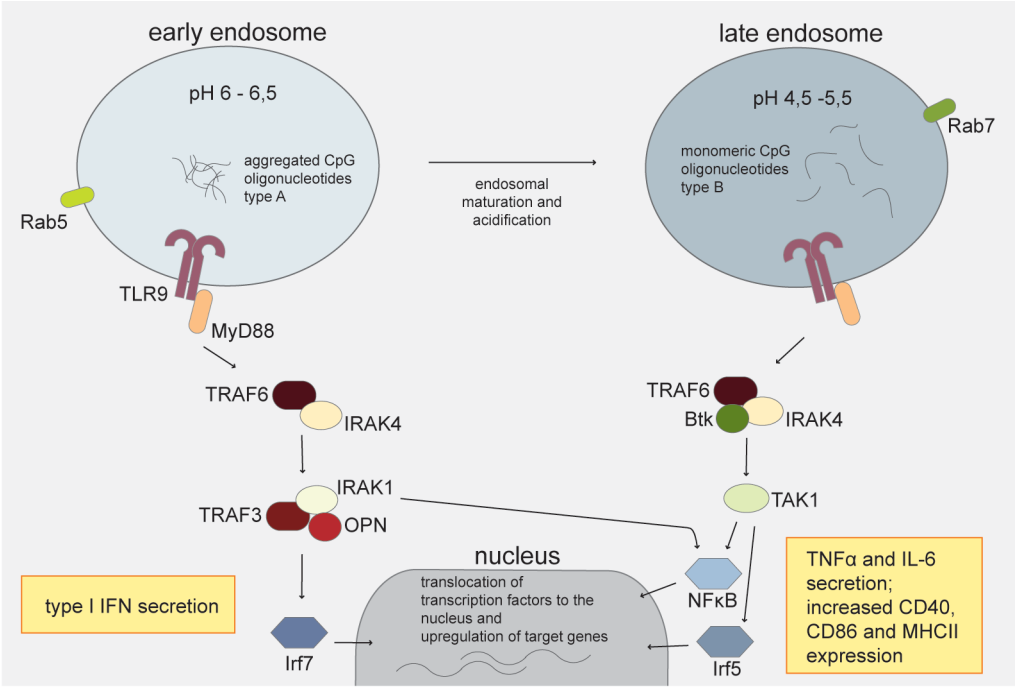

Figure 1.1 | pDCs respond differently to CpG oligonucleotide-mediated stimulation in early and late endosomes.
Type A CpG oligonucleotides tend to aggregate which causes them to be retained in and signal from early endosomes. They induce a signaling cascade that terminates in phosphorylation of Irf7 and secretion of type I IFN. On the other hand, endosomes containing monomeric type B CpG oligonucleotides rapidly acidify and become late endosomes. CpG-B signaling via TLR9 form late endosomes induces a different signaling cascade which will lead to activation of NFκB and Irf5 and subsequent secretion of proinflammatory cytokines like IL-6 and TNFα as well as upregulation of molecules needed for antigen presentation. TLR9, toll-like receptor 9; Rab, Ras-related in brain protein; MyD88, myeloid-differentiation primary response gene 88; TRAF, TNF receptor associated factor; IRAK, interleukin 1 receptor associated kinase 4; Btk, Bruton's tyrosine kinase; OPN, osteopontin; Irf, IFN regulatory factor; TAK, TGF β-activated kinase; NFκB, nuclear factor 'kappa-light-chain-enhancer' of activated B-cells. Adapted from[72]

Oligonucleotides that contain unmethylated CpG-motifs (CpG oligonucleotides) are frequently used *in vitro* for experimental stimulation of TLR9. They are distinguished as type A, B or C depending on their sequence and the response they induce upon binding to their receptor. Firstly, CpG-A oligonucleotides form large multimeric aggregates due to a polyG tail. Because of this, CpG-A oligonucleotides are retained in early endosomes for an extended time and the signaling cascade induced will finally lead to phosphorylation and translocation of IFN regulatory factor 7 (Irf7), the master transcription factor for IFN

synthesis, to the nucleus[68,73,74]. In contrast, CpG-B oligonucleotides remain monomeric[74]. For reasons not yet understood, monomeric DNA binds to TLR9 only in the late endosomes and induces a different signaling cascade that leads to activation of the nuclear factor 'kappa-light-chain-enhancer' of activated B-cells (NFκB)[74,75]. In addition, so-called C type CpG oligonucleotides exist which signal from both early and late endosomes[74].

1.2.3 pDCs as type I IFN producing cells

The main antiviral effector function of pDCs is the secretion of type I IFN. IFNs are grouped into three distinct families of which type I and type III IFN have the highest potential to literally interfere with viral replication. The most important type I IFNs are IFNα and IFNβ. Type I as well as type III IFN bind to heterodimers of IFNα receptor 1 and 2 (IFNAR1 and 2) that signal via the Janus kinase/signal transducers and activators of transcription (JAK-STAT) pathway. This involves phosphorylation of STAT1 and STAT2, their dimerization with Irf9 to form IFN stimulated gene factor 3 which translocates to the nucleus and induces expression of a range of IFN-stimulated genes (ISGs) by binding to upstream IFN-stimulated regulatory elements[76]. ISGs include a large number of proteins, some of which sensitize cells to pathogen detection, like pattern recognition receptors[77]. Others directly interfere with viral entry, replication or egress. These include, among others, myxovirus resistance 1 (Mx1) and 2'-5'-oligoadenylate sythetase (OAS). Mx1 binds incoming viral components and targets them for degradation while OAS activates the endoribonuclease RNase L that degrades viral RNA in the cytoplasm[78,79].

On the large scale, type I IFN does not only prepare individual cells for the detection and eradication of viral infection, but it also contributes to an appropriate antiviral response of the innate and adaptive immune system. To date a range of different effects on other DCs, natural killer (NK) cells, T cells and B cells has been described. It is important to note that the precise effect of type I IFN on a given immune cell seems to be highly context dependent and type I IFN secretion by pDCs may have both pro- as well as anti-inflammatory effects. For example, IL-12 production by DCs requires stimulation with type I IFN[80] while high levels of type I IFN, on the contrary, inhibit IL-12 secretion[81,82]. Type I IFN also promotes the activation of immature DCs and increases their ability for T cell activation by upregulation of MHCII and costimulatory molecules[83,84] as well as the ability of DCs to cross-present antigens[85,86]. Furthermore, the migration of DCs to lymph nodes for interaction with T cells is improved in response to IFN due to upregulation of chemokine receptors[87,88]. In NK cells, type I IFN induces production of IFNγ and cytolytic effector functions[89,90]. With regard to leukocytes, type I IFN increases the ability of $CD4^+$ T cells to provide B cell help[85] as well as survival and clonal expansion[91]. On the other hand, however, IFNα also has anti-proliferative

effects including the induction of Fas/Fas ligand upregulation and subsequently increased activation-induced cell death[92,93]. Type I IFN lowers the threshold for B cell receptor dependent activation of B cells[94] and increases antibody production[95]. Interestingly, on the other hand, a recent publication has shown that the presence of IFNα increases secretion of the anti-inflammatory cytokine IL-10 by B cells[96].

Nearly all cells in the body are capable of secreting type I IFN in response to viral infections. The most important difference of pDCs to other IFN secreting cells, however, is both the amount and the speed of IFN secretion. pDCs are unique in that they constitutively express sufficient levels of Irf7[71,97]. In all other cells, Irf7 is expressed at minor levels and IFN secretion is low until Irf7 is upregulated in response to an auto- and paracrine feedback loop[98]. pDCs are therefore likely needed to ensure that the IFN concentration during very early infection is sufficiently high to control spread of the pathogen before type I IFNs are produced more broadly by other cells. Accordingly, pDCs appear to be more important during acute infections while their activation may even prevent clearance of pathogens during chronic infections[99,100].

1.2.4 pDCs as antigen-presenting cells

Compared to IFN secretion, antigen-presentation is a by far less understood effector function of pDCs. Molecules upregulated by pDCs after CpG-B induced maturation include MHCII as well as the costimulatory molecules CD40, CD80 and CD86[101,102]. The phagocytic capacity of pDCs remains controversial although several studies show that pDCs efficiently take up endogenous and exogenous antigen[36,103,104]. It has also been shown that pDCs prime T cells after activation *in vivo*[105–107] and cross-present antigen to naïve T cells in mice after they have been pre-activated by CpG oligoneucleotides[108]. As mentioned earlier, however, several lines of evidence prove that even after maturation pDCs do not present antigen as efficiently as cDC and, in addition, the function of antigen presentation by pDCs is likely to be different from that of cDCs. Consistently, the expression of MHC and costimulatory molecules by mature pDCs remains, despite its increase after activation, lower than in cDCs[33]. In contrast to cDCs, MHCII expression is not downregulated after pDC activation implying that the composition of antigen-loaded MHCII molecules on the cell surface is constantly altered[109]. Third, although pDCs migrate to lymph nodes during infection, their frequency in draining lymph nodes is not significantly increased compared to the steady state as would be the case for cDCs[110].

On the contrary, several observations argue for a role of antigen-presenting pDCs in the induction of regulatory T cell responses. For example, presentation of oral antigen by pDCs

to naïve T cells in the liver induces anergy and deletion of antigen-specific T cells which is essential for the establishment of oral tolerance[111]. pDCs have also been implicated in the formation of an immunosuppressive environment in cancer by induction of $CD8^+$ regulatory T cells[112] as well as in the suppression of graft rejection and graft versus host disease[113,114]. Finally, pDCs that have been activated by polysaccharide A derived from the gut commensal *Bacteroides fragilis* via TLR2 promote IL-10 production by $CD4^+$ T cells in the gut and their depletion is associated with more severe pathology in a mouse model of colitis[115]. Moreover, several publications propose a regulatory role of pDCs in the maintenance of immune tolerance towards self antigens which will be discussed in the next part.

1.2.5 Contribution of pDC dysregulation to autoimmunity

In accordance with their putative dual role during immune responses, IFN secretion and antigen presentation by pDCs may either aggravate disease or limit autoimmune responses depending on the pathophysiological context. Hence, overactivation of pDCs and increased IFN secretion are hallmark features of some autoimmune diseases like systemic lupus erythematosus (SLE) and psoriasis[116] while the opposite is assumed for MS as discussed below. In still other pathologies, like type I diabetes, both aggravating and protective roles of pDCs also with regard to antigen presentation have been shown so that the precise contribution of pDCs to the pathophysiology yet remains to be resolved[117,118].

SLE is a rare autoimmune disease characterized by the production of anti-nuclear and anti-dsDNA antibodies, deposition of immune complexes and consequent tissue inflammation that causes organ damage, for example of the kidneys[119]. It has been proposed that one critical step in the pathogenesis of lupus is the access of pDCs to self-DNA released during NETosis, a specialized type of cell death during which neutrophils release chromatin-containing neutrophil extracellular traps (NETs)[120,121]. In SLE degradation of NETs is impaired [122,123] and it has been shown that NETs can activate pDCs after endocytosis via TLR7 which results in massive secretion of IFNα[124,125]. Increased IFN production contributes to SLE pathogenesis in different ways including priming of neutrophils to undergo further NETosis thereby establishing a detrimental feed forward mechanism[125]. Consistently, peripheral blood mononuclear cells (PBMCs) of patients suffering from SLE exhibit a characteristic IFN-induced gene signature that correlates with disease activity[126,127] and pDC depletion in SLE mouse models ameliorates disease[128,129].

Although the underlying mechanisms are less clear compared to SLE, there is strong evidence for an involvement of altered pDC function and IFN secretion in MS which derives from a range of observations in patients and mouse models. First, pDCs are present in white

matter lesions and the CSF of MS patients[27,28]. Several publications prove that effector functions of pDCs isolated from MS patients are impaired in *ex vivo* experiments, including reduced upregulation of costimulatory molecules and decreased ability to stimulate T cell proliferation as well as IFNα secretion[28,130]. Consistently, the amount of type I IFN in serum of MS patients is decreased[131]. The most striking evidence, however, derives from the efficiency of IFNβ in MS therapy making it the therapeutic agent of choice for the treatment of many RRMS patients. Since it was originally thought that MS might be triggered by viral infection, the efficiency of treatment with IFNβ in RRMS patients was investigated from the early 1990s on. Strikingly, administration of IFNβ resulted in reduced relapse rate and disease progression reflected by decreased *de novo* appearance and number of active lesions detected by magnetic resonance imaging[132–134]. Later on, IFNβ was also found to be efficient in patients with SPMS and superimposed relapses[135] as well as in patients presenting with clinically isolated syndrome in which treatment significantly delayed progression to definite disease[136,137]. In general, two different types of IFNβ, IFNβ 1a and 1b, are licensed for use in MS patients which differ in their structure and way of production. Of these IFNβ 1a is identical to natural human IFNβ and more active than IFNβ 1b[138]. Treatment with type I IFN is generally well tolerated and occurring adverse effects are normally mild[136,139]. Still, depending on the preparation used between 6% and 48% of patients develop neutralizing antibodies to IFNβ which reduces treatment efficacy in the long term[140]. Intensive research has been invested to elucidate the mechanisms underlying disease amelioration after type I IFN treatment and revealed a range of anti-inflammatory effects. These include, for example, enhanced regulatory T cell responses[141], but reduced $CD4^+$ and $CD8^+$ T cell activation[142] and decreased expression of matrix metalloproteases which have been associated with blood-brain barrier disruption and CNS infiltration of immune cells[143]. Moreover, IFN treatment was shown to alter effector function of pDCs including the induction of increased TLR7 expression and thus responsiveness[144]. However, many aspects are still under investigation and no overall concept of the action of IFNβ in MS patients could yet be established.

In addition to the considerable amount of human data, further evidence for the importance of pDCs in the IFN response derives from studies in mice where several, however not entirely conclusive, findings suggest that pDCs may limit pathology in EAE. First, absence of type I IFN signaling in myeloid cells aggravates EAE symptoms and is associated with an altered activation state as well as dysregulated cytokine and chemokine production by these cells[145]. Of note, IFNβ increases secretion of IL-27 by macrophages[146], a cytokine that has been shown to inhibit the development of Th17 responses in CNS inflammation[147]. Consistently, increased IL-17 production during EAE in IFNAR-deficient mice has been demonstrated[146].

Furthermore, IFNβ treatment of mice during EAE ameliorates disease, an effect that nevertheless requires the presence of B cells[148]. In addition to these IFN-mediated effects, antigen presentation by pDCs in draining lymph nodes during EAE promotes regulatory T cell responses as has been shown in mice lacking MHCII expression specifically in pDCs[149]. Furthermore, transfer of MOG-loaded pDCs after immunization ameliorates EAE symptoms by increasing pDC development in the bone marrow as well as the frequency of CNS-infiltrating pDCs which is, however, independent of both IFN secretion and antigen presentation[150].

Altogether, these observations underline the importance of a tight control of pDC activation for the maintenance of tolerance against self which in turn requires precise regulation of the endosomal compartment from which pDC activation is initiated. Still, many questions remain with respect to how endosomal physiology including endosome maturation, a process that involves acidification of the endosomal compartment, is controlled. In this context, this thesis studies the role of the voltage-gated proton channel Hv1 which is shown further on to be expressed in pDCs. Hence, the next chapter provides an overview of the structure and function of Hv1 proton channels, particularly with regard to their well established role in phagocytic immune cells.

1.3 Voltage-gated proton channels

1.3.1 Introduction to the voltage-gated proton channel Hv1

The existence of proton currents was described for the first time in the early 1980s in depolarized neurons of the snails *Helix aspersa* and *Lymnea stagnalis*[151,152]. These proton currents, which were proposed to be necessary to counteract rapid intracellular acidification after action potentials in these cells[153], were assigned to a then still unidentified highly selective proton channel. Notably, they had distinctive features compared to other ionic currents in that they not only depended on membrane depolarization, but were also strongly influenced by the difference between internal and external pH and sensitive to the presence of external divalent cations[151,152]. While similar depolarization-activated proton currents were afterwards soon recognized in a range of different species and cell types, it was only in 2006 that the genes encoding the underlying human and murine proton channel were identified independently by two different groups using bioinformatic tools[154,155]. With regard to its functional and structural characteristics the authors termed the channel voltage-gated proton channel 1 (Hv1)[154] and voltage-sensor domain-only protein (VSOP)[155]. The latter term relates to the most striking structural feature of the identified ion channel. Voltage-gated proton channels have only four transmembrane domains which are homologous to the voltage-

sensor domain of other voltage-gated ion channels, but lack a separate pore domain (**figure 2A**). Other voltage-gated ion channels comprise six transmembrane domains and it is the domains S5 and S6 that form the actual ion permeable pore in these multimeric channels[156,157]. Consequently, the proton permeable pore of Hv1 must lie within the transmembrane segments S1 to S4, the mechanism of which will be discussed below. Remarkably, mutation of only one single arginine residue in the voltage-sensing domain of other voltage gated ion channels artificially induces proton permeability[158].

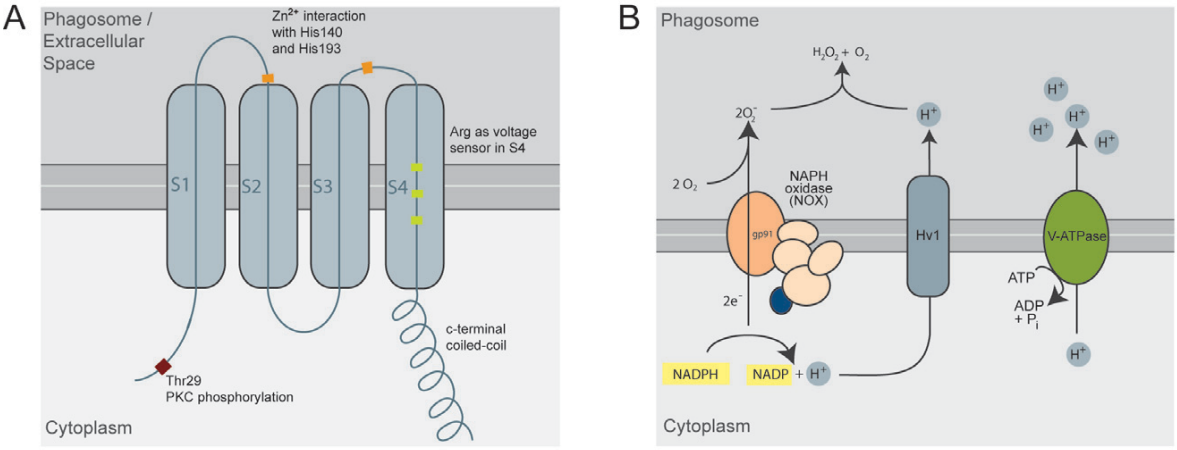

Figure 1.2 | The voltage-gated proton channel Hv1
(**A)** Hv1 proton channels comprise four transmembrane domains. Arginine residues in S4 are important for voltage-sensing and proton selectivity. Inhibition by extracellular Zn^{2+} ions is mediated by histidine residues in the extracellular loop. Enhanced gating is induced by N-terminal phosphorylation at threonine 29. (**B)** In different immune cells Hv1 localizes to the phagosomal membrane where it counteracts cytoplasmic accumulation of protons during oxidation of NADPH by NOX enzymatic complexes. Inside the phagosomal lumen, protons are available to react with superoxide anion to give rise to hydrogen peroxide thereby further contributing to the generation of reactive oxygen species. Therefore, proton flux through Hv1 might not significantly contribute to intraphagosomal acidification which is instead mediated by V-ATPases. PKC, protein kinase C; Asp, aspartate; Arg, arginine, ATP, adenosine triphosphate; ADP, adenosine diphosphate, NADPH, nicotinamide adenine dinucleotide phosphate. **B** is adapted from[159,160]

1.3.2 Structure and gating of Hv1

Human Hv1 is a 273 amino acid protein encoded by the *HVCN1* gene on chromosome 12 at q24.11[154]. Two isoforms of Hv1 exist, the shorter one lacking the first 20 amino acids of the N-terminus due to an alternative start codon[161]. Phosphorylation of human Hv1 at the threonine at position 29 in the N-terminus by protein kinase C induces a state of enhanced gating[162,163] characterized by faster channel opening and slower closing as well as elevated maximum proton conductance[164]. The C-terminus has been shown to form an α-helical coiled-coil structure in extension of the voltage-sensor domain[165,166]. Physiologically, Hv1 exist as homodimers that show cooperative gating[167–170] and dimerization of Hv1 requires both the N- and C-terminal domains[166,167,169]. Two dimeric interfaces have been described, one between S1 and the two adjacent extracellular loops and the second at the intracellular

coiled-coil domains of the C-terminus[171]. If one of the channels within a dimer is open the opening probability of the other subunit is increased by 60 times. Accordingly, both channels within a dimer are most likely in the same opening state[172]. Nevertheless, there is also voltage-dependent proton permeation in monomers and monomeric Hv1 has been described to open at more negative membrane potentials[167,170]. In order for Hv1 to open, three distinct conformational changes seem to be necessary of which the first two appear to be voltage-dependent[173]. Similar to other voltage-gated channels, the S4 domain of Hv1 contains three arginine residues which move outward when the membrane is depolarized and inward upon membrane hyperpolarization[170,174,175]. As a consequence of S4 movement, there is also a voltage-dependent transition of S1, possibly the opening transition, during which the pore widens giving intracellular solution access to the selectivity filter[176].

Voltage-gated proton channels are perfectly selective for protons. Physiologically, this is of utmost importance as proton concentrations are normally much lower than that of most other major ions which would therefore tend to permeate the channel much more often when competing with protons for access[177]. In addition to its importance for voltage-sensing, the arginine residue at position 211 (Arg211) in S4 has also been implied in the selectivity filter of Hv1. After movement of the S1 and S4 segments upon depolarization Arg211 interacts with an aspartate at position 112[178–182] via formation of two hydrogen bonds that occlude the pore but that can nevertheless transiently break due to thermal fluctuations thereby allowing access of hydronium ions[176,178,181]. Protonation of the aspartate by the hydronium ion results in energetically favorable interactions that open the pore, allow the hydronium ion to pass as a neutral water molecule and retrieve the proton on the other side of the selectivity filter. According to this mechanism, permeation is only possible for protons whereas permeation of anions or other cations is impossible[181].

As mentioned above, gating of Hv1 is not only regulated by the membrane potential, but it is also remarkably sensitive to the difference between the intra- and extracellular concentration of its permeating ion (ΔpH). At equal intra- and extracellular pH Hv1 opens at a membrane potential slightly above 0 mV. For every change in ΔpH by one unit the threshold potential is shifted by approximately 40 mV. Intracellular acidification or extracellular alkalization move the current-voltage relationship in the positive direction which means that Hv1 opens already at more negative membrane potentials[155,183]. The physiological importance of Hv1's pH-sensitivity is highlighted by the fact that the threshold potential at physiological intra- and extracellular pH is always more positive than the reversal potential for protons and endogenous proton currents therefore only exist as outward rectifying currents[155]. This allows the channel to extrude protons after intracellular acidification and thereby maintain the

intracellular pH at resting levels. Still, most studies in which selected residues have been mutated to identify a proton regulatory site within the channel have not been successful[184,185]. The presence of submillimolar concentrations of extracellular divalent cations inhibits voltage-gated proton currents by slowing channel opening and shifting the voltage dependence to more positive values[151,152,154,186]. It has been shown that Zn^{2+} ions bind at the dimer interface between the complementary histidine residues at position 193 and 140 of both monomers[154,168] thereby impairing the movement of S1 in the dimer relative to each other that is needed for channel opening. In addition, Hv1 mediated proton currents are highly temperature-dependent and channel opening with rising temperature occurs already at more negative membrane potentials without generally affecting the current-voltage relationship[183,187].

1.3.3 Cellular functions of Hv1

The regulation of intracellular or extracellular pH is relevant for a wide range of cellular functions and Hv1 expression has consistently been identified in a variety of different tissues and cell types. In all of these except one[188], its principal task is to extrude protons from the cytoplasm although in very different functional contexts. Phylogenetically Hv1 has diverged from other voltage-gated ion channels in bacteria more than a billion years ago[179]. It is therefore not surprising that Hv1 is expressed in different species including unicellular organisms like dinoflagellates[188]. Still, the functions of Hv1 discussed here will only refer to its expression in mammalian immune cells which is most relevant for the work presented further on. In this context, the generation of Hv1-deficient mouse models in 2009[189,190] has facilitated research and therein massively augmented our understanding of the physiological function of Hv1.

The best described function of Hv1 channels to date is its importance for the respiratory burst in phagocytic immune cells, including neutrophils[191], cDCs[192], macrophages[193] and microglia[194]. During the respiratory burst, massive amounts of reactive oxygen species (ROS) are generated in the phagosome to kill engulfed pathogens. Fundamental to this is the nicotinamide adenine dinucleotide phosphate (NADPH) oxidase (NOX) complex in the phagosomal membrane, an enzymatic complex that oxidizes NADPH in the cytoplasm and subsequently mediates the transport of electrons across the phagosomal membrane (**figure 1.2 B**). These electrons will then be available to react with oxygen giving rise to superoxide anions as a precursor of different ROS[195,196]. Activity of NOX will inevitably cause local cytoplasmic acidification due to the protons released by NADPH oxidation as well as depolarization of the phagosomal membrane caused by electron transport. As both of this impairs NOX function a counteractive mechanism is indispensable[197,198]. Being activated

both by depolarization and decreased intracellular pH Hv1 channels are ideally suited to allow proton currents into the phagosome under these circumstances. Indeed, Hv1 has been shown to colocalize with NOX at the phagosomal membrane and absence of Hv1 impairs ROS production after NOX activation[189,190]. Nevertheless, ROS production is not abrogated completely implying that other Hv1-independent mechanisms for charge compensation might exist[189,199].

In most phagocytic cells, the respiratory burst goes along with alterations in phagosomal pH. According to the physiological function of phagosomes in different cell types, phagosomal pH is regulated differently in distinct immune cells[200,201]. In this context, phagocytic cells express distinct phagosomal proteases to digest engulfed pathogenic material and the activity of these enzymes is optimal at different phagosomal pH. M2 macrophages, for example, rapidly acidify their phagosome[200] while the phagosomal pH in neutrophils is maintained neutral to ensure full functionality of neutral proteases like neutrophil elastase[202,203]. It is important to note that proton fluxes via Hv1 are not assumed to directly contribute to phagosomal acidification since they are rapidly dismutated by reaction with superoxide anion. Instead, active transport of protons by V-ATPases into the phagosomal lumen is the main source of intraphagosomal acidification (**figure 1.2 B**)[204]. Still, it has been proposed that in some cells NOX activity regulates V-ATPase abundance on phagosomes or its activity once inserted into the phagosomal membrane[205]. Accounting for the differences in its regulation, the impact of Hv1-deficiency on phagosomal pH varies among different cell types. For example, Hv1-deficiency significantly reduces phagosomal acidification in macrophages. In neutrophils, on the other hand, maintenance of neutral pH is impaired and phagosomal acidification is observed in most cells, possibly due to an altered recruitment of V-ATPases[193]. In addition to direct interference with proper endosomal function, Hv1-deficiency also impairs Ca^{2+} entry and signaling in neutrophils, probably as a reason of cell depolarization, eventually leading to diminished responses to chemoattractants and decreased migration[206].

Hv1 expression in immune cells is, however, not only confined to the intracellular membranes. After intracellular acidification of neutrophils during the respiratory burst protons are not only extruded into the phagosome, but also into the extracellular space. It has been shown that this is necessary to specifically control the release of azurophilic granules, which is massively increased in Hv1-deficient neutrophils[208]. In B cells, Hv1 associates with the B cell receptor on the cytoplasmic membrane and is necessary for sustained B cell activation [207]. Interestingly, basophils which lack NOX expression also highly express Hv1[209] to counteract cytoplasmic acidification which has been observed after IgE-stimulation. Consequently, Hv1 deficiency reduces histamine release after IgE-stimulation[210].

In conclusion, Hv1 deficiency results in impaired function of all immune cells in which it has been analyzed to date and is thus likely to affect different aspects of the initiation and regulation of immune responses. Of particular interest in the context of this thesis, recently published work described a lupus-like autoimmune phenotype in Hv1-deficient mice characterized by increased T cell activation, elevated concentrations of antibodies against double-stranded DNA and glumerolonephritis[211]. While the underlying mechanisms are to date still unknown, this finding illustrates the overall relevance of Hv1 proton channels for the maintenance of proper immune cell function and thus immune homeostasis.

1.4 Purpose of the presented work

Dysregulation of pDC activation and effector functions has been shown to be involved in different autoimmune pathologies. Importantly, the main route of pDC activation is via stimulation of endosomal TLRs. To understand the causative events leading to inappropriate pDC activation it is thus particularly important to understand how endosomal function, especially endosomal maturation and pH, are regulated in these cells. In this context, data presented further on reveals that pDCs express the voltage-gated proton channel Hv1. Since Hv1 has been implied in the maintenance of normal phagosomal function and pH in other immune cell populations it was investigated here whether Hv1 is functionally involved in endosomal homeostasis and thus activation of pDCs. In addition, the impact of Hv1-deficiency on autoimmunity was also analyzed in the context of the pathophysiology of EAE, the mouse model of MS. To this end, four different questions are addressed in this thesis:

1. What is the expression level of Hv1 in different immune cell populations, particularly DCs?
2. Does Hv1 affect endosomal pH and activation of pDCs?
3. What is the impact of Hv1 on autoimmune pathogenesis, especially with regard to the IFN response in EAE, a mouse model of MS?
4. Is the immune phenotype of Hv1-deficient mice altered at the steady state thereby predisposing to the development of autoimmunity?

2 Material and methods

2.1 Material

2.1.1 Laboratory animals

C57BL6/J mice were obtained from Charles River Laboratories, Germany.

Hvcn1$^{-/-}$ mice were generated by Scott Ramsey and colleagues[189] and received from David Clapham, Boston, Massachusetts, USA.

All mice were housed under specific pathogen-free conditions at the Central Animal Facility of the University Medical Center Hamburg-Eppendorf (UKE) and at the Center for Molecular Neurobiology Hamburg (Zentrum für Molekulare Neurobiologie Hamburg, ZMNH). All animal experiments were approved by the local ethics committee (Behörde für Soziales, Familie, Gesundheit und Verbraucherschutz in Hamburg) as part of the application G13/022.

2.1.2 Human sample material

Blood samples for the isolation of PBMCs were obtained from healthy human volunteers recruited among co-workers at the ZMNH. None of the donors was diagnosed with an immunological disease at the time of blood sampling.

2.1.3 Cell lines

MS-5 murine stromal cells (DSMZ number ACC 441) were obtained from the German Collection of Microorganisms and Cell Cultures (Deutsche Sammlung von Mikroorganismen and Zellkulturen, DSMZ).

The human pDC cell line GEN2.2 was obtained from Laurence Chaperot, Grenoble, France.

2.1.4 Chemicals and reagents

If not stated otherwise all chemicals used were bought from either Sigma-Aldrich or Roth.

Table 2.1 | Reagents for animal experiments

Reagent	Company
Incomplete Freund's adjuvant	Difco laboratories
MOG_{35-55} peptide	Schafer-N
Mycobacterium tuberculosis H37Ra	Difco laboratories
Pertussis toxin (*Bordetella pertussis*)	Calbiochem

Table 2.2 | Reagents for cell culture

Reagent	Company
Alpha MEM	PAN Biotec
Beta-mercaptoethanol	Sigma
CD135/recombinant murine Flt3L	Immunotools
Class A CpG oligonucleotide ODN1585	Invivogen
Class B CpG oligonucleotide ODN 1668	Invivogen
Class C CpG oligonucleotide ODN 2395	Invivogen
Class A CpG oligonucleotide, 5' Atto 647N	MWG
Class B CpG oligonucleotide, 5' Atto 647N	MWG
Class A CpG oligonucleotide, 5' Oregon Green 488	MWG
Class B CpG oligonucleotide, 5' Oregon Green 488	MWG
Collagenase A	Roche
Collagenase D	Roche
DNaseI	Merck Milipore
Ethanol absolute	Th. Geyer
Ethylendiaminetetraacetic acid (EDTA), 0.5 M	DAKO
Fetal calf serum (FCS)	Biochrom
HEPES	Life Technologies
Interferon alpha, recombinant murine	Biolegend
L-glutamine	Life Technologies
Lipopolysaccharide from *salmonella typhi*	Sigma-Aldrich
Penicillin-streptavidin 10,000 U/ml	Life Technologies
Percoll	GE Healthcare
RPMI1640	PAN Biotec
RPMI1640 with GlutaMax	Life Technologies
Sodium pyruvate	Life Technologies
Trypanblue solution	SigmaAldrich
TryPLE	Thermo Fisher Scientific
Tuerck's solution	Merck

Table 2.3 | Reagents for polymerase chain reaction (PCR) and agarose gel electrophoresis

Reagent	Company
Agarose Ultra Pure	Life Technologies
dNTP Mix	Fermentas
Hot Start Taq DNA polymerase	Thermo Fisher Scientific
GeneRuler 1 kb Plus DNA ladder	Thermo Fisher Scientific
QuickExtract	Epicentre
RotiSafe gel stain	Roth

Table 2.4 | Reagents for molecular cloning

Reagent	Company
Ampicillin	Roth
FastDigest BglII	Thermo Fisher Scientific
FastDigest EcoRI	Thermo Fisher Scientific
FastDigest HindIII	Thermo Fisher Scientific
Kanamycin	Roth
NucleoBond Xtra Midi EF	Macherey Nagel
NucleoSpin Gel and PCR Clean Up	Macherey Nagel
NucleoSpin Plasmid Easy Pure	Macherey Nagel
T4 DNA Ligase (with ligase buffer)	Thermo Fisher Scientific
XL1 Blue competent bacteria	Agilent Technologies

Table 2.5 | Reagents for cell staining and microscopy

Reagent	Company
Cell-Tak Cell and Tissue Adhesive	Corning
Cytopainter Orange	Abcam
Paraformaldehyde	Roth
Rotimount with DAPI	Roth

Table 2.6 | Reagents for flow cytometry

Reagent	Company
Alexa700 Fixable Viability Stain	BD Biosciences
Anti-Rat and Anti-Hamster Igκ / Negative Compensation Particles Set	BD Biosciences
BD TrueCount Tubes	BD Biosciences
Brilliant Stain Buffer	BD Biosciences
FACS Clean	BD Biosciences
FACS Flow	BD Biosciences
Life/Dead Fixable Near-IR Dead Cell Staining Kit	Life Technologies
Sodium azide	Roth

Table 2.7 | Reagents for RNA isolation, cDNA synthesis and quantitative real-time PCR (RT-PCR)

Reagent	Company
RevertAid H Minus First Strand cDNA Synthesis Kit	Thermo Fisher Scientific
RNase-free DNase	Qiagen
RNeasy Micro Kit	Qiagen
RNeasy Mini Kit	Qiagen
TaqMan Gene Expression Master Mix	Applied Biosystems
QIAshredder	Qiagen

Table 2.8 | Reagents for enzyme-linked immunosorbent assay (ELISA)

Kit	Company
Mouse IFN alpha Platinum ELISA	eBioscience
Mouse IL-6 ELISA Ready-SET-Go!	eBioscience
Mouse IL-10 ELISA Ready-SET-Go!	eBioscience
Mouse TNF alpha ELISA Ready-SET-Go!	eBioscience

2.1.5 Buffer, solution and media

Phosphate buffered saline (PBS)
137 mM NaCl
2.7 mM KCl
10 mM Na_2HPO_4
1.8 mM KH_2HPO_4
in ddH_20, pH 7.4

MACS Buffer
0.5% BSA
2 mM EDTA
in 1x PBS

Fluorescence-activated cell sorting (FACS) Buffer
0.1% BSA
0.02% NaN_3
in 1x PBS

Erylysis Buffer	150 mM NH_4Cl 10 mM $KHCO_3$ 0.1 mM Na_2EDTA in ddH_2O, pH 7.2-7.4
50x TAE buffer	2 M TRIS-base 0.5 M EDTA 57.1 ml acetic acid in 1l ddH_2O, pH 8.3
ELISA wash buffer	0.05% Tween 20 in PBS
ELISA stoppping solution	1 M H_2SO_4 in ddH_20
Mouse complete medium	10% FCS 2 mM L-Glutamine 50 µM 2-Mercaptoethanol 1% penicillin/streptavidin in RPMI1640
GEN2.2 medium	10% FCS 2 mM L-Glutamine 1% penicillin/streptavidin In RPMI1640
MS-5 medium	10% FCS 2 mM L-glutamine 2mM sodium pyruvates 1% penicillin/streptavidin in Alpha MEM
Lysogeny broth (LB)	10 g tryptone 5 g yeast extract 10 g NaCl in 1l ddH_2O

2.1.6 Antibodies

Table 2.9 | Antibodies against mouse antigens for flow cytometry

Antigen	Fluorochrome	Clone	Company
CD3	PE-CF594	145-2C11	BD Biosciences
CD3	PerCP-Cy5.5	145-2C11	Biolegend
CD4	FITC	GK1.5	Biolegend
CD4	BV605	RM4-5	Biolegend
CD8	PE-Cy7	53-6.7	Biolegend
CD11b	APC	M1/70	eBiosciences
CD11b	PE-CF594	M1/70	BD Biosciences
CD11c	FITC	N418	Biolegend
CD11c	PE-Cy7	N418	Biolegend
CD16/32 (FcBlock)	-	93	Biolegend
CD19	APC	1D3	BD Biosciences
CD19	BV510	6D5	Biolegend
CD19	BV605	6D5	Biolegend
CD19	PE-Cy7	1D3	BD Biosciences
CD21/35	BV605	7G6	BD Biosciences
CD23	BV510	B3B4	BD Biosciences
CD25	Alexa488	PC61.5	eBioscience
CD40	APC	3/23	Biolegend
CD44	APC	IM7	Biolegend
CD45	APC-Cy7	30-F11	Biolegend
CD45R/B220	AF647	RA3-6B2	BD Biosciences
CD86	PerCP-Cy5.5	GL-1	Biolegend
CD93	BV650	AA4.1	BD Biosciences
CD115	PE	T38-320	BD Biosciences
CD317 (PDCA1)	PE	927	Biolegend
F4/80	BV421	T45-2342	BD Biosciences
I-A/I-E (MHCII)	Pacific Blue	M5/114.15.2	Biolegend
IgD	BV711	11-26c.2a	BD Biosciences
IgM	FITC	R6-60.2	BD Biosciences
Ly6G	BV711	1A8	BD Biosciences
NK1.1	BV605	PK136	Biolegend
NK1.1	PE-Cy7	PK136	BD Biosciences
Siglech F	BB515	E50-2440	BD Biosciences

Table 2.10 | Antibodies against human antigens for flow cytometry

Antigen	Fluorochrome	Clone	Company
CD3	FITC	HIT3a	Biolegend
CD3	PerCP-Cy5.5	UCHT1	Biolegend
CD4	APC-Cy7	RPA-T4	eBioscience
CD8	FITC	HIT8a	Biolegend
CD11c	BV421	3.9	BD Biosciences
CD14	FITC	M5E2	BD Biosciences
CD14	V450	RPA-T8	BD Biosciences
CD16	FITC	B73.1	Biolegend
CD16	APC	B73.1	BD Biosciences
CD19	PE-CF594	HIB19	BD Biosciences
CD19	FITC	HIB19	BD Biosciences
CD20	BV711	2H7	BD Biosciences
CD20	FITC	2H7	BD Biosciences
CD56	FITC	MEM-188	Biolegend
CD123	BV605	6H6	Biolegend
CD303	APC	AC144	eBioscience
CD304	PE-Vio770	AD5-17F6	Miltenyi Biotec
HLA-DR	PE	L243	Biolegend

2.1.7 Material for genotyping, cloning and RT-PCR

Table 2.11 | Primer for Hv1 genotyping

Primer	Sequence (5‘-3‘)
Hv1 Fwd	gagatccatctgcctccgttatgagtg
Hv1 Rev	gacgtcctaacatcactgagaccatg
betaGeo Rev	gacagtatcggcctcaggaagatcg

Table 2.12 | Plasmids

Plasmid	Company
pENTR-THT, Addgene number 55790	Addgene
pGLTR-X-GFP, Addgene number 58245	Addgene

Table 2.13 | Primer for sequencing during molecular cloning

Primer	Sequence (5‘-3‘)
pENTR-THT Seq Fwd	ctgcaggaattcgaacgctgacg
pENTR-THT Seq Rev	tgtaaaacgacggccagt
pGLTR-X-GFP Seq Rev	gctcaccgcagatatcctg

Table 2.14 | Oligonucleotides for cloning of E2-2 knockdown constructs

Oligo	Sequence (5'-3')
#1 top strand	gatccccgaaaggaatctgaatccgaaatcaagagtttcggattcagattccttttcttttttg gaaa
#1 bottom strand	agcttttccaaaaagaaaggaatctgaatccgaaactcttgatttcggattcagattccttt cggg
#1 scrambled top strand	gatccccggaaagcagtcaagatcaaattcaagagatttgatcttgactgctttccttttttg gaaa
#1 scrambled bottom strand	agcttttccaaaaaggaaagcagtcaagatcaaatctcttgaatttgatcttgactgctttc cggg
#2 top strand	gatccccacacgaaatcttcggaggacaatcaagagttgtcctccgaagatttcgtgtttt tggaaa
#2 bottom strand	agcttttccaaaaacacgaaatcttcggaggacaactcttgattgtcctccgaagatttcg tgtggg
#2 scrambled top strand	gatccccgacatgaatacccggagacatatcaagagtatgtctccgggtattcatgtcttt ttggaaa
#2 scrambled bottom strand	agcttttccaaaaagacatgaatacccggagacatactcttgatatgtctccgggtattca tgtcggg

Table 2.15 | RT-PCR Assays for mouse samples

Target	ID	Company
Cybb	Mm01287743_m1	Life Technologies
Hvcn1	Mm00503873_m1	Life Technologies
Mx1	Mm00487796_m1	Life Technologies
Oas3	Mm00460944_m1	Life Technologies
Ifna4	Mm00833969_s1	Life Technologies
Irf7	Mm00516793_g1	Life Technologies
Tbp	Mm01277042_m1	Life Technologies

Table 2.16 | RT-PCR Assays for human samples

Target	ID	Company
HVCN1	Hs01032838_m1	Life Technologies
TBP	Hs00427620_m1	Life Technologies

2.1.8 Consumables

Table 2.17 | Consumables

Consumable	Company
Multiwell plates (96-well, 24-well, 6-well)	Greiner
Multiwell plate for suspension culture, 6 well, PS	Greiner
Cell culture flask 75 cm^2, PS, filter cap	Sarstedt
Cell culture flask for suspension culture 250 ml, PS, filter cap	Greiner
CELLSTAR EASYstrainer (40 µm and 100 µm)	Greiner
Coverslips	Roth
Eppendorf tubes (0.2 ml)	Thermo Fisher Scientific
Eppendorf tubes (1.5 ml and 2 ml)	Sarstedt
Eppendorf tubes (5 ml)	Eppendorf
FACS tubes (5 ml)	Sarstedt
Falcon tubes (15 ml and 50 ml)	Greiner
Liquid reservoir for multichannel pipettes	Roth, Integra
MicroAmp optical 384-well reaction plate	Applied Biosystems
Neubauer counting chamber	Brand
Parafilm N	Roth
PCR plate sealing tape	Sarstedt
Pipette tips	Sarstedt, Nerbe Plus
Serological pipettes (2ml, 5ml, 10ml and 25ml)	Greiner
Superfrost Plus Slides	VWR
Syringes and needles	Braun, BD

Table 2.18 | Equipment

Device	Company
ABI Prism 7900 HAT Fast Real-Time PCR System	Applied Biosytsems
BD FACS Aria Cell Sorter	BD Biosciences
BD FACS Aria IIIu Cell Sorter	BD Biosciences
BD FACS Aria Fusion Cell Sorter	BD Biosciences
BD FACS LSR II FACS analyser	BD Biosciences
BluePower 500 power supply	Serva
Eppendorf 5417C centrifuge	Eppendorf
FlexCycler2	Analytik Jena
Fridges (4°C) and freezers (-20°C and -80°C)	Liebherr, Sanyo
HeraCell 240 incubator	Thermo Fisher Scientific
INC153 incubator	Memmert
LSM800 Confocal Laser Scanning Microscope	Zeiss
Multifuge 3 S-R	Heraeus
Nanodrop Nd-1000	Peqlab
PerfectBlue Horizontal Gel System	Peqlab
Picus 120 electronic pipet	Sartorius
Picus 1200 electronic multichannel pipet	Sartorius
Pipets	Eppendorf, Gilson
Pipetgirl and pipetboy pipette controller	Integra
Safe 2020 sterile bank	Thermo Fisher Scientific
SevenCompact pH meter	Mettler Toledo
Spark 10M multimode plate reader	Tecan
Thermomixer	Eppendorf
UV transilluminator	Peqlab
Water bath with shaker	GFL

Table 2.19 | Software

Software	Company
FACSDiva	BD Biosciences
FlowJo V7.6 and V10	TreeStar
Mendeley	Elsevier
NanoDrop ND1000 V3.5.2	ThermoScientific
Prism	GraphPad Software
RQ Manager	Applied Biosystems
SDS V2.4	Applied Biosystems
Sparkcontrol	Tecan
ZEN Blue	Zeiss

2.2 Methods

2.2.1 Genotyping

Tail biopsies were taken from each newborn mouse. DNA was extracted from the biopsy using QuickExtract reagent and used as a template in a genotyping PCR (**table 2.18**). The amplification program used was as follows: 5 minutes of incubation at 94 °C, 35 cycles with 30 seconds at 94 °C, 1 minute at 63 °C and 1 minute at 72 °C, 10 minutes at 72 °C. The fragment size of the PCR product was analyzed on a 1% agarose gel containing RotiSafe Gel Stain. The amplicons from wild type samples were 1910 base pairs long while 1500 base pair fragments were amplified from samples of Hv1-deficient mice.

Table 2.20 | Protocol for the genotyping of Hv1-deficient mice

	[µl]
H_2O	14.75
Hot Start Taq Buffer (10x)	2.5
$MgCl_2$ (25 mM)	2
dNTPs (10 mM)	0.5
Primer Hvcn1 Fwd (10 µM)	1
Primer Hvcn1 Rev (10 µM)	1
Primer betaGeo Rev (10 µM)	1
Hot Start Taq	0.25
Template	2
Σ	25

2.2.2 Cloning of lentiviral expression constructs and infection of GEN2.2 pDCs

Visualization of chromatin immunoprecipitation sequencing (ChIP-Seq) data

ChIP-Seq data on genomic binding of E2-2 published by Ghosh and colleagues[212] was analyzed for E2-2 binding to the *HVNC1* gene with the help of Dr. Jan-Broder Engler (INIMS). In brief, FASTQ read files of the study were downloaded from the short read archive. FASTQ files from ChIP input and E2-2 immunoprecipitation were aligned to the human reference genome hg38. Reads falling into the region of the *HVCN1* gene were projected to their genomic coordinates to produce a coverage graph. Enrichment peaks were identified and annotated using the default parameters of MACS 1.4.0 software.

Cloning of small hairpin RNA (shRNA) expressing constructs for E2-2 knockdown

To establish a system for the knockdown of the transcription factor E2-2 in the human pDC cell line GEN2.2 cloning of a lentiviral vector for inducible shRNA expression was chosen. The vectors used were designed for Gateway Recombination Cloning (Life Technologies). In total two vectors with different shRNAs and two corresponding vectors encoding scrambled shRNAs were cloned. Oligonucleotides encoding the shRNAs were designed according to sequences described by Cheng and colleagues[213] (**table 2.12**) and annealed at a concentration of 50 µM in ligase buffer by heating the reaction to 95 °C for 4 minutes and subsequent cooling to room temperature for 10 minutes. Double-stranded oligonucleotides were then ligated into the linearized entry vector pENTR-THT at the BglII and HindIII restriction sites by incubation with T4 DNA ligase for 1 hour at room temperature. Plasmids were transformed into XL-1 Blue competent bacteria and cultured on LB agar plates containing 50 µg/ml kanamycin. Individual colonies were picked and grown in miniprep cultures with 5 ml LB and 50 µg/ml kanamycin. To identify colonies formed by bacteria containing plasmids with an inserted shRNA, plasmids were isolated from the miniprep cultures and digested with BglII. Insertion of the shRNA destroys the BglII restriction site and vectors containing an insert were consequently identified by agarose gel electrophoresis as non-linearized plasmid DNA. Selected vectors were sequenced using pENTR-THT sequencing primers (**table 2.11**). pENTR-THT encodes an inducible H1 promoter that was subsequently subcloned along with the shRNAs into pGLTR-X-GFP, a lentiviral expression vector that allows constitutive expression of green fluorescent protein (GFP) and tetracycline repressor (**figure 2.1**)[214]. Again, XL-1 Blue competent bacteria were transformed with these plasmids and grown on LB agar plates containing 100 µg/ml ampicillin. Individual colonies were picked and digested with EcoRI. Similar to the BglII site in pENTR-THT, the EcoRI restriction site is lost after efficient recombination of the insert so that insert-containing plasmids can be identified by agarose gel electrophoresis. Individual colonies were again picked and amplified in midiprep cultures with 100 ml LB and 100 µg/ml ampicillin. Plasmid DNA was isolated as an endotoxin-free preparation using the NucleoBond Xtra Midi EF kit according to the manufacturer's instructions. The DNA concentration was measured using the NanoDrop and the sequence of all vectors used for viral production was verified by sequencing using the pENTR Seq Fwd and the pGLTR-X-GFP Seq Rev primers (**table 2.11**) by the service group for bioanalytics at the ZMNH. Lentiviruses were generated by the UKE vector facility.

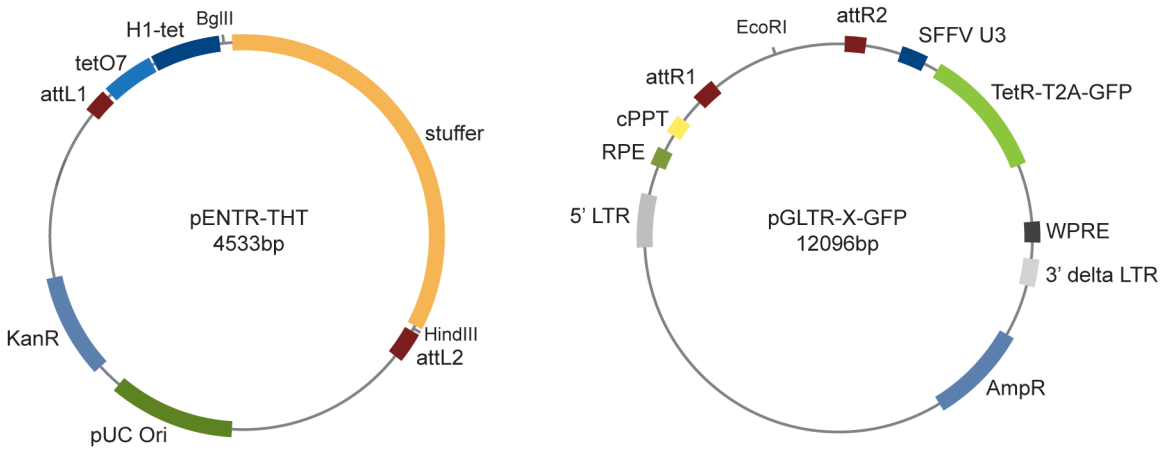

Figure 2.1 | pENTR-THT and pGLTR-X-GFP vector maps
shRNAs were ligated into the pENTR-THT entry vector in exchange for the stuffer after digestion with BglII and HindIII. The shRNA and the upstream H1-tet promoter were then recombined into the pGLTR-X-GFP expression vector between the attL and attR sites. H1, RNA-polymerase III promoter; tetO7, tetracycline operator 7; att (L and R) attachment site; LTR, long terminal repeat; RRE, rev response element; cPPT, central polypurine tract; SFFV U3, spleen focus forming virus U3 promoter; WPRE, woodchuck hepatitis posttranscriptional response element; AmpR, ampicillin resistance; KanaR, kanamycin resistance; TetR, tetracycline repressor; T2A, 2A-like cis-acting hydrolase elements of *Thosea asigna* virus; GFP, green fluorescent protein, pUC Ori, pUC origin of replication; bp, base pairs. Adapted from[214]

Culture and lentiviral infection of the human pDC cell line GEN2.2

For the culture of GEN2.2 cells, MS-5 murine stromal cells were seeded at a density of 5 x 10^5 cells in a 75 cm^2-culture flask with 20 ml of MS-5 medium. The next day, GEN2.2 cells were harvested and seeded at a density of 2 x 10^6 in GEN2.2 medium on the then subconfluent layer of MS-5 feeder cells. Both cell lines were cryopreserved in FCS containing 10% DMSO. All cells used for experiments were not passaged more than 20 times.

If GEN2.2 pDCs were prepared for lentiviral infection, MS-5 cells were seeded on a 6-well plate at a density of 0.6 x 10^5 cells per well one day before the experiment. On the day of infection 1.2 x 10^6 GEN2.2 pDCs were seeded on the subconfluent MS-5 feeder cells and incubated for 6 hours at 37 °C and 5% CO_2. Cells were then infected with lentiviruses at a multiplicity of infection (MOI) of 15 or 25. After 5 days, GFP expression was either analyzed by flow cytometry or cells were seeded on coverslips coated with Cell-Tak for subsequent microscopic analysis.

Staining of GEN2.2 pDCs

To enable adherence of suspension cells, coverslips were coated in 24-well plates with Cell-Tak at a concentration of 3.5 µg/cm^2 for 30 minutes at room temperature according to the manufacturer's instructions. Per well, 2 x 10^5 cells were added in 400 µl of serum-free RPMI medium and allowed to sink to the bottom of the well for 5 minutes. Plates were then spun for 1 minute at 200 x g and incubated for another 30 minutes at 37 °C. After washing three times

for 5 minutes with PBS, cells were immediately fixed using PBS containing 1% PFA for 10 minutes at room temperature followed by three additional washes in PBS to take off residual PFA. Staining was performed at room temperature. Cells were incubated with a 1:1000 dilution of Cytopainter Orange in PBS for 90 minutes. After three final washing steps with PBS, coverslips were mounted on microscope slides using Rotimount with DAPI.

2.2.3 Isolation of human and murine primary cells

Isolation of immune cells from spleen and lymph nodes

Mice were sacrificed by CO_2 inhalation and spleens and lymph nodes were prepared. Spleens were comminuted through a 40 µm cell strainer and spun down at 300 x g and 4 °C for 10 minutes. To lyse erythrocytes, the cells were resuspended in 5 ml erylysis buffer and incubated for 5 minutes on ice. The reaction was stopped by adding 45 ml of cold PBS. Cells were then spun down and resuspended in cold PBS or MACS buffer depending on the downstream experiments. To isolate immune cells from lymph nodes, tissue was put into RPMI containing 400 U/ml collagenase D and 50 µg/ml DNaseI and cut into small pieces using a sterile scissor. The tissue was then digested for 30 minutes in a shaking water bath at 37 °C. After 25 minutes of incubation 10 µM EDTA was added. The samples were comminuted through a 40 µm cell strainer and spun down at 300 x g and 4 °C for 10 minutes. Depending on the downstream experiments cells were resuspended in PBS or MACS buffer.

Isolation of CNS infiltrating immune cells

To isolate infiltrating immune cells from the CNS, mice were sacrificed by CO_2 inhalation and immediately perfused intracranially using 10 ml PBS. The brain and spinal cord were prepared, dissected using a scalpel and digested in RPMI containing 1 mg/ml collagenase A for 30 minutes at 37 °C in a shaking water bath. The digested tissue was then minced through a 40 µm cell strainer and washed once with PBS (300 x g, 10 minutes, 4 °C). Separation of infiltrating immune cells and microglia from myelin was achieved using a discontinuous Percoll gradient. Cells were resuspended in 30% isotonic Percoll and transferred into a 15 ml Falcon tube. The homogenate was then underlayered with 78% isotonic Percoll and centrifuged at 2500 rpm for 30 minutes at 4 °C without using the break. Cells were taken from the interphase and washed twice by resuspending the cell pellet in PBS and two centrifugation steps at 1800 rpm and 1500 rpm for 10 and 5 minutes, respectively. Cells were then resuspended in PBS or MACS buffer for downstream experiments.

Differentiation of pDCs from bone marrow cultures (Flt3L-cultures)

Mice between 8 and 12 weeks of age were sacrificed and cells were isolated from femur, tibiae and humerus by flushing the bones with ice-cold PBS using a 23G needle. Cells were dispersed by pipetting up and down, put through a 40 µm cell strainer and spun down at 300 x g for 10 minutes at 4 °C. Erythrocytes were lysed by 2-minute treatment with erylysis buffer. Cells were washed once in ice-cold PBS and then seeded at a density of 5 x 10^6 cells per well on a 6-well plate for suspension culture or 30 x 10^6 cells in a 75 cm² flask for suspension culture in mouse complete RMPI medium containing 100 ng/ml Flt3L. Cells were cultured for 7 to 8 days at 37 °C and 5% CO_2.

Isolation of PBMCs from human blood samples

Blood was diluted with room temperature PBS and immediately layered on top of 15 ml Ficoll. The gradients were spun at 2000 rpm for 30 minutes at room temperature without using the break. The serum on top of the gradient was carefully taken off until approximately 5 ml were left just above the interphase. PBMCs were cautiously taken from the interphase of the gradient and washed twice in ice-cold PBS: first by spinning the cells at 1800 rpm for 10 minutes and secondly with a spin at 300 x g for 5 minutes. The cells were then resuspended in PBS and counted in a Neubauer chamber.

2.2.4 Flow cytometry

2.2.4.1 Analysis of immune cell populations and expression of surface molecules

Determination of cell numbers by flow cytometry

TrueCount Tubes (BD Bioscience) were used to determine the total number of immune cells isolated from spleens, lymph nodes or CNS. Per tube 100 µl of cell suspension were stained for CD45 expression at 4 °C for 15 minutes. Buffer was then added to a total volume of 300 µl and the number of beads and $CD45^+$ cells was immediately recorded by flow cytometry. Each TrueCount Tube contains a known number of beads which can be identified due to their uniform size and autofluorescence. From each tube 10,000 beads were recorded. The number of $CD45^+$ cells recorded in the meantime was then used to calculate the total number of cells in the sample using the following formula:

$$total\ number\ of\ cells\ in\ the\ sample = \frac{total\ number\ of\ beads\ in\ the\ tube}{recorded\ number\ of\ beads} \times recorded\ number\ of\ cells \times dilution$$

Staining and gating strategies

To identify dead cells by flow cytometry, samples were washed by adding 1ml PBS and centrifugation at 300 x g for 5 minutes before staining with Alexa700 Fixable Viability Stain or Life/Dead Fixable Near-IR Dead Cell Stain diluted 1:1000 in PBS for 15 minutes at 4 °C. The samples were then washed once more with PBS. Extracellular FACS staining was performed in a total volume of 100 µl FACS buffer for 30 minutes at 4 °C. If antibodies coupled to fluorophores of the Brilliant Violet family were used, antibodies and cells were diluted in Brilliant Stain Buffer instead of FACS buffer. In both cases, unbound antibody was washed off using FACS buffer. Cells were immediately fixed by incubation with 1% PFA for 10 minutes at room temperature, washed once in FACS buffer and resuspended in 300 µl of FACS buffer for analysis.

For the analysis of mouse immune cell populations in samples obtained from the CNS or secondary lymphoid organs, different stainings and gating strategies were used. Only one panel was used for the analysis of all immune subsets among CNS-infiltrating cells (**figure 2.2**). In samples isolated from mouse spleen and lymph nodes, distinct panels were used to identify T cells (**figure 2.3**), DCs (**figure 2.4**) and other immune cells including NK cells, granulocytes, macrophages and monocytes (**figure 2.5**). For the immunephenotyping of T cells and DCs the activation markers CD44 or CD40 and CD86, were also stained. Moreover, in samples obtained from mouse spleen, different B cell subpopulations were distinguished (**figure 2.6**) while B cells isolated from lymph nodes were identified by adding an anti-CD19 antibody to the panel depicted in **figure 2.5** and gated as $CD19^+$ cells prior to gating for CD11b.

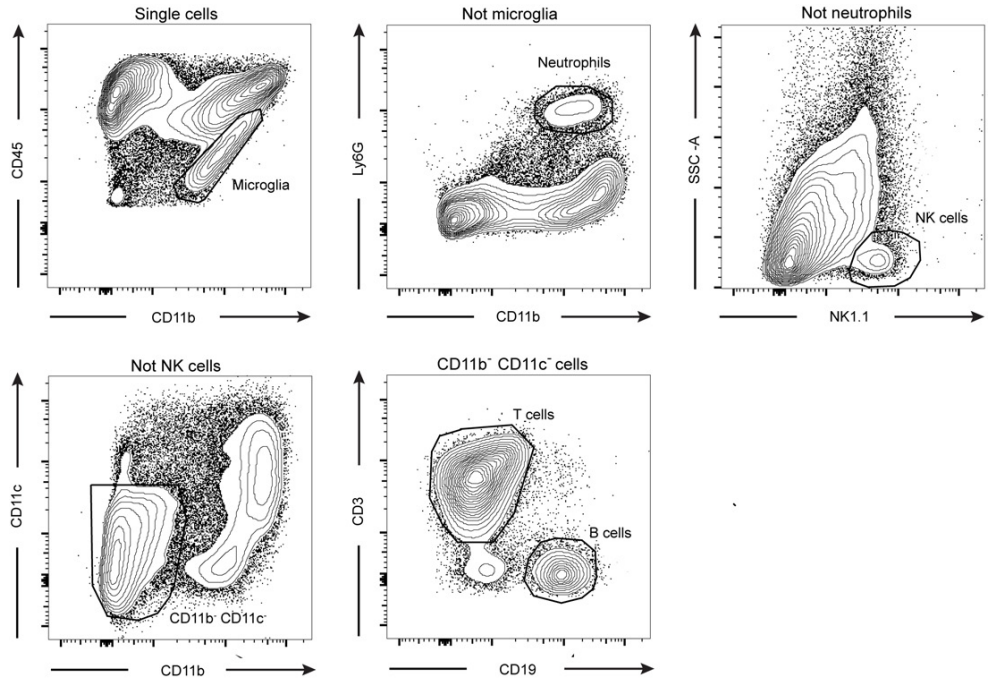

Figure 2.2 | Gating strategy for the identification of different populations CNS-infiltrating immune cells
Single cells were plotted for their expression of CD45 and CD11b to distinguish CNS-resident microglia cells as being $CD45^{int}$ and $CD11b^{+}$. By gating on the remaining cells neutrophils and NK cells were identified in two consecutive steps. The remaining cells were plotted for their expression of CD11c and CD11b and the double-negative cells were further analyzed for their expression of CD3 and CD19 to identify T cells and B cells, respectively. All cells outside the $CD11b^{-}$ $CD11c^{-}$ gate were considered to be myeloid cells including macrophages and DCs.

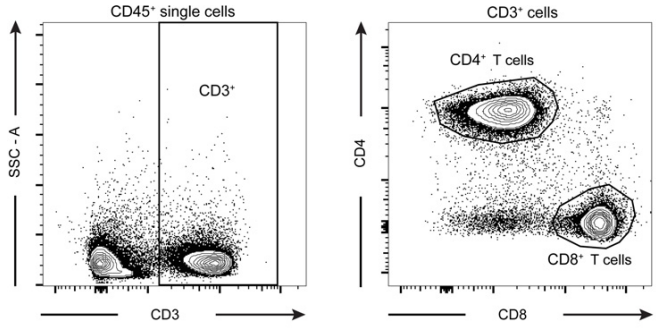

Figure 2.3 | Gating strategy for the identification of $CD4^{+}$ and $CD8^{+}$ T cells
$CD45^{+}$ single cells were plotted for their expression of CD3. Among the $CD3^{+}$ cells the $CD4^{+}$ and $CD8^{+}$ populations were gated as the respective T cell subsets. The same gating strategy was used for the sorting of T cells while for some experiments an antibody against CD19 was added to additionally identify and sort B cells in the $CD3^{-}$ population.

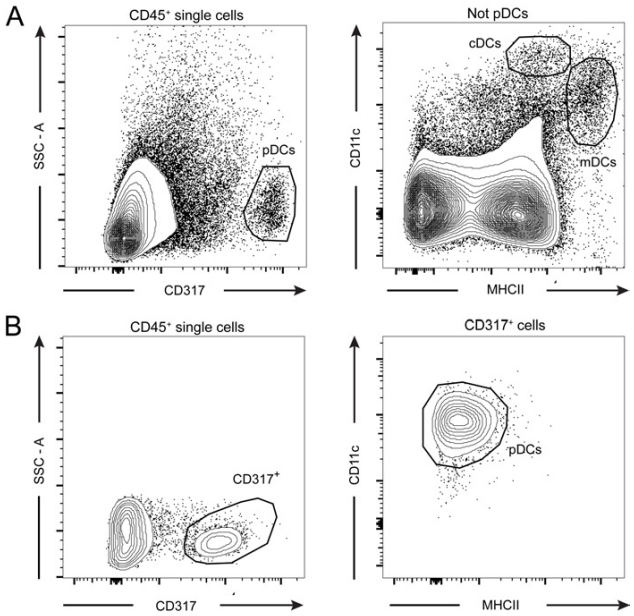

Figure 2.4 | Gating strategy for the identification of DCs
Staining of the same combination of surface markers was used for the identification of different subsets of DCs in spleen and lymph nodes (**A**) as well as for the identification of pDCs in Flt3L-cultures (**B**). Among all $CD45^+$ singlets, pDCs were first identified as $CD317^+$ cells which were then also plotted for their expression of CD11c and MHCII and gated as $CD11c^+$ $MHCII^{lo}$ cells. Among the $CD317^-$ cells present in samples isolated from lymph nodes, cDCs were gated as $CD11c^{hi}$ $MHCII^+$ and migratory DCs (mDCs) as $CD11c^+$ $MHCII^{hi}$. **A** shows a representative example for cells isolated from lymph nodes. While mDCs are absent in the spleen, gating of pDCs and cDCs from splenocytes was nevertheless the same as in **A**.

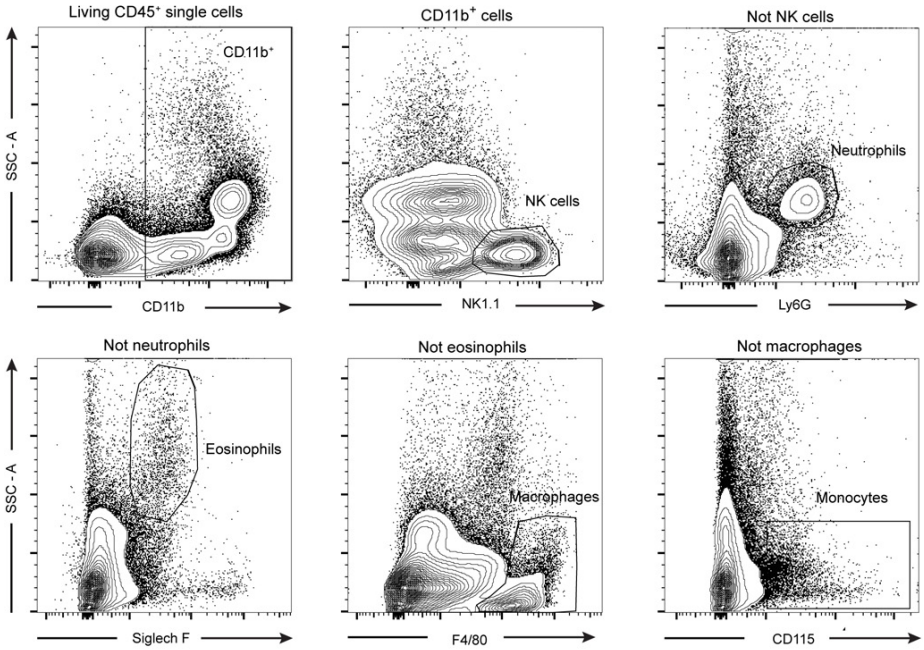

Figure 2.5 | Gating strategy for the identification of additional immune cell populations in spleen and inguinal lymph nodes
$CD11b^+$ cells were gated among all living $CD45^+$ single cells. From these, NK cells were identified as staining $NK1.1^+$. Among non-NK cells $Ly6G^+$ neutrophils and Siglech F^+ eosinophils were identified in two consecutive steps. Both populations show intermediate to high granularity when plotted for the side scatter. The remaining cells were first analyzed for their expression of F4/80 to define a $F4/80^+$ macrophage population and finally all $CD115^+$ monocytes were identified among the $F4/80^-$ cells.

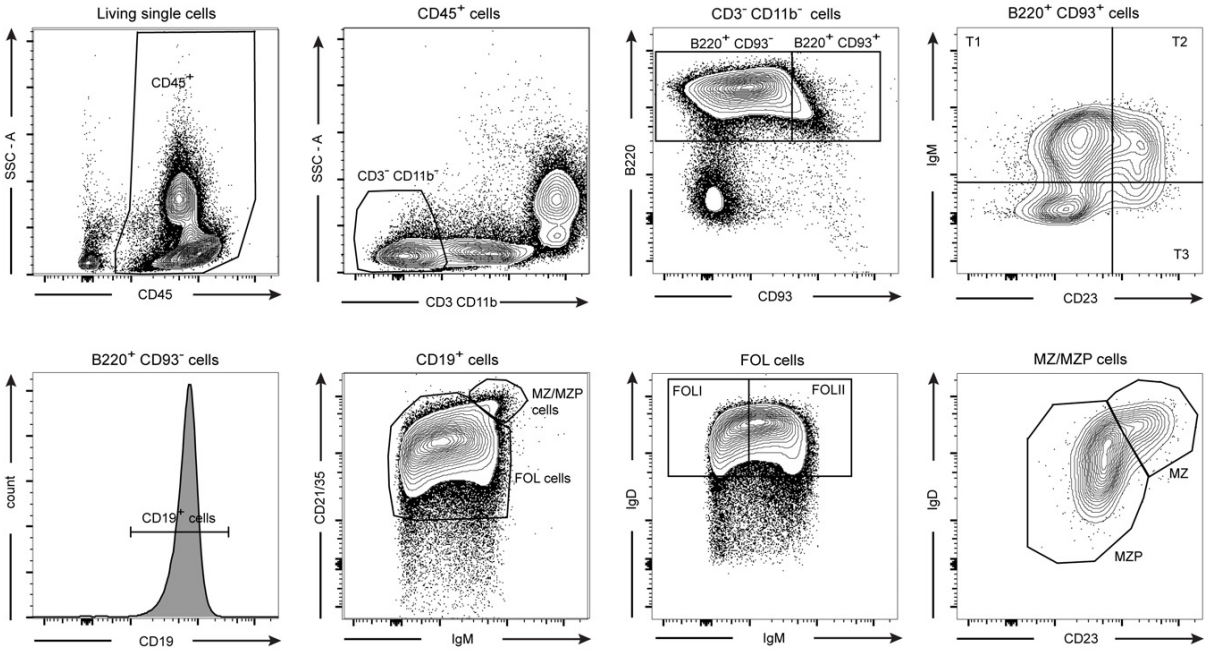

Figure 2.6 | Gating strategy for the identification of different splenic B cell subsets
$CD45^+$ cells among all living single cells plotted for their expression of CD3 and CD11b which were both stained with antibodies coupled to the same fluorophore. The double negative population was then assessed for their expression of B220 and CD93. $B220^+$ $CD93^+$ cells are transistional B cells that were further subdivided into T1, T2 and T3 subsets according to their expression of IgM and CD23. Among the $B220^+$ $CD93^-$ cells, nearly all of which were $CD19^+$, a population of $CD21/35^{hi}$ IgM^+ marginal zone (MZ) and their precursor (MZP) cells was distinguished from the remaining $CD21/35^+$ follicular (FOL) B cells. Among the latter population FOLI and FOLII cells were identified as being both IgD^+, but IgM^- or IgM^+, respectively. MZ and MZP cells were gated according to their expression of CD23 and IgD.

The optimum concentrations of all antibodies for staining were titrated and Fluorescence Minus One controls were used to adjust the gating of each individual population. Compensation controls were measured using stained and unstained compensation particles according to the manufacturer's instructions and compensation values calculated using FACS DIVA software.

Measurement of endosomal pH

Flt3L-cultures were harvested, counted and cells were seeded at a density of 1.5×10^5 cells per well in triplicates on a 96-well plate. CpG oligonucleotides labelled with Atto 647N were mixed with CpG oligonucleotides labelled with Oregon Green 488 at a 1:1 ratio and cells were stimulated with 10 µg/ml of oligonucleotides from this premix for 90 minutes at 37 °C and 5% CO_2. The cells were then harvested, washed in PBS and stained for 15 minutes with Alexa700 Fixable Viability stain diluted 1:1000 in PBS at 4 °C. After an additional washing step with PBS, cells were stained for 30 minutes at 4 °C against CD45 and CD317 to enable identification of pDCs. The samples were washed once more and diluted in FACS buffer for analysis by flow cytometry.

2.2.4.2 FACS

For the isolation of distinct immune cell subsets by FACS, cells were stained at a concentration of 200 x 10^6 cells/ml in MACS buffer for 30 to 45 minutes at 4 °C. MACS buffer was then added and cells were spun down at 300 x g for 10 minutes at 4 °C to take off unbound antibody. The cells were resupended in PBS containing 10 µM EDTA and gently put through a 40 µm cell strainer or, in the case of human samples, a 100 µm cell strainer. The final concentration of the samples was 20 x 10^6 cells/ml. All samples were sorted at a BD FACS Aria IIIu and BD FACS AriaFusion (UKE Sorting Core Facility) or a BD FACS Aria III (INIMS). The purity of the obtained samples was above 90%.

To sort pDCs from Flt3L-cultures as well as primary DCs from spleen or lymph node-derived samples, the same gating strategy as used for the immune phenotyping was applied (**figure 2.4**). T cells were gated as the $CD3^+$ population among $CD45^+$ single cells and, if required, further separated into $CD4^+$ T cells and $CD8^+$ T cells. For the isolation of mouse immune cell populations for *Hvcn1* expression analysis, B cells were gated in the same panel as $CD3^-$ $CD19^+$ cells (**figure 2.3**). For all other *in vitro* experiments, B cells were sorted as $CD19^+$ cells among $CD45^+$ singlets. Finally, with the intention to sort human immune cell subpopulations from PBMCs, two additional stainings were established (**figure 2.7 and 2.8**). Again, antibody concentrations were titrated to optimal dilutions and all gates were placed according to Fluorescence Minus One controls. The calculation of compensation values was performed using FACS DIVA software after measurement of stained and unstained Compensation Particles according to the manufacturer's instructions.

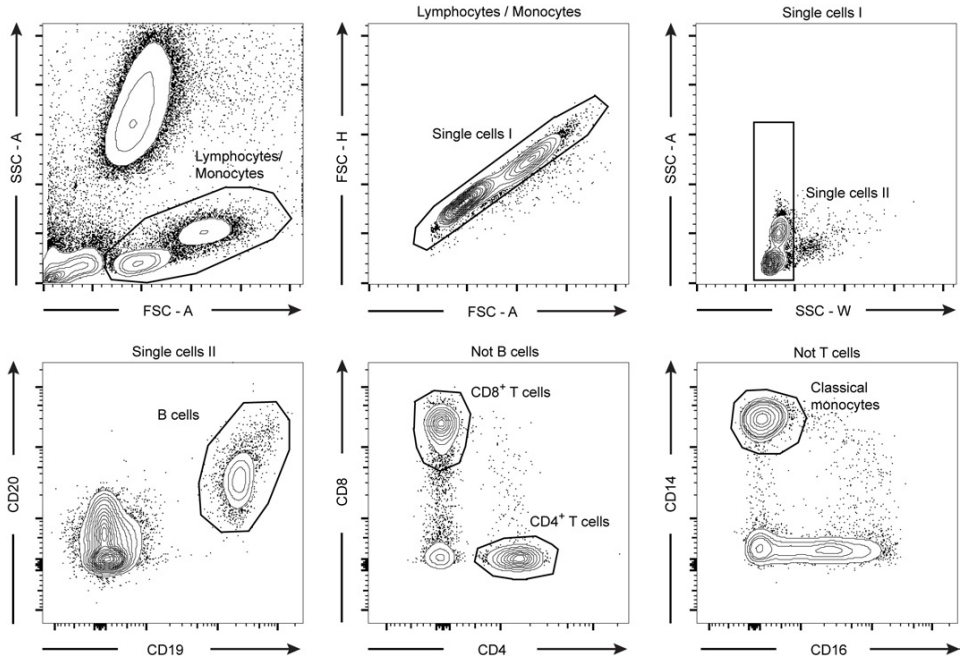

Figure 2.7 | Gating strategy for sorting of human immune cells
Lymphocyte/monocyte populations were identified according to their size and granularity and doublets were excluded by plotting height against area of the forward scatter as well as area against width of the side scatter. First, B cells were gated as $CD19^+$ $CD20^+$. All remaining cells were subdivided into $CD4^+$ and $CD8^+$ T cells. $CD4^-$ $CD8^-$ cells were plotted for CD14 and CD16 to identify classical monocytes as the $CD14^+$ $CD16^-$ population. FACS plots show data obtained from staining of whole blood.

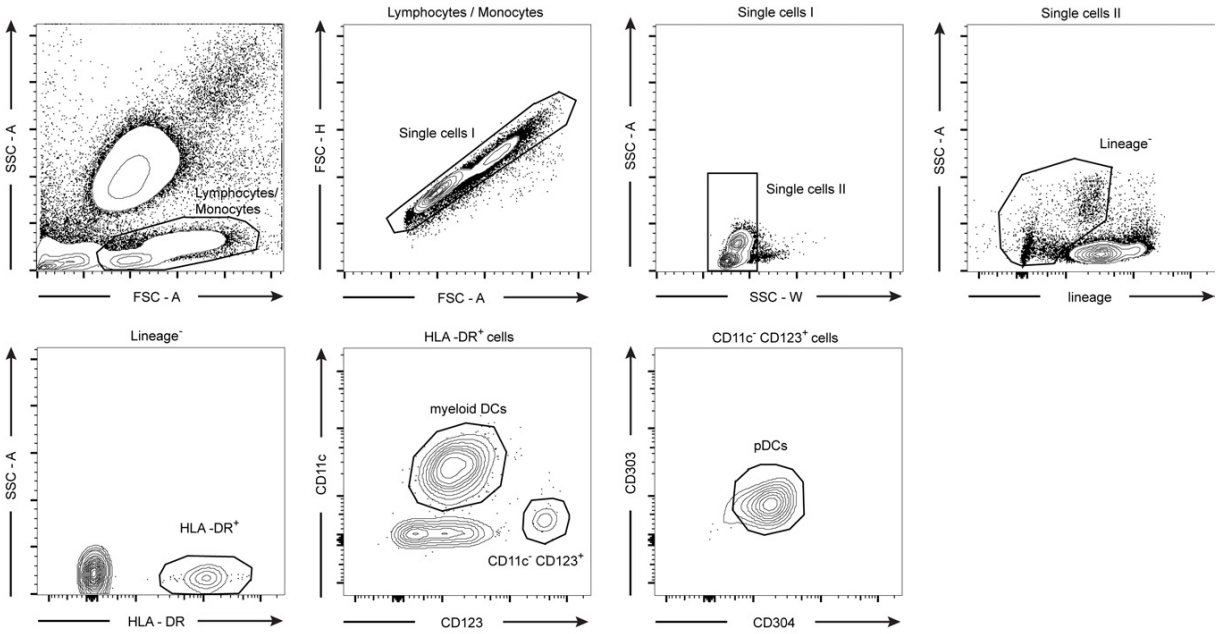

Figure 2.8 | Gating strategy for sorting of human DCs
Lymphocytes/monocytes were first gated by plotting side scatter against forward scatter. After excluding doublets by plotting of first forward scatter height against forward scatter area and second side scatter area against side scatter width, $lineage^+$ cells were excluded. The lineage cocktail contained antibodies against CD3, CD14, CD16, CD19, CD20 and CD56 all labelled with the same fluorophore. Remaining cells were plotted for their expression of HLA-DR. Among the positive cells myeloid DCs were identified as $CD11c^+$ $CD123^-$ cells. pDCs were gated as $CD11c^-$ $CD123^+$ $CD303^+$ $CD304^+$ cells. FACS plots show data from staining of whole blood.

2.2.5 *in vitro* stimulation of immune cells

Stimulation of pDCs with CpG oligonucleotides

For the analysis of pDC activation after stimulation with CpG oligonucleotides, pDCs were differentiated from bone marrow by addition of Flt3L and sorted as described above. 5 x 10^4 cells were plated per well on a 96-well plate and stimulated with CpG-A or CpG-B oligonucleotides for 18 hours at 37 °C and 5% CO_2. Supernatants were then transferred to a new plate and stored at -20 °C until analyzed by ELISA. Cells were harvested and either spun down and snap frozen as a dry pellet for RNA isolation and subsequent analysis of gene expression by RT-PCR or immediately stained for flow cytometry.

Stimulation of pDCs with IFNα

pDCs were differentiated in Flt3L-cultures and sorted as described above. 4 x 10^4 cells were seeded per well on a 96-well plate and stimulated with 100 U/ml or 400 U/ml mouse recombinant IFNα. After 1 hour or 18 hours at 37 °C and 5% CO_2, the cells were harvested, spun down and the pellets were snap frozen in liquid nitrogen for RNA isolation.

Stimulation of T cells with IFNα

$CD3^+$ T cells were sorted from splenocytes as described above. 2 x 10^5 cells per well were seeded in 200 µl of complete RPMI medium on a 96-well plate and stimulated with 100 U/ml or 400 U/ml mouse recombinant IFNα for 1 hour or 24 hours at 37 °C and 5% CO_2. Cells were then harvested, spun down and snap frozen as a dry pellet in liquid nitrogen for RNA isolation.

Stimulation of B cells with CpG-B oligonucleotides and LPS

$CD19^+$ B cells were isolated from splenocytes by FACS as described above. 2 x 10^5 cells were seeded per well on a 96-well plate in complete RPMI containing either 2.5 µg/ml or 10 µg/ml lipopolysaccharide (LPS) or 2.5 µg/ml or 10 µg/ml CpG-B oligonucleotides. After incubation for 24 hours at 37 °C and 5% CO_2 supernatants were collected and stored at -20 °C until being analyzed by ELISA.

Stimulation of B cells in pDC-cocultures

pDCs were isolated from Flt3L-cultures and $CD19^+$ B cells were isolated from splenocytes by FACS as described above. Per well 1.5 x 10^5 B cells were seeded with pDCs at a ratio between 1:3 and 1:50 on a 96-well plate and stimulated with 1 µM CpG-C oligonucleotides for 48 hours. Supernatant was then collected to analyze IL-10 concentrations by ELISA.

2.2.6 ELISA

All ELISAs were performed according to the manufacturer's instructions. In brief, 96-well plates were either bought pre-coated or coated with capture antibody over night. All subsequent incubation steps were performed at room temperature under mild agitation. Unspecific binding was reduced by incubation with blocking buffer for 1 hour. Standard and samples were then added in duplicates and incubated on the plate for 2 hours. Cell culture supernatants used to detect TNFα, IL-6 and IL-10 were diluted 1:2, cell culture supernatants for the detection of IFNα were diluted 1:2 to 1:20 according to the expected concentration. The bound cytokine of interest was subsequently detected with a horseradish peroxidase-coupled detection antibody during an one-hour incubation. A colorimetric reaction was then induced by addition of substrate solution and the reaction was stopped after 15 to 30 minutes depending on the assay. The absorbance at 450 nm and 570 nm was measured using the Tecan plate reader. For analyzation of data, the absorbance at 570 nm was subtracted from the absorbance at 450 nm. A standard curve was plotted using Prism software and the concentrations were calculated accordingly.

2.2.7 RNA isolation, cDNA synthesis and RT-PCR

RNA was isolated from snap-frozen cell pellets using the RNeasy Micro Kit or the RNeasy Mini Kit according to the manufacturer's instructions. For samples containing more than 1 x 10^5 cells the RNeasy Mini Kit was chosen while the RNeasy Micro Kit was used for all samples containing less than 1 x 10^5 cells. Reverse transcription of RNA was performed using the RevertAid H Minus First Strand cDNA Synthesis Kit as follows: Random hexamers were annealed at 65 °C for 5 minutes. Samples were immediately put on ice to add reaction buffer, dNTPS, RNase inhibitor and reverse transcriptase. Reverse transcription was performed by incubation at 25 °C for 5 minutes, 42 °C for 60 minutes and 70 °C for 5 minutes. cDNA was stored at -20 °C until being used for RT-PCR.

To analyze gene expression by RT-PCR, TaqMan Gene Expression Assays (**Table 2.13 and 2.14**) and TaqMan Gene Expression Master Mix were used. Assays were performed with 10 µl reaction volume per well using 384-well plates. All cDNA samples were diluted 1:2 to 1:5 in H_2O prior to measurement.

2.2.8 EAE

10 week old mice were immunized by subcutaneous injection of an emulsion containing 100 µg MOG_{35-55} peptide and complete Freund's adjuvant with 2 mg/ml *Mycobacterium tuberculosis* above the flanks. Additionally, mice received an intravenous injection of 100 ng pertussis toxin (PTX) into the tail vein. PTX administration was repeated two days after

immunization. Mice were weighted daily and disease symptoms were scored according to a five-point scale (0: no disease symptoms; 1: limp tail; 2: hind limb paresis; 3: partial hind limb paralysis; 3.5: complete hind limb paralysis; 4: hind limb paralysis and fore limb paresis; 5: moribund or dead). Mice exhibiting a complete paralysis of their hind limbs on three consecutive days or having a weight loss above 20% were euthanized.

2.2.9 Statistical analysis

All data is presented as the mean values with the standard error of the mean (SEM). Significant results are indicated as * ($p \leq 0,05$) and ** ($p \leq 0,01$), *** ($p \leq 0,001$) and **** ($p \leq 0,0001$). To compare mean differences between two experimental groups an unpaired, two-tailed Student's *t*-test was used. For all other experiments shown in this thesis a two-way analysis of variance (ANOVA) with Bonferroni's *post hoc* test was performed. All statistical analysis was calculated using Prism software.

3 Results

3.1 Expression of *Hvcn1* in pDCs

3.1.1 *Hvcn1*/*HVCN1* expression in the immune system

Data on the function of Hv1 in different types of immune cells has been published in recent years. As an initial experiment for this project, the expression of *Hvcn1*/*HVCN1* in different immune cell populations was analyzed to reproduce published results as well as to complement them with data on its expression in subtypes of DCs in which little is known about the role and expression level of Hv1. To this end, different populations of immune cells were isolated from the spleen and inguinal lymph nodes of wild type mice as well as from PBMCs by FACS. Expression of *Hvcn1*/*HVCN1* was then analyzed on the mRNA level by RT-PCR.

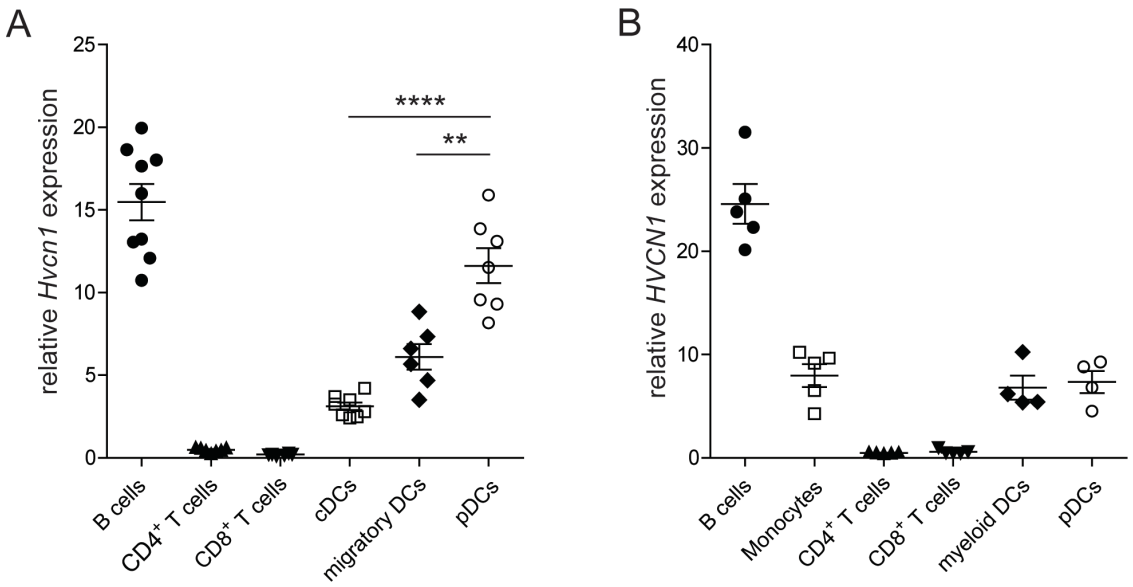

Figure 3.1 | The voltage-gated proton channel Hv1 is expressed in pDCs.
RT-PCR was performed for the quantification of *Hvcn1/HVCN1* mRNA in different immune cell populations isolated from spleen and inguinal lymph nodes of mice (**A**) and human PBMCs (**B**) by FACS. In **A,** migratory DCs were isolated from inguinal lymph nodes, cDCs and pDCs from lymph nodes and spleen and B cells and T cells only from spleen samples. n = 6 - 9 for murine samples and n = 4 - 5 for human samples. The expression level in each cell type is shown relative to the expression of the housekeeping gene *Tbp/TBP* as mean ± SEM. Statistical analysis was performed by student's *t*-test and significance is indicated by ** ($p \leq 0{,}01$) or **** ($p \leq 0{,}0001$).

Hvcn1/*HVCN1* is expressed by all mouse (**figure 3.1 A**) and human (**figure 3.1 B**) immune cells examined in this experiment and its expression is highest in B cells which is in accordance with published data. In addition, *Hvcn1*/*HVCN1* expression is detectable in $CD4^+$ and $CD8^+$ T cells although at very low levels. Of note, *Hvcn1*/*HVCN1* is also expressed in all

subsets of DCs that were analyzed here including pDCs. Even more so, *Hvcn1* expression levels in mouse cells are significantly higher in pDCs compared to migratory DCs or cDCs. Comparing human myeloid DCs and pDCs, however, no difference could be detected. In the human samples, *HVCN1* expression was also analyzed in monocytes which show an intermediated expression level comparable to that of DCs.

Altogether, the data obtained on *Hvcn1*/*HVCN1* expression is in accordance with earlier publications and, in addition, proves expression of *Hvcn1*/*HVCN1* in pDCs, which at least in mice is significantly higher than in other DC subsets. This finding is novel since no data has yet been published on the expression of this proton channel in pDCs and its particular function in this cell type.

3.1.2 Analysis of the transcription factor E2-2 as a potential regulator for Hv1 expression in pDCs

The relatively high expression of *Hvcn1*/*HVCN1* in pDCs, particularly in mouse samples, raises the question whether Hv1 expression in these cells might be explicitly regulated by the pDC-specific transcription factor E2-2 which is itself encoded by the *TCF4* gene in humans. Interestingly, Ghosh and colleagues investigated genomic E2-2 binding sites by ChIP-Seq analysis, a method for the examination of interaction between proteins and nucleic acids, and the data obtained in this study is openly accessible[212]. The dataset was therefore searched for E2-2 binding sites within the region of the *HVCN1* gene. The data indeed shows three statistically significant binding sites of E2-2 within or close to the *HVCN1* coding region (**figure 3.2 A**). Of note, only two of three different *HVCN1* transcript variants are depicted in figure 3.2 A. Variant 1 encodes the longer Hv1 isoform, while an alternative downstream start codon is used for the transcription of variant 3 which encodes the shorter Hv1 isoform. Variant 2 is not depicted here since it encodes the same protein as variant 1 and only differs in its 5' untranslated region[161].

Still, it remains to be tested whether E2-2 not only binds to the *HVCN1* gene, but also regulates its expression. Therefore, a system for the knockdown of E2-2 in the human pDC-like cell line GEN2.2 was established by molecular cloning of lentiviral vectors encoding shRNAs targeting *TCF4* mRNA. If E2-2 binding to *HVCN1* as shown in the ChIP-Seq data was to increase its transcription, its knockdown should consequently be associated with a reduced *HVCN1* expression which can be monitored by RT-PCR and western blot. pGLTR-X-GFP was chosen as a vector backbone for this experiment in which shRNA expression is controlled by a tetracycline operator (TetO)-flanked H1 promoter and thus inducible by the addition of tetracycline. In addition, pGLTR-X-GFP confers constitutive expression of green fluorescent protein (GFP) making it possible to identify infected cells by flow cytometry or

microscopy (**figure 3.2 B and C**). Both methods prove that lentiviral infection of GEN2.2 pDCs is efficient. Moreover, cell survival after infection was well above 80%.

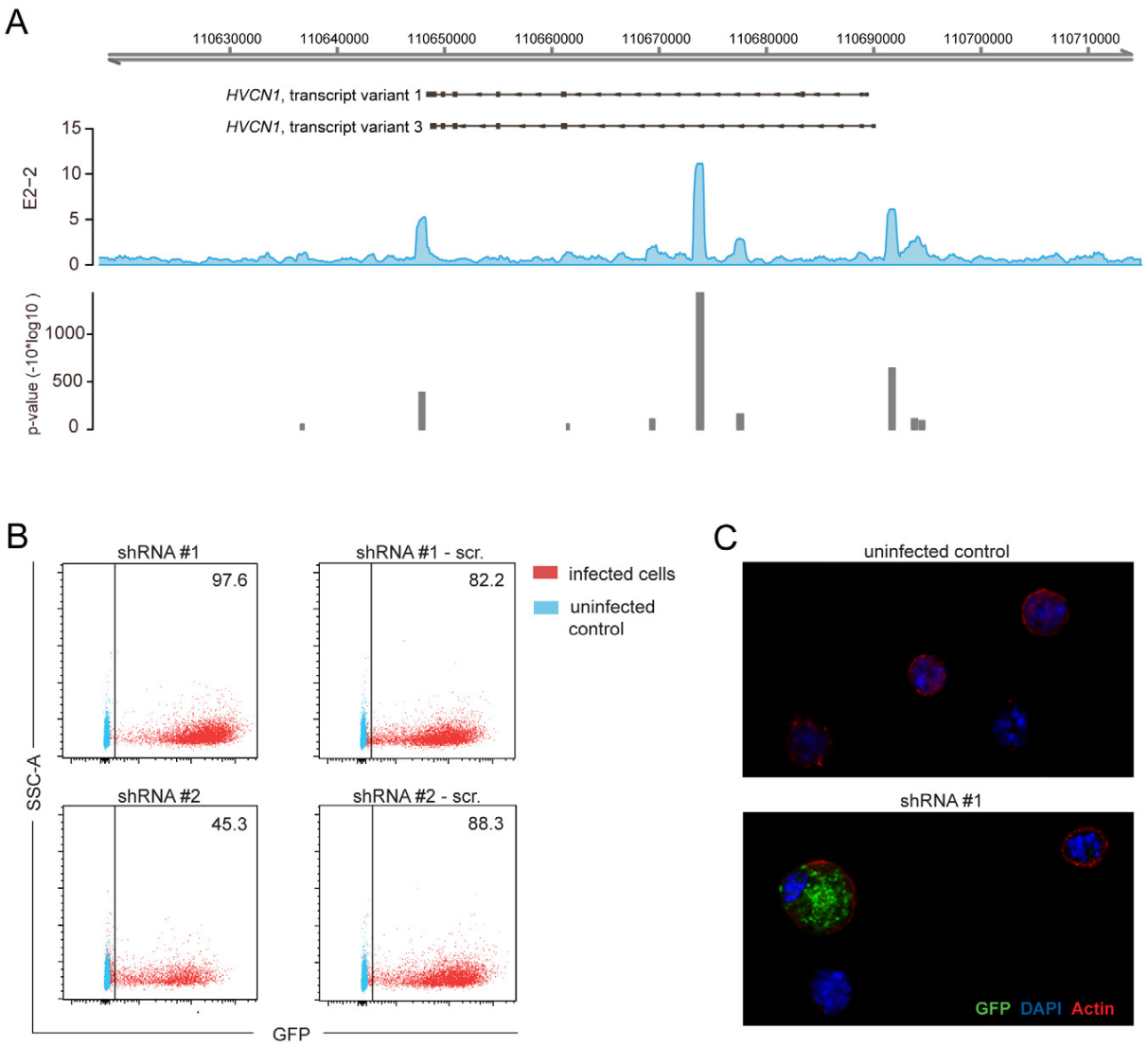

Figure 3.2 | Establishment of a lentiviral expression system for the knockdown of E2-2 in GEN2.2 pDCs
(**A**) Visualization of chromatin enrichment peaks according to ChIP data published by Ghosh and colleagues illustrating three significant binding sites of E2-2 within or close to the *HVCN1* coding region. (**B**) Representative FACS plots showing GFP-expression of GEN2.2 pDCs on day 5 after lentiviral infection with different pGLTR-X-GFP constructs encoding shRNA or scrambled controls at an MOI of 25. (**C**) GFP expression in cells infected with an MOI of 15 as in **B** and documented by confocal microscopy after staining of F-Actin and nuclei.

To conclude, E2-2 is a likely regulator of Hv1 expression in pDCs according to published ChIP-Seq data. Using the pGLTR-X-GFP expression system to knockdown E2-2 after lentiviral infection of pDCs which has successfully been established in his project, it will be possible to directly test whether E2-2 affects Hv1 expression in GEN2.2 pDCs *in vitro.*

3.2 Analysis of the impact of Hv1 on pDC function

3.2.1 Analysis of *Hvcn1* expression in pDCs after stimulation with CpG oligonucleotides

As shown in figure 3.19 in section 3.4.2 of this chapter, the frequency of pDCs in spleen and lymph nodes of wild type mice is less than 0.4%. It is thus difficult to obtain sufficient numbers of primary pDCs for functional experiments and instead pDCs isolated from Flt3L-stimulated bone marrow cultures were used for all *in vitro* experiments presented in this thesis.

To prove whether these cells express *Hvcn1*, which is an obvious prerequisite for their use in functional experiments, RNA was isolated from pDCs derived from wildtype and knockout cultures and the expression of *Hvcn1* on the mRNA level was assessed by RT-PCR. In addition, sorted cells were stimulated with 10 µg/ml CpG oligonucleotides type A or type B for 18 hours to test whether pDC activation alters *Hvcn1* expression levels. Furthermore, the expression of two additional functionally related genes, *Tlr9* and *Cybb*, was assessed. TLR9 is the endosomal receptor to which both types of oligonucleotides bind, although at different stages of endosome maturation, and from which the signaling cascade leading to pDC activation is initiated[57]. The *Cybb* gene, on the other hand, encodes NOX2 which is part of the NOX enzymatic complex needed for ROS production in phagosomes and which activity has been shown to depend on co-localization with Hv1[189].

Hvcn1 mRNA is detectable in unstimulated wild type pDCs isolated from Flt3L-cultures and its expression is significantly upregulated after stimulation with CpG-A, but not CpG-B oligonucleotides (**figure 3.3 A**). At the same time, both types of oligonucleotides enhance expression of *Tlr9,* notably, to a similar degree in both wild type and Hv1-deficient cells (**figure 3.3 B**). Nevertheless, expression of *Cybb* is only significantly higher after stimulation with CpG oligonucleotides type A, but not CpG oligonucleotides type B while again the response in wild type cells is equal to that in Hv1-deficient pDCs (**figure 3.3 C**).

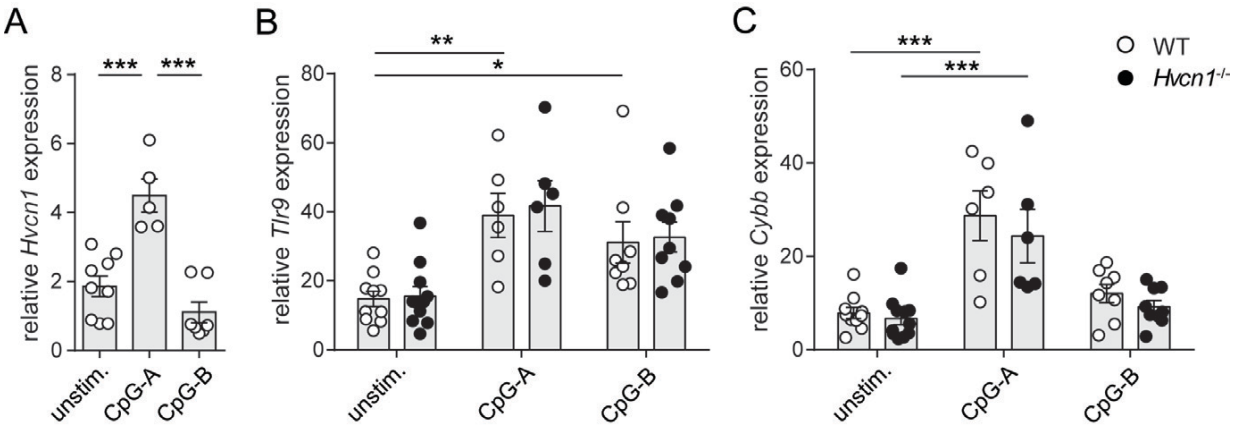

Figure 3.3 | The expression of *Hvcn1*, *Tlr9* and *Cybb* is enhanced after stimulation with CpG-A oligonucleotides.
pDCs were isolated from Flt3L-cultures and stimulated with 10 µg/ml CpG oligonucleotides type A or type B for 18 hours. The expression of *Hvcn1* (**A**), *Tlr9* (**B**) and *Cybb* (**C**) was measured by RT-PCR. Data is pooled from two independent experiments (n = 5 - 9) and is shown relative to the expression of the housekeeping gene *Tbp* as mean ± SEM. In **B**, the difference between *Hvcn1*$^{-/-}$ unstimulated cells also reached statistical significance when compared to samples stimulated with CpG-A ($p \leq 0{,}001$) or CpG-B ($p \leq 0{,}05$). Statistical analysis was performed by student's *t*-test in **A** and two-way ANOVA with Bonferroni's *post hoc* test in **B** and **C**. Significance is indicated by * ($p \leq 0{,}05$), ** ($p \leq 0{,}01$), *** ($p \leq 0{,}001$) or **** ($p \leq 0{,}0001$).

The data thus confirms the expression of *Hvcn1* on the RNA level in pDCs sorted from Flt3L-cultures. Importantly, it also shows that *Hvcn1* expression is massively upregulated after stimulation with CpG oligonucleotides type A which is in turn paralleled by increased expression of *Cybb* which encodes NOX2, a protein shown to be functionally related to Hv1 in other immune cells.

3.2.2 Endosomal pH in Hv1-deficient pDCs

As mentioned above, Hv1 localizes to the phagosomal membrane in phagocytic immune cells where it is essential for sustained ROS production by the NOX complex[189]. With regard to this already established function of the proton channel in other immune cells as well as its upregulation after stimulation of endosomal TLR9 in pDCs, further experiments where conducted to test whether Hv1 is required for endosomal function and signaling in pDCs. As a starting point it was tested whether absence of Hv1 affects the endosomal pH which is frequently used to monitor proper endosomal function. For this purpose, wild type and Hv1-deficient pDCs from Flt3L-cultures were stimulated for 90 minutes with fluorescently-labelled CpG oligonucleotides type A and type B targeting early and late endosomes, respectively. A 1:1 ratio of oligonucleotides coupled to either the pH-insensitive dye Atto 647N or the pH-sensitive dye Oregon Green 488 was used. Oregon Green 488 was chosen as the pH-sensitive fluorophore in this experiment since its fluorescence is not affected by ROS concentrations[215], a parameter that might be altered in the absence of Hv1. The fluorescence intensity of Oregon Green 488 is increasing with rising pH, so that the ratio of the mean

fluorescence intensity (MFI) of Oregon Green 488 normalized to the MFI of Atto 647N was used as an indicator for endosomal pH. It is published that CpG oligonucleotides type A and type B accumulate in the early and late endosomes, respectively, after 90 minutes of incubation[216]. By using fluorescently-labelled oligonucleotides for this experiment the pH could thus be recorded specifically in these distinct endosomal compartments and in a physiologically relevant setting.

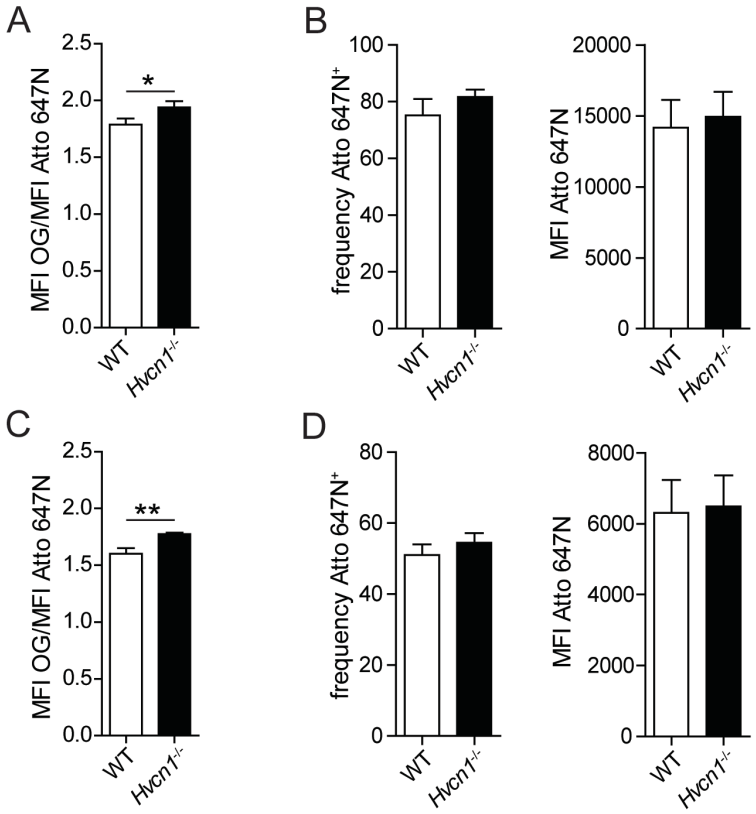

Figure 3.4 | The pH in early and late endosomes after stimulation with CpG oligonucleotides is increased in the absence of Hv1.
Flt3L cultures were stimulated with CpG oligonucleotides type A (**A** and **B**) and type B (**C** and **D**) for 90 minutes using 5 µg/ml CpG oligonucleotides labelled with Atto 647N and 5 µg/ml CpG oligonucleotides labelled with Oregon Green 488 for each sample. MFIs of both dyes were recorded among $CD45^+$ $CD317^+$ pDCs by flow cytometry. Pooled data from two independent experiments is shown and includes samples from individual cultures derived from 6 animals per genotype from each of which three independent stimulations were measured. OG, Oregon Green 488. Data is shown as mean ± SEM. Statistical analysis was performed by student's *t*-test and significance is indicated by * ($p \leq 0{,}05$) and ** ($p \leq 0{,}01$).

When comparing the data obtained in samples from wild type and Hv1-deficient cells, significantly higher MFI (Oregon Green 488)/MFI (Atto 647N) ratios were recorded in Hv1-deficient pDCs in early and late endosomes (**figure 3.4 A and C**). This indicates that the endosomal pH in both early and late endosomes of pDCs is more alkaline in the absence of Hv1 proton channels which, in conclusion, points towards a requirement of Hv1 in the regulation of endosomal pH in this cell type. In addition, the frequency of pDCs which were positive for Atto 647N was analyzed as a readout for the percentage of cells that have

efficiently endocytosed oligonucleotides as well as their MFI for Atto 647N as an indicator for the amount of oligonucleotides on average taken up by each cell. However, both parameters are not different between wild type and Hv1-deficient pDCs neither after stimulation with oligonucleotides type A nor with oligonucleotides type B (**figure 3.4 B and D**). This indicates that absence of Hv1 does not impair the general capacity of pDCs for endocytosis.

3.2.3 Response to TLR9 stimulation in Hv1-deficient pDCs

As a next step it was tested whether the altered endosomal pH observed in Hv1-deficient cells would also be associated with impaired pDC activation after stimulation of endosomal TLR9. As described earlier, CpG oligonucleotides type A bind to TLR9 in the early endosome and induce secretion of IFNα[72]. Hence, pDCs sorted from Flt3L-cultures were first stimulated with different concentrations of CpG-A oligonucleotides for 18 hours and the concentration of IFNα in the supernatant was measured by ELISA as a readout for the degree of pDC activation.

Hv1-deficient pDCs secreted significantly lower amounts of IFNα compared to wild type cells (**figure 3.5 A**). Moreover, RNA was isolated from the same samples to analyze the expression of relevant genes by RT-PCR. Consistent with the results obtained by ELISA, expression of *Ifna4* which encodes one isoform of IFNα also showed a tendency towards decreased expression in Hv1-deficient samples when stimulated with up to 5 µg/ml CpG oligonucleotides which, however, did not reach statistical significance (**figure 3.5 B**). Nevertheless, expression of *Irf7*, the master transcription factor for type I IFN synthesis, as well as expression of the two IFN response genes *Mx1* and *Oas3* were significantly higher in wild type compared to Hv1-deficient samples (**figure 3.5 C to E**). Even with rising concentrations of CpG oligonucleotides, the expression level of these genes could not be increased.

In contrast to CpG-A oligonucleotides, CpG oligonucleotides type B signal from the late rather than from the early endosome. This induces a different activation status characterized by the upregulation of molecules involved in antigen-presentation and the release of proinflammatory cytokines while only negligible amounts of type I IFN are secreted[72]. In order to investigate whether TLR9 signaling was also impaired from this more acidified endosomal compartment, pDCs sorted from Flt3L-cultures were stimulated with CpG-B oligonucleotides for 18 hours.

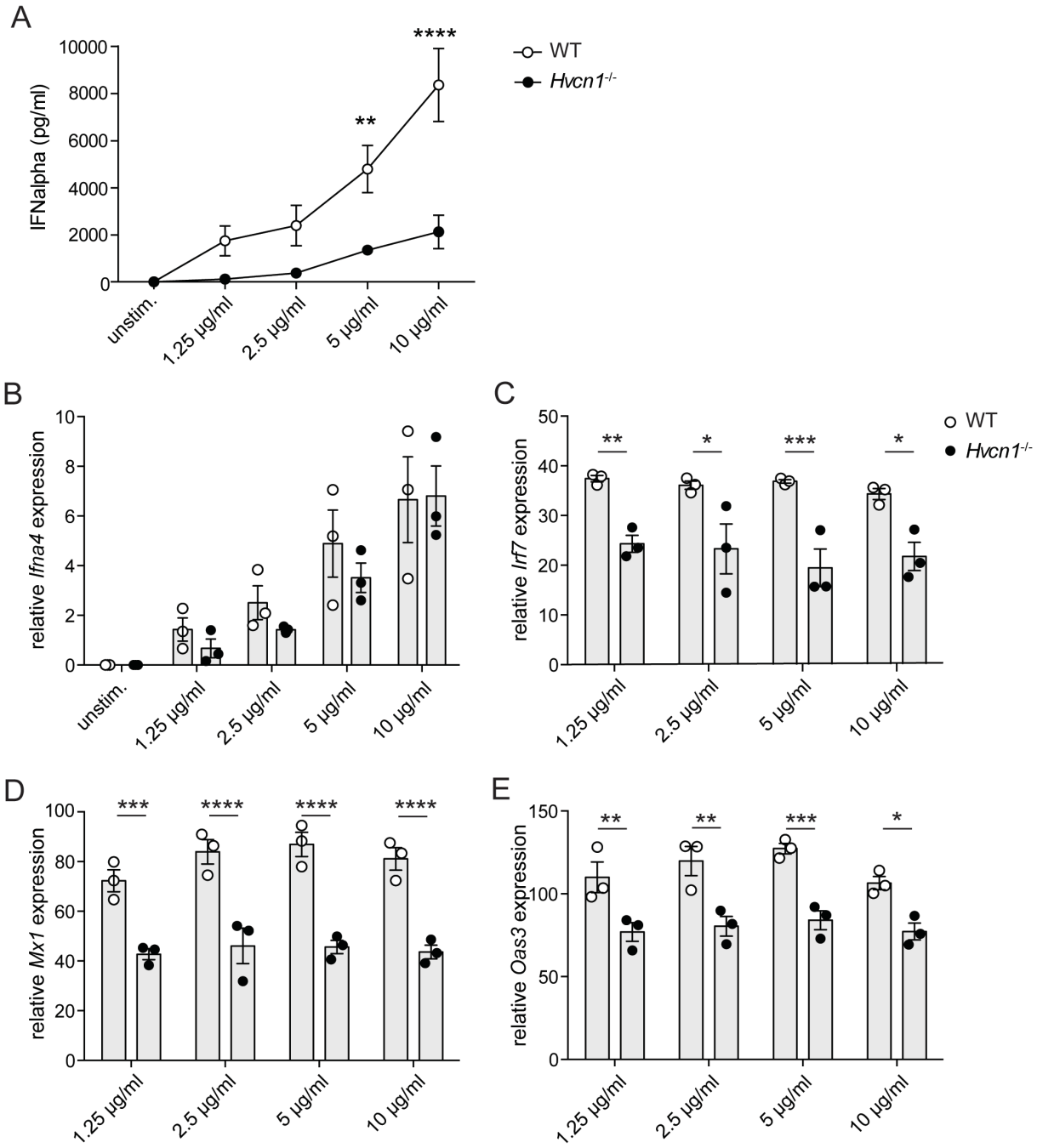

Figure 3.5 | pDC activation after stimulation with CpG-A oligonucleotides is decreased in the absence of Hv1.
pDCs were sorted from Flt3L-cultures and stimulated with CpG oligonucleotides type A for 18 hours. The concentration of IFNα in the supernatant was measured by ELISA (**A**) and the expression of *Ifna4* (**B**), *Irf7* (**C**), *Mx1* (**D**) and *Oas3* (**E**) were analyzed by RT-PCR. Representative data from one experiment out of 3 stimulations is shown with n = 3 as the mean ± SEM. Statistical analysis was performed by two-way ANOVA with Bonferroni's *post hoc* test and significance is indicated by * ($p \leq 0,05$) and ** ($p \leq 0,01$), *** ($p \leq 0,001$) and **** ($p \leq 0,0001$).

Indeed, secretion of IL-6 and TNFα as measured by ELISA were significantly reduced in cultures of Hv1-deficient pDCs (**figure 3.6 A**). Furthermore, surface expression of the costimulatory molecule CD40 was lower in Hv1-deficient compared to wild type cells indicating decreased cell activation and capacity for antigen presentation (**figure 3.6 B**).

Expression of CD86 was, however, not altered. Furthermore, cell survival was not different between wild type and knockout cells (**figure 3.6 C**).

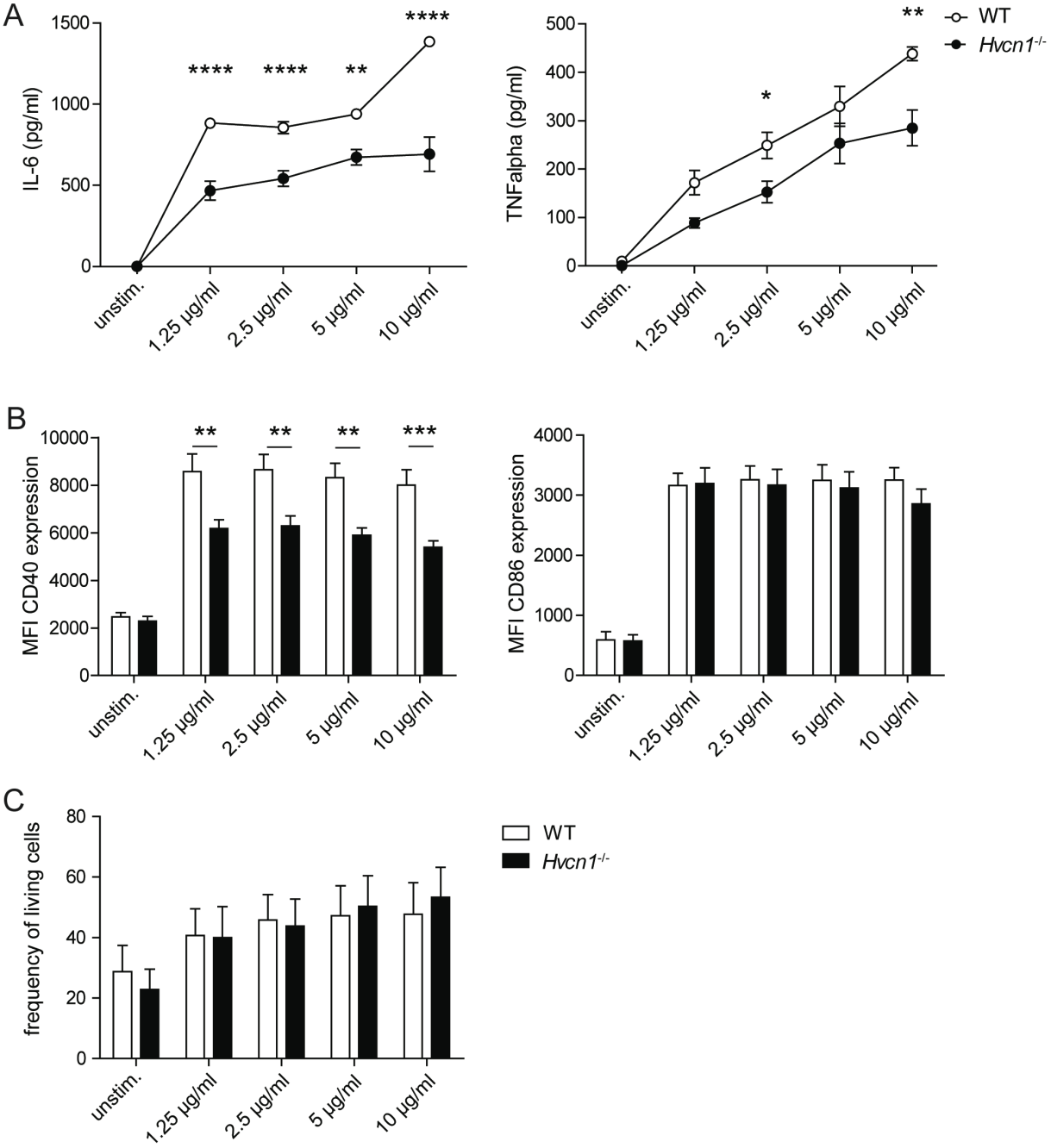

Figure 3.6 | pDC activation after stimulation with CpG-B oligonucleotides is decreased in the absence of Hv1.
pDCs were sorted from Ftl3l-cultures and stimulated with different concentrations of CpG-B oligonucleotides for 18 hours. (**A**) IL-6 (n = 5) and TNFα (n = 5 - 11) concentration were measured in the supernatant by ELISA. (**B**) Surface expression of CD40 and CD86 (n ≥ 6) measured as the MFI by flow cytometry. (**C**) The percentage of living cells was measured by flow cytometry as the percentage of negative cells after staining with fixable viability stain. Pooled data from two or three out of three independent experiments is shown in **A** for IL-6 and TNFα, respectively**. B** and **C** show pooled data from four independent experiments (n = 12 – 15). All data is shown as mean ± SEM. Statistical analysis was performed using two-way ANOVA with Bonferroni's *post hoc* test and significance is indicated by by * ($p \leq 0,05$) and ** ($p \leq 0,01$), *** ($p \leq 0,001$) and **** ($p \leq 0,0001$).

Altogether, these results demonstrate that pDCs require Hv1 for proper activation in response to stimulation with CpG oligonucleotides targeting TLR9 in both early and late endosomes. Consequently, both the secretion of type I IFN as well as the secretion of proinflammatory cytokines and the ability to present antigen are impaired in Hv1-deficient pDCs *in vitro*.

3.2.4 Type I IFN response in Hv1-deficient pDCs

Secretion of type I IFN is enhanced by an autocrine and paracrine feedback loop, meaning that type I IFN secreted by an individual cell will also bind to IFN receptors on the same as well as neighboring cells and elicit an intracellular signaling cascade that will further promote phosphorylation of Irf7 and IFN secretion[217]. To test whether the responsiveness of Hv1-deficient pDCs to IFN is altered which might contribute to the observed decreased IFN secretion after stimulation with CpG oligonucleotides type A described above, pDCs were isolated from Flt3L-cultures and stimulated with 100 U/ml or 400 U/ml recombinant murine IFN for 1 or 18 hours. The expression of the IFN response gene *Oas3* was measured by RT-PCR (**figure 3.7**). No significant differences comparing the IFN response of wild type and Hv1-deficient pDCs were detected at neither time point, indicating that Hv1 is not required for auto- and paracrine sensing of type I IFN in pDCs.

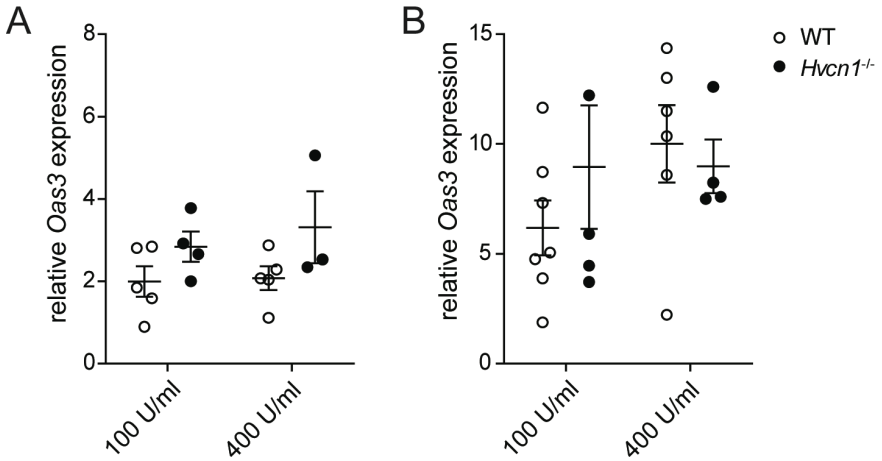

Figure 3.7 | The IFN response is not different between wild type and Hv1-deficient pDCs.
pDCs were sorted form Flt3L-cultures and stimulated with 100 U/ml or 400 U/ml recombinant murine IFNα for 1 hour (**A**) or 18 hours (**B**). The expression of the IFN response gene *Oas3* was measured by RT-PCR in two independent experiments (n = 3 - 7) and is depicted relative to the expression in unstimulated cells. Statistical analysis was performed by two-way ANOVA with Bonferroni's *post hoc* test and data is shown as mean ± SEM.

3.2.5 IL-10 secretion of Hv1-deficient B cells after TLR-mediated stimulation

Similar to pDCs, B cells express TLR9 and can be stimulated with CpG oligonucleotides type B or type C[218,219]. The response induced by this pathway is, however, different and includes

secretion of the anti-inflammatory cytokine IL-10[220]. If Hv1-deficiency would not only impair TLR9-mediated stimulation of pDCs, but also of B cells, this would hint at a more general role of this proton channel in normal endosomal function in diverse immune cells. Therefore, IL-10 secretion of $CD19^+$ B cells from wild type and Hv1-deficient animals was analyzed after stimulation with CpG oligonucleotides type B and lipopolysaccharide (LPS). LPS induces IL-10 secretion via a distinct signaling pathway that involves ligand binding to TLR4 on the plasma membrane and the response to LPS-stimulation is thus independent of endosomal function[221,222]. The IL-10 concentration in the supernatant was subsequently measured by ELISA.

IL-10 secretion was significantly decreased after stimulation with both concentrations of CpG oligonucleotides (**figure 3.8**). For the LPS-stimulated samples, a similar tendency was observed in all three independent experiments which did, however, not reach statistical significance. It thus seems that Hv1-deficiency indeed impairs IL-10 secretion by B cells and that this effect is more pronounced after stimulation via the endosomal TLR9. Nevertheless, it might be that Hv1-deficiency is also associated with a generally decreased ability of the $CD19^+$ population to secrete IL-10 which is independent of its possible involvement in endosomal function.

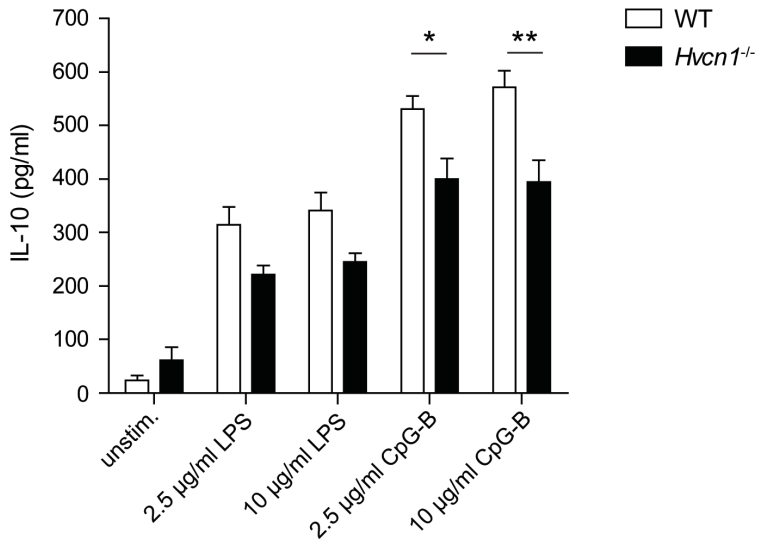

Figure 3.8| IL-10 secretion by $CD19^+$ B cells after stimulation with LPS or CpG-B oligonucleotides is decreased in the absence of Hv1.
B cells were sorted as $CD19^+$ cells from wild type and Hv1-deficient splenocytes and stimulated for 24 hours with 2.5 µg/ml or 10 µg/ml LPS or CpG-B oligonucleotides. IL-10 concentration in the supernatant was measured by ELISA. Results are pooled from three independent experiments and shown as mean ± SEM (n=15) Statistical analysis was performed by two-way ANOVA with Bonferroni's *post hoc* test and statistical significance is indicated by * ($p \leq 0,05$) or ** ($p \leq 0,01$)

3.3 Experimental autoimmune encephalomyelitis

3.3.1 EAE in Hv1-deficient mice

During EAE, the mouse model of MS, an autoimmune T cell reaction against MOG-peptide is experimentally induced that causes immune cell infiltration, inflammation and demyelination in the CNS. Since activation of Hv1-deficient pDCs is impaired *in vitro* and dysregulation of the IFN response has been implied in the pathophysiology of EAE, the *in vivo* effect of Hv1-deficiency was analyzed in this model of autoimmunity. For this purpose, wild type and Hv1-deficient mice were immunized by subcutaneous injection of MOG-peptide and complete Freund's adjuvant (CFA). PTX was additionally administered intravenously directly after MOG-injection as well two days thereafter.

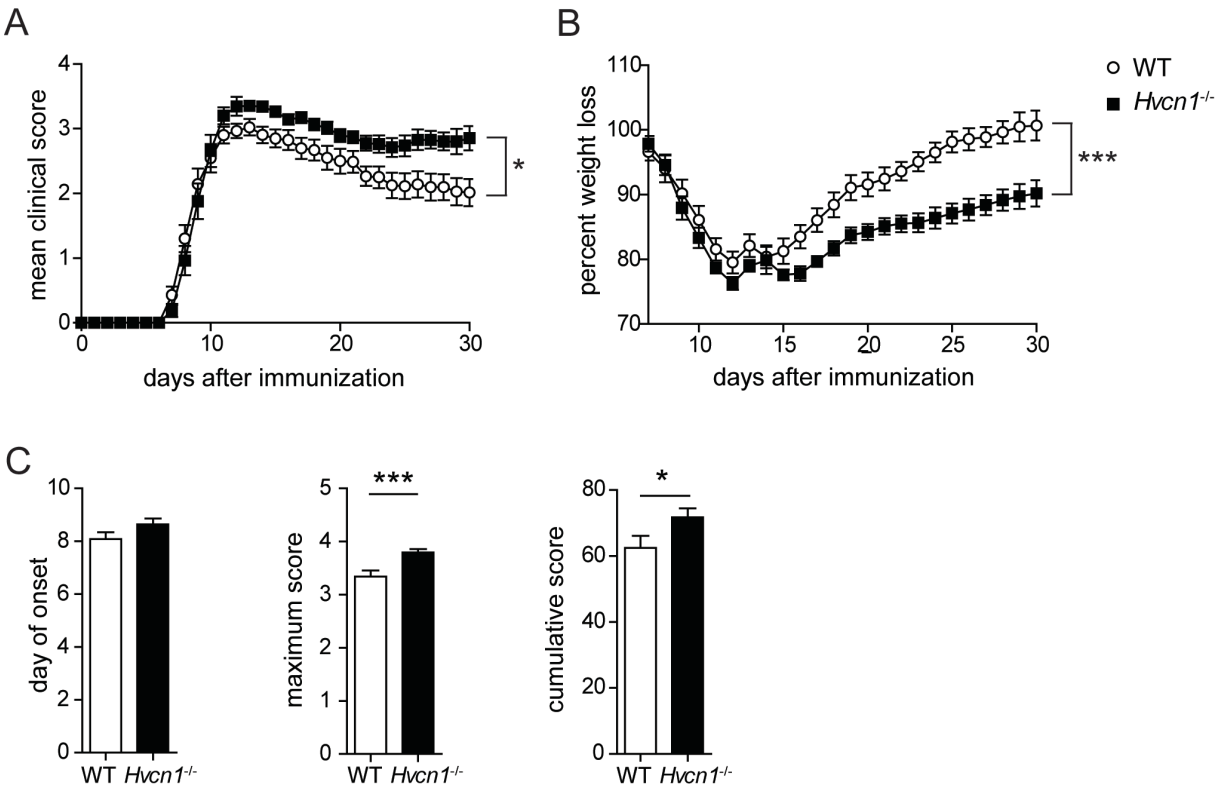

Figure 3.9 | EAE is aggravated in the absence of Hv1.
Mice were immunized with MOG/CFA and PTX and the disease severity was recorded as the mean clinical score (**A**) and percent weight loss (**B**). The maximum score, the cumulative score and the day of onset were calculated from the daily mean clinical scores (**C**). Data from two independent immunizations is shown as mean ± SEM (n = 24 for wild type mice and 25 for Hv1-deficient mice). Statistical analysis was performed by two-way ANOVA with Bonferroni's *post hoc* test in A and B and student's *t*-test in C and statistical significance is indicated by * ($p \leq 0,05$) and *** ($p \leq 0,001$).

Both genotypes developed a classical EAE course with an onset of symptoms around day 7 after immunization and gradually exacerbating symptoms until day 14 after immunization (**figure 3.9 A**). Thereafter, symptoms slightly ameliorated reaching a plateau until day 30 after immunization. Of note, Hv1-deficient mice reached higher disease scores than wild type

animals from around day 11 after immunization on until the end of the experiment. This significant exacerbation of EAE symptoms was also reflected by an increased body weight loss (**figure 3.9 B**) as well as increased maximum and cumulative scores of the knockout animals (**figure 3.9 C**). No difference was, however, observed in the day of disease onset.

3.3.2 CNS infiltration in acute and chronic EAE

On the background of the known expression of *Hvcn1* in almost all populations of immune cells, the frequency and absolute numbers of CNS infiltrating immune cells was assessed during acute (day 14 after immunization) and chronic (day 30 after immunization) EAE to test for possible alterations which might explain the increased disease severity in knockout animals. To this end, CNS infiltrating cells were isolated from the brain and spinal cord and the frequency of different immune cell populations was analyzed in detail by flow cytometry. At both acute and chronic EAE, mice with a similar range of disease scores were chosen from both genotypes with the intention to control for a possibly confounding effect of the on average increased disease severity in Hv1-deficient mice.

During acute EAE a non-significant trend towards increased absolute numbers of $CD45^+$ CNS infiltrating immune cells was observed when comparing the mean number of infiltrating cells derived from all mice in the experiment irrespective of disease score (**figure 3.10 A**), but also when comparing wild type and Hv1-deficient mice that were assigned similar disease severity on the day of the experiment (**figure 3.10 B**). Importantly, this number does not include $CD45^+$ CNS-resident microglia cells. Among all subsets of immune cells analyzed, the only statistically significant differences could be recorded with regard to the absolute number of infiltrating $CD4^+$ T cells as well as myeloid cells. The latter population includes macrophages and dendritic cell subsets including pDCs which were not distinguished further in this experiment (**figure 3.10 C**).

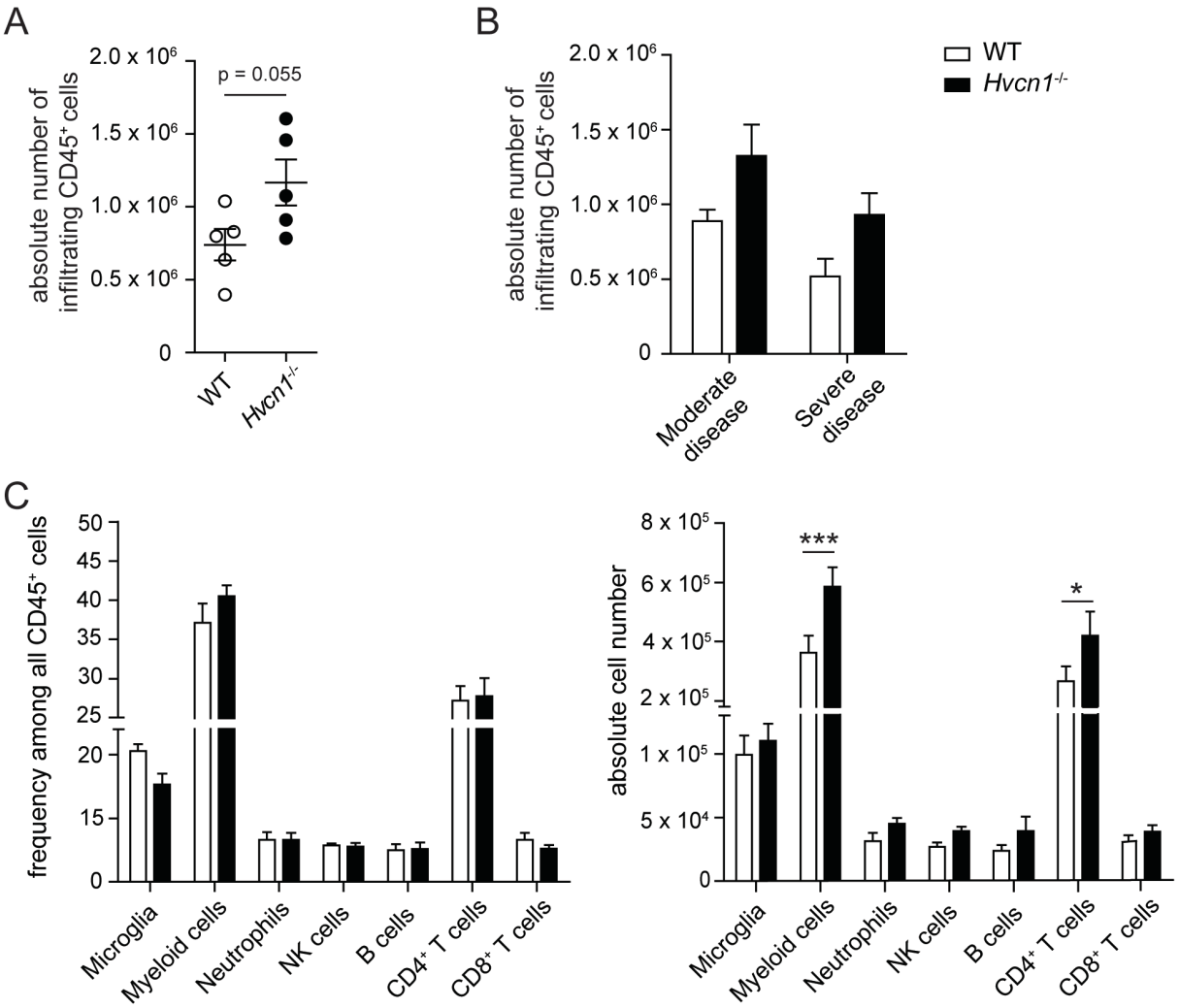

Figure 3.10 | CNS infiltration of myeloid cells and CD4$^+$ T cells is increased during acute EAE in the absence of Hv1.
CNS infiltrating cells were isolated at day 14 after immunization and analyzed by flow cytometry. (**A**) Absolute number CD45$^+$ CNS infiltrating cells in wild type and Hv1-deficient mice (**B**) Absolute number of CD45$^+$ CNS infiltrating cells grouped for wild type and Hv1-deficient mice with the same disease severity. (**C**) Percentage and absolute cell count of different infiltrating immune cell subpopulations. Moderate disease is defined as disease score of 3.0 or lower, severe EAE is defined as a disease score above 3.0. Results from only one experiment are shown as mean ± SEM (n = 5). Statistical analysis was performed by student's t-test in **A** and two-way ANOVA with Bonferroni's post hoc test in **B** and **C** and significance is indicated by * ($p \leq 0,05$) and *** ($p \leq 0,001$).

Different to what was observed in acute EAE, similar numbers of CD45$^+$ CNS infiltrating cells were isolated from Hv1-deficient mice and wild type controls during the chronic phase of the disease (**figure 3.11 A**). Also, when comparing mice with different genotypes that were scored with similar disease severity on the day of the experiment, no difference between the number of CD45$^+$ infiltrating cells was detected (**figure 3.11 B**). Furthermore, no differences were recorded with regard to the frequency or absolute numbers of different immune cell types among CD45$^+$ infiltrating cells (**figure 3.11 D**).

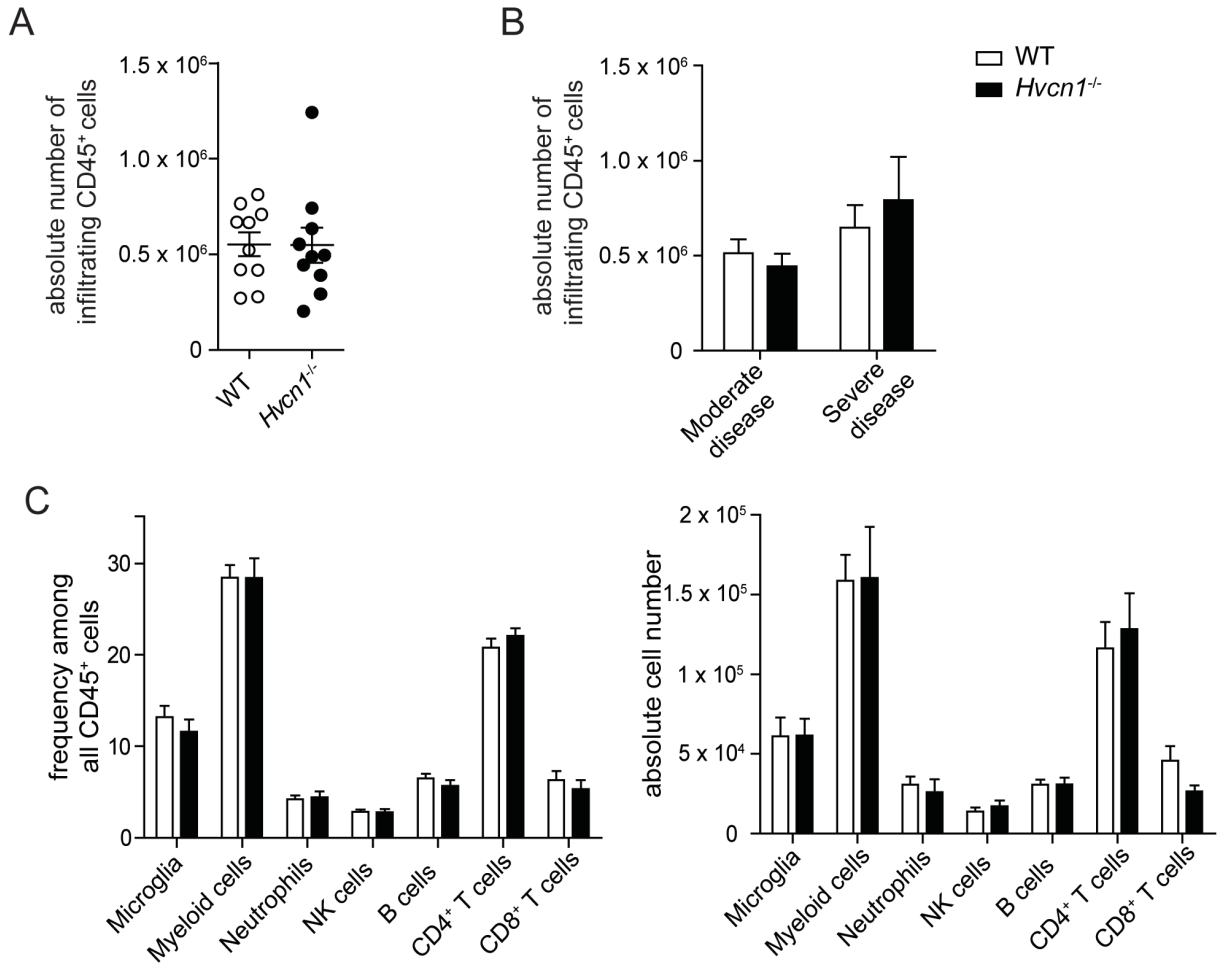

Figure 3.11 | CNS infiltration of immune cells during chronic EAE is not different between wild type and Hv1-deficient mice.
CNS infiltrating cells were isolated at day 30 after immunization and analyzed by flow cytometry. Absolute number of $CD45^+$ CNS infiltrating cells (**A**), absolute number of $CD45^+$ CNS infiltrating cells grouped for the same range of disease scores (**B**), mean EAE score of all animals at the day of experiment (**C**) and frequency and absolute number of different CNS-infiltrating immune cell subsets (**D**) were analysed. Moderate disease is defined as a disease score of 3.0 or lower, severe EAE is defined as a disease score above 3.0. experiment. Results from two experiment are shown as mean ± SEM (n = 10). Statistical analysis was performed by student's *t*-test in **A** and two-way ANOVA with Bonferroni's *post hoc* test in **B** and **C**.

Altogether, the analysis of CNS infiltration during acute and chronic EAE thus shows that EAE in Hv1-deficient mice is associated with significantly increased infiltration of myeloid cells and $CD4^+$ T cells during acute EAE, differences that nevertheless cease when reaching the chronic stage of disease.

3.3.3 Type I IFN response in CNS infiltrating cells during chronic EAE

The significantly impaired ability of Hv1-deficient pDCs to become activated after stimulation with CpG oligonucleotides *in vitro* suggests that pDC activation might also be impaired *in vivo* during EAE. Since, in addition, a reduction in the type I IFN response is in particular known to aggravate autoimmune pathology in EAE[145], it was investigated whether the IFN response in Hv1-deficient mice was altered. However, it is difficult to directly assess the

concentration of type I IFN in the CNS and therefore the expression of different IFN response genes, which are upregulated in all cells in response to type I IFN, was measured as an indirect readout. For this purpose, infiltrating $CD3^+$ T cells were isolated from the CNS of wild type and Hv1-deficient mice at day 30 after immunization and the expression of *Irf7*, *Mx1* and *Oas3* was recorded by RT-PCR. All genes analyzed had similar expression levels when comparing wild type and Hv1-knockout cells indicating that there was no difference in the concentration of type I IFN in the CNS during chronic EAE (**figure 3.12**).

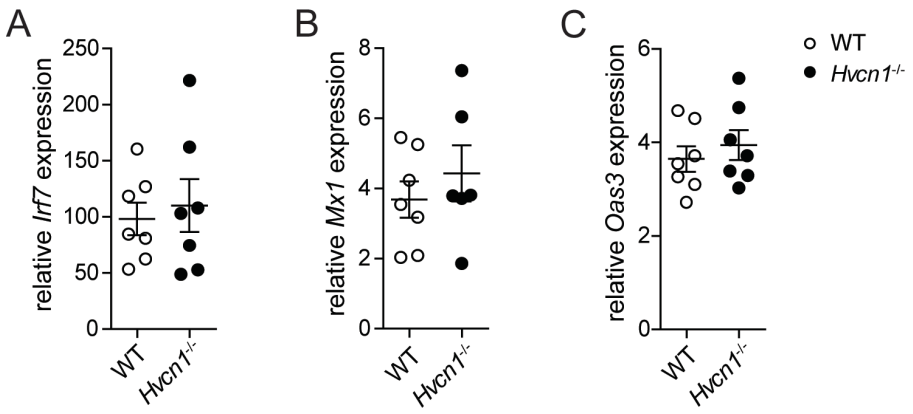

Figure 3.12 | The IFN response is not altered in CNS-infiltrating T cells of Hv1-deficient mice during chronic EAE.
Mice were sacrificed at day 30 after immunization and CNS-infiltrating immune cells were isolated from brain and spinal cord. $CD3^+$ T cells were sorted and the expression of the IFN response genes *Irf7* (**A**), *Mx1* (**B**) and *Oas3* (**C**) was measured by RT-PCR. Data from two independent immunizations (n = 6 – 7) is shown as mean ± SEM. Statistical analysis was performed by two-way ANOVA with Bonferroni's *post hoc* test.

In principle, Hv1-deficiency could alter the responsiveness of T cells to type I IFN thereby masking existing differences in local IFN concentration in the chosen experimental setup. To validate that T cells from wild type and Hv1-deficient mice were equally responsive to the presence of type I IFN, $CD3^+$ cells were sorted from the spleen of healthy mice and stimulated with different concentrations of murine recombinant IFNα *in vitro*. No difference in the upregulation of the IFN response genes *Mx1* and *Oas3* was, however, detected between wild type and Hv1-deficient T cells (**figure 3.13**). This means that absence of Hv1 does not alter the ability of T cells to respond to the presence of IFNα by upregulation of IFN response genes. Hence, the expression of IFN response genes as measured above seems to be truly reflective of the concentration of type I IFN encountered by these cells.

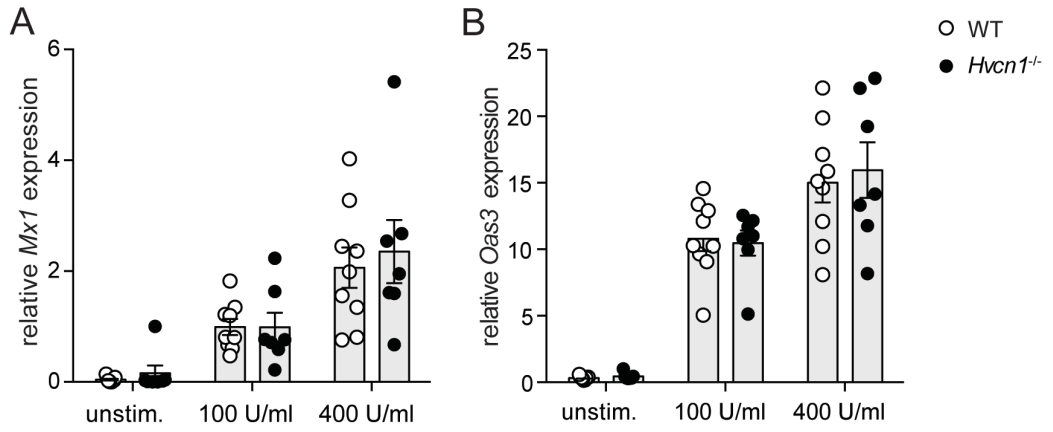

Figure 3.13 | The response of T cells to stimulation with IFNα is not altered in the absence of Hv1.
$CD3^+$ T cells were sorted from wild type and Hv1-deficient splenocytes and stimulated with 100 U/ml or 400 U/ml murine recombinant IFNα for 24 hours. Expression of the IFN response genes *Mx1* (**A**) and *Oas3* (**B**) was measured by RT-PCR. Results from two independent experiments are presented as mean ± SEM (n = 6 - 9). Statistical analysis was performed by two-way ANOVA with Bonferroni's *post hoc* test.

3.3.4 IL-10 secretion of B cells in pDC co-cultures

It has recently been published that IFN-secreting human pDCs *in vitro* promote the secretion of IL-10 by B cells[96]. A possible interaction between IFN-producing pDCs and IL-10 producing regulatory B cells is particularly interesting in the context of EAE and MS considering that the mechanisms by which type IFN limits autoimmunity in these pathologies are still unclear. In fact, IL-10 secretion by regulatory B cells has been shown to ameliorate disease in the early phases of EAE and its absence severely aggravates disease pathology[223]. Consequently, the hypothesis was tested whether the diminished ability of pDCs to secrete type I IFN *in vitro* would also translate into an impaired ability of pDCs to promote the secretion of IL-10 by B cells which could be an explanation for the increased disease severity in knockout animals. To this end, $CD19^+$ B cells were co-cultured with different concentrations of pDCs for 48 hours in the presence of CpG oligonucleotides type C which induce both IFNα secretion by pDCs as well as IL-10 secretion by B cells. The concentration of IL-10 in the supernatant was then measured by ELISA. Since B cells highly express Hv1 both wild type (**figure 3.14 C**) and Hv1-deficient (**figure 3.14 D**) B cells were stimulated in separate experiments to control for possible differences in the ability to secrete IL-10 between both genotypes.

The presence of IFN-secreting pDCs significantly enhanced IL-10 secretion by B cells when cultured at a ratio of pDCs to B cells of 1:3 (**figure 3.14 A**). At lower pDC concentrations the measured IL-10 concentrations in the supernatant were not significantly different from those of B cells stimulated in the absence of pDCs. When comparing wild type and knockout pDCs in their ability to promote IL-10 secretion, no statistically significant difference could be

detected at any B cell to pDC ratio analyzed (**figure 3.14 C and D**). This shows that Hv1-deficiency does not impair pDCs in their ability to promote IL-10 secretion by B cells. Furthermore, the IL-10 secretion by B cells from wild type and Hv1-deficient mice showed a non-significant trend towards less IL-10 secretion by B cells that lack Hv1 expression (**figure 3.14 B**) again giving a hint that B cells might require Hv1 for proper activation by CpG oligonucleotides and IL-10 secretion.

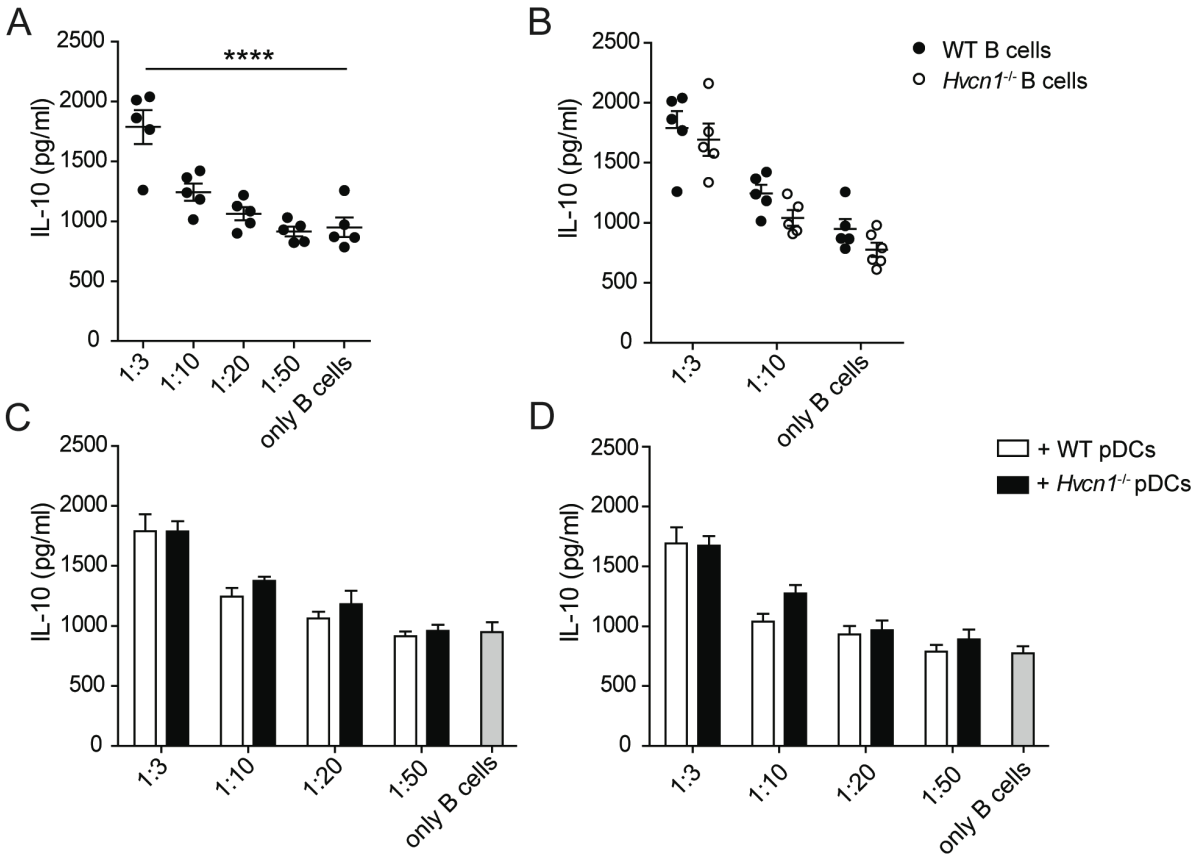

Figure 3.14 | IL-10 secretion by CD19$^+$ B cells is not different after stimulation with CpGC oligonucleotides in co-cultures with wild type or Hv1-deficient pDCs.
pDCs were sorted from Flt3L-cultures and CD19$^+$ B cells were sorted from splenocytes. B cells were seeded with different ratios of pDCs and stimulated with 10 µM CpG-C oligonucleotides for 48 hours. Supernatant was collected and the concentration of IL-10 was measured by ELISA. Data from different combinations of wild type and Hv1-deficient cells is depicted: wild type B cells and wild type pDCs (**A**), wild type or Hv1-deficient B cells and wild type pDCs (**B**), wild type B cells with wild type or Hv1-deficient pDCs (**C**) and Hv1-deficient B cells with wild type or Hv1-deficient pDCs (**D**). Data is pooled from two independent experiments (n = 5 - 6) and shown as mean ± SEM. Statistical analysis was performed by by two-way ANOVA with Bonferroni's *post hoc* test and significance is indicated as **** ($p \leq 0{,}0001$).

3.4 Immune phenotype of Hv1-deficient mice

3.4.1 Analysis of the size of spleens and LN in Hv1-deficient mice

It has been published that mice of the Hv1-deficient strain generated by Okochi and colleagues in 2009 exhibit an altered immune phenotype with splenomegaly and lupus-like pathology at the age of 6 months[190,211]. Of note, any alteration in the frequency or activation status of peripheral immune cells at the time of immunization could contribute to the exaggerated autoimmune disease observed in Hv1-deficient mice in EAE. However, the Hv1-deficient mouse strain used in this project was generated by another group[189] and it was thus tested whether it would also exhibit similar differences at the steady state. To this end, spleens and inguinal lymph nodes were prepared from healthy wild type and Hv1-dficient mice and the spleen size as well as the number and composition of $CD45^+$ immune cells obtained from these tissues was analyzed by flow cytometry.

Among female animals, spleens of Hv1-deficient mice were significantly larger compared to those of wild type mice, however, not only at 6 months, but already at 3 months of age (**figure 3.15 A and B**). Notably, the differences in spleen size measured at the age of 3 and 6 months did not reach significance among male mice. Since all mice used for functional experiments in this thesis including the EAE were between 8 and 12 weeks old, all additional data acquired with regard to the immune phenotype which is presented in this section was obtained from mice at the age of 10 to 12 weeks.

In line with the difference in size an increased number of $CD45^+$ cells in the spleen was observed in both female and male animals. On the other hand, there was no difference in the number of $CD45^+$ cells in inguinal lymph nodes (**figure 3.15 C**) or total cells without erythrocytes obtained from the bone marrow (**figure 3.15 D**) of wild type and Hv1-deficient mice.

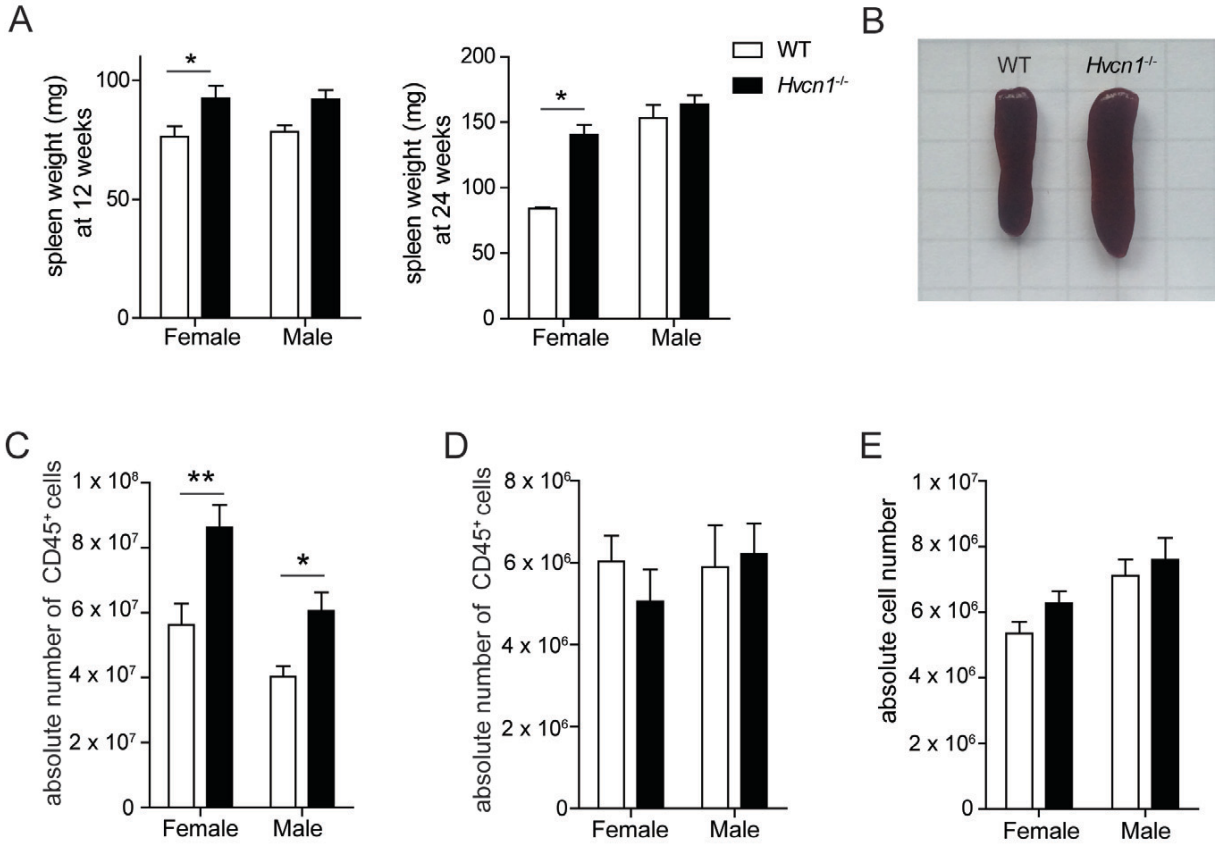

Figure 3.15 | Spleen size and splenic CD45$^+$ cell counts are increased in Hv1-deficient mice. (**A**) Weight of spleens prepared from wild type and Hv1-deficient mice at the age of 12 and 24 weeks (n = 9 – 14 for 12 weeks and n = 4 - 7 for 24 weeks) (**B**) Representative image of spleens prepared from a female wild type mouse and a female Hv1-deficient mouse at the age of 24 weeks. (**C**) Number of CD45$^+$ cells in spleen and inguinal lymph node of 10 to 12 week old healthy mice as measured by flow cytometry using TruCount Tubes (n = 15 for spleen and n = 10 for lymph nodes). (**D**) Total number of cells isolated from bone marrow after erylysis and counted in a Neubauer chamber (n = 13 - 16). Results are shown as mean ± SEM. Statistical analysis was performed by two-way ANOVA with Bonferroni's *post hoc* test and statistical significance is indicated by * ($p \leq 0,05$) and ** ($p \leq 0,01$).

3.4.2 Analysis of the frequency and activation state of different immune cell populations

The observed differences raised the question whether the increase in CD45$^+$ cells was driven by one subset of immune cells in particular or whether it was due to a more general expansion of several immune cell subpopulations. In addition, and despite equal total numbers of cells, the frequency of different immune populations was also looked at in lymph nodes. To this end, cells were isolated and stained for the identification of different immune cell populations by flow cytometry. Of note, there was a significant decrease in the frequency of CD4$^+$ and CD8$^+$ T cells in the inguinal lymph nodes of Hv-1 deficient mice (**figure 3.16 B**), but no significant difference in the spleen (**figure 3.16 A**). At the same time, surface expression of CD44 was increased on CD4$^+$ T cells isolated from lymph nodes of knockout mice indicating a generally higher activation status of these cells at the steady state and confirming published data.

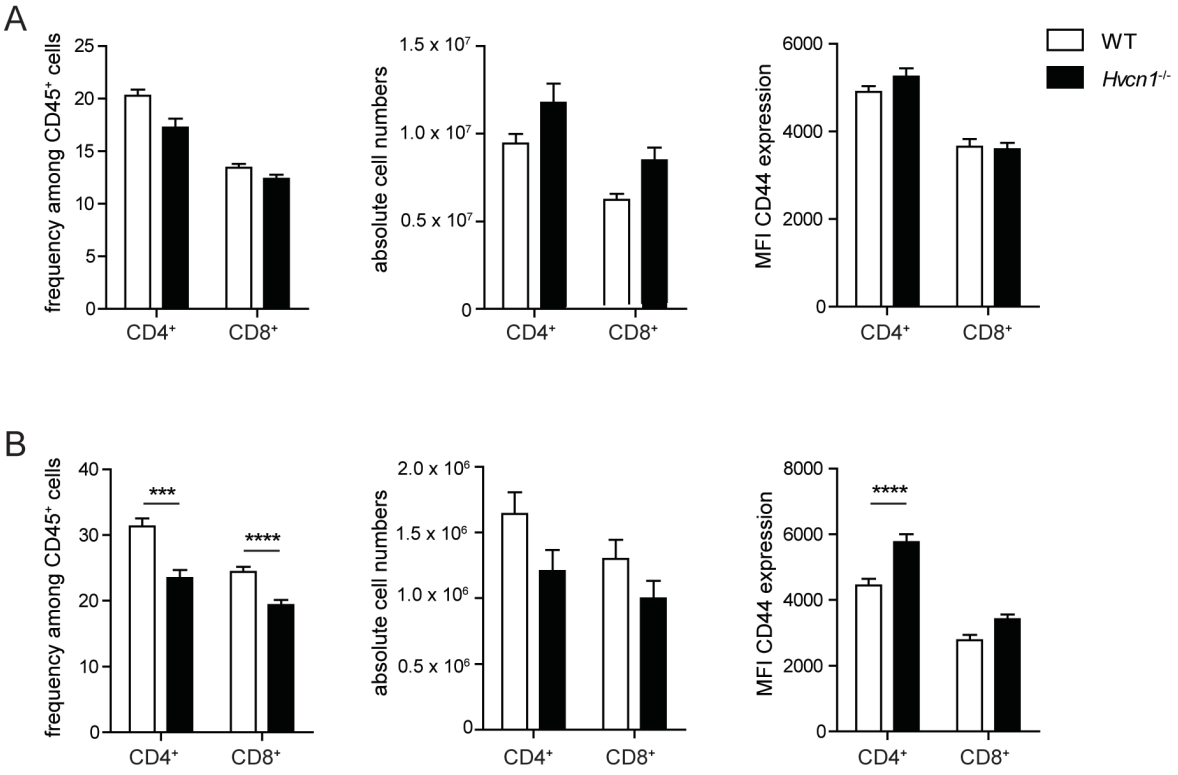

Figure 3.16 | The frequency of T cells is decreased in inguinal lymph nodes while activation of CD4$^+$ T cells is increased.
Cells were isolated from spleen (**A**) and inguinal lymph nodes (**B**) of healthy wild type and Hv1-deficient mice at the age of 10 to 12 weeks. The frequencies of CD4$^+$ and CD8$^+$ T cells were measured by flow cytometry and the total cell count for each population was calculated according to the total number of CD45$^+$ cells recorded in TruCount Tubes. The surface expression of CD44 on CD4$^+$ T cells and CD8$^+$ T cells was analyzed by flow cytometry and is shown as the MFI. Data from two independent experiments is shown as the mean ± SEM (n = 10). Statistical analysis was performed by two-way ANOVA with Bonferroni's *post hoc* test and statistical significance is indicated by *** ($p \leq 0{,}001$) and **** ($p \leq 0{,}0001$).

In contrast to what was observed for T cells, significantly higher frequencies of CD19$^+$ B cells were detected in both spleens and lymph nodes of Hv1-deficient mice (**figure 3.17**). In the murine spleen, different B cell subsets exist. These include transitional B cell, a population made up of B cells which only recently left the bone marrow. Transitional B cells are divided into three subpopulations, T1, T2 and T3, which have been proposed to represent three consecutive developmental stages[224]. Transitional B cells give rise to either marginal zone (MZ) B cells or follicular B cells. MZ B cells are sessile cells residing, as their name implies, in the marginal zone of the splenic white pulp and are mainly contributing to T cell-independent B cell responses[225]. Follicular B cells, on the contrary, are recirculating cells which mainly mediate T cell-dependent B cell responses[226]. Moreover, follicular B cells are further subdivided into type I and type II follicular B cells with respect to their expression of IgM. The differences between these two subsets are not entirely elucidated, but type II follicular B cells are thought to form a reservoir for MZ B cells[227].

In order to check for alterations among the frequency of individual splenic B cell subpopulations, more detailed flow cytometry was performed. Among all subsets analyzed, only follicular type I B cells were significantly increased in frequency in spleens of Hv1-deficient mice (**figure 3.17 A**). At the same time neither the frequencies of the $CD19^-$ transitional B cells nor of follicular type II B cells, marginal zone B cells or their direct precursors were different.

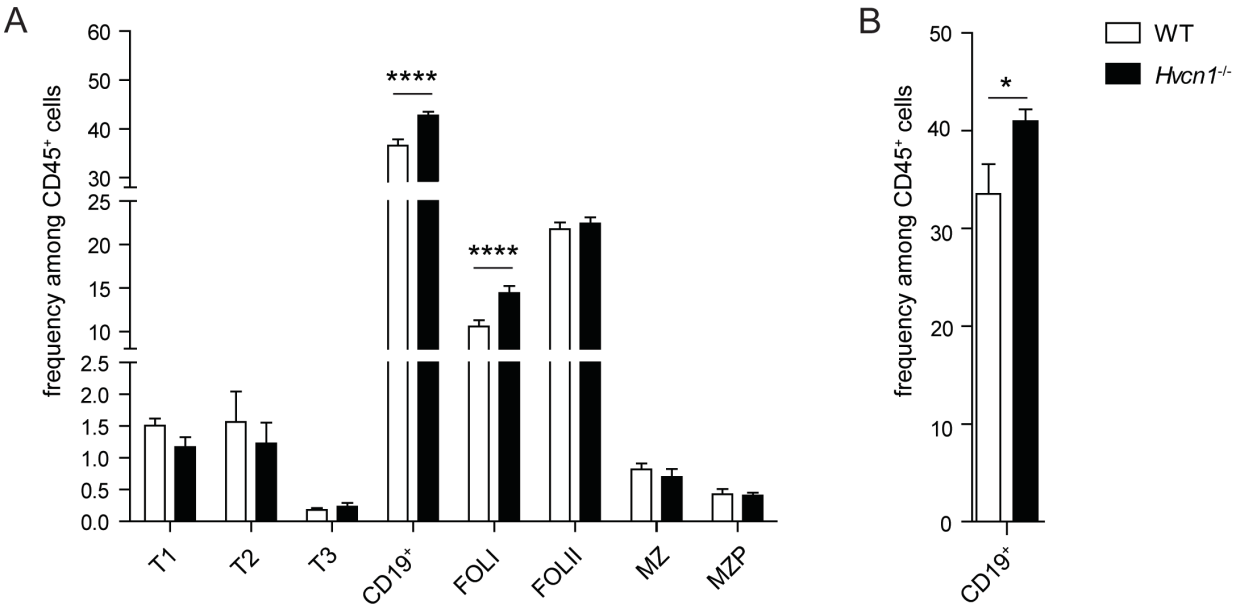

Figure 3.17 | The frequency of $CD19^+$ B cells is increased in the spleen and inguinal lymph nodes of Hv1-deficient mice.
Cells were isolated from spleen (**A**) and inguinal lymph nodes (**B**) of healthy wild type and Hv1-deficient mice at the age of 10 to 12 weeks and B cell frequencies were measured by flow cytometry. Data from two independent experiments is shown as mean ± SEM (n = 10). Statistical analysis was performed by two-way ANOVA with Bonferroni's *post hoc* test in **A** and by student's *t*-test in **B**. Statistical significance is indicated by * ($p \leq 0,05$) and **** ($p \leq 0,0001$).

In addition to T and B lymphocytes, also the frequency of several populations of innate immune cells was analyzed. However, no additional significant differences were recorded with regard to NK cells, granulocytes, macrophages or monocytes in spleen or inguinal lymph nodes (**figure 3.18**).

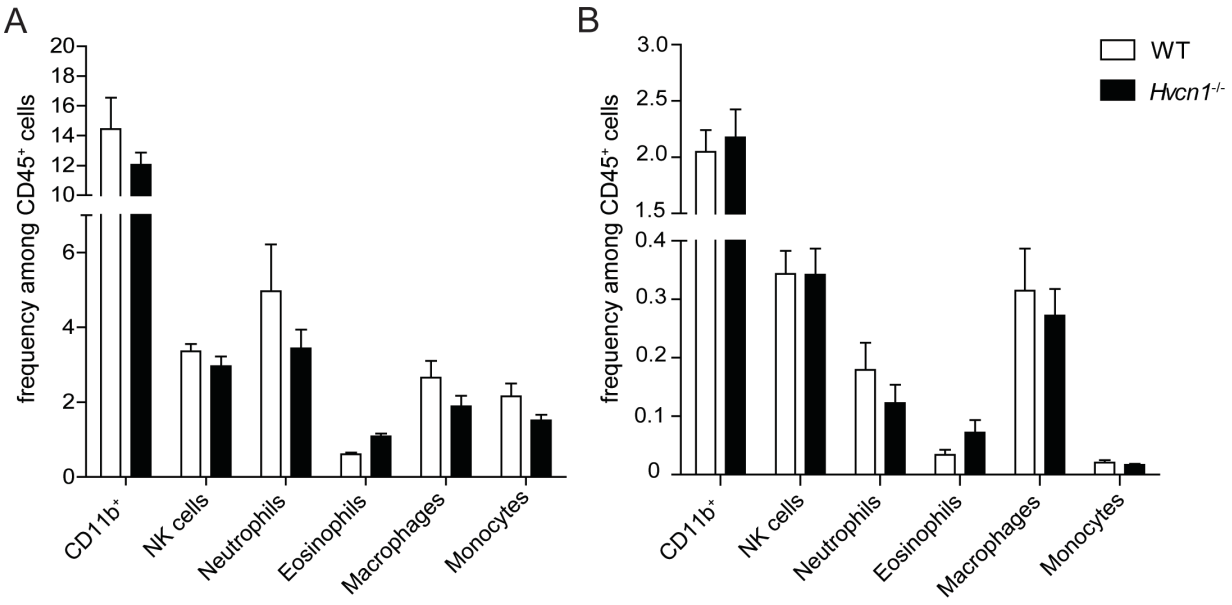

Figure 3.18 | The frequency of CD11b$^+$ cells and NK cells is not altered in spleen and inguinal lymph nodes of Hv1-deficient mice.
Cells were isolated from spleen (**A**) and inguinal lymph nodes (**B**) of healthy 10- to 12-week old wild type and Hv1-deficient mice and the frequencies of different CD11b$^+$ subpopulations and NK cells among CD45$^+$ cells were recorded by flow cytometry. Data from two independent experiments is shown as the mean ± SEM (n = 10) and statistical analysis using two-way ANOVA with Bonferroni's *post hoc* test was performed.

A detailed analysis of the frequency of different subpopulations of DCs, however, revealed further alterations in this compartment which is particularly interesting in the context of this thesis. First, the frequency of pDCs was nearly doubled in the samples of inguinal lymph nodes obtained from knockout animals. A significantly increased frequency was also observed for migratory DCs (mDCs) (**figure 3.19 B**). In the spleen, no difference was observed with regard to the frequency of pDCs, while the frequency of cDCs was decreased (**figure 3.19 A**). To test whether the increase of pDCs in the inguinal lymph nodes was paralleled by an altered activation status the surface expression of different activation markers was assessed by flow cytometry in the same samples. Interestingly, the expression of activation markers in pDCs was unchanged. On the other hand, CD86 expression was significantly decreased on classical dendritic cells in the spleen, but increased on migratory dendritic cells in the inguinal lymph nodes.

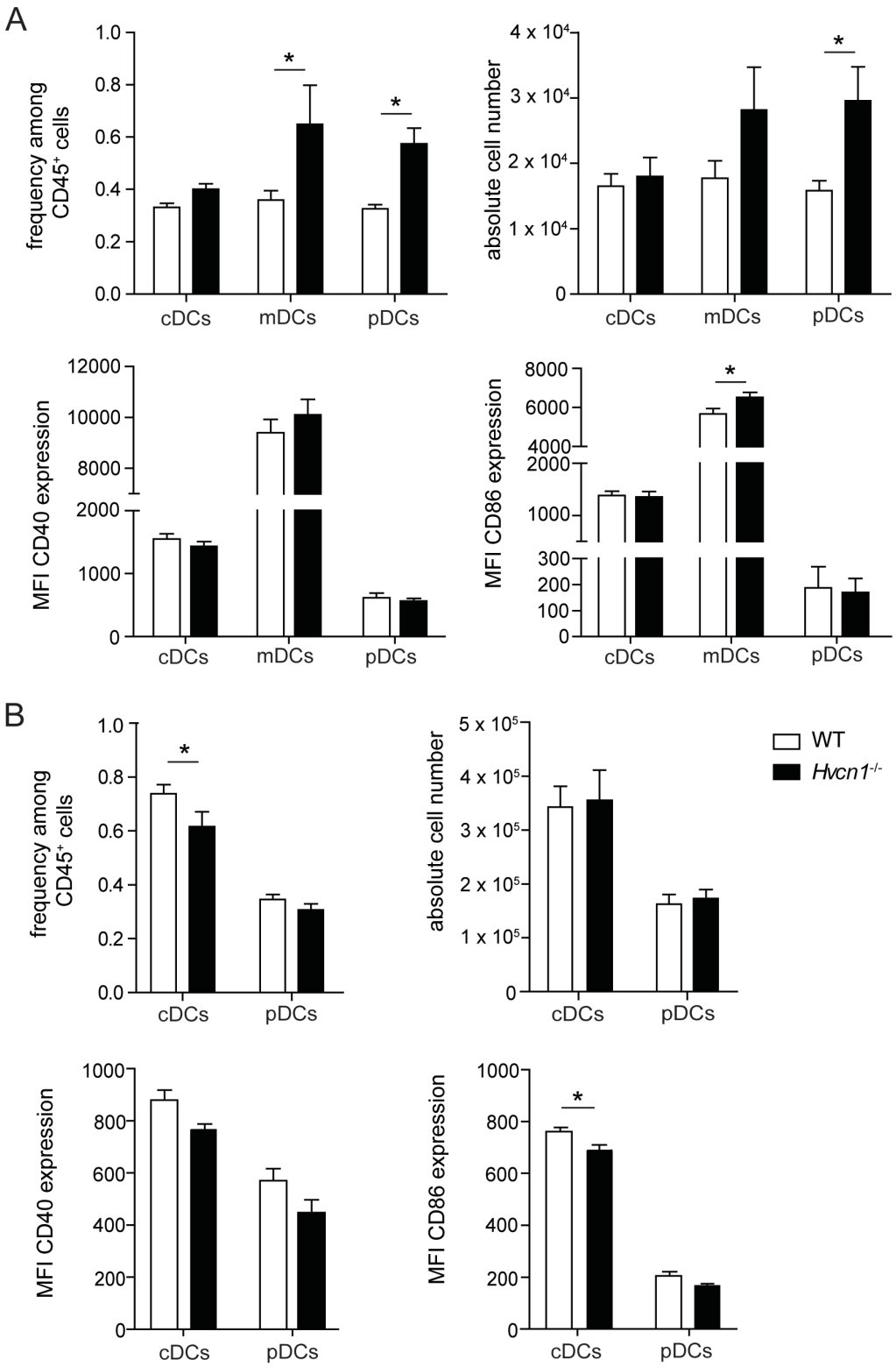

Figure 3.19 | The frequency and absolute number of pDCs is increased in inguinal lymph nodes of Hv1-deficient mice while their expression of costimulatory molecules is not altered.
Cells were isolated form inguinal lymph nodes (**A**) and spleen (**B**) of mice at the age of 10 to 12 weeks. The frequency of different DC subpopulations among $CD45^+$ cells as well as their expression of activation markers was recorded by flow cytometry and the absolute cell numbers were calculated according to the total number of $CD45^+$ cells. Results are from three independent experiments (n = 15) for frequency and count and one representative experiment out of two for CD40 and CD86 expression (n = 5). Statistical analysis using two-way ANOVA with Bonferroni's *post hoc* test was performed and statistical significance is indicated by * ($p \leq 0,05$).

In conclusion, Hv1-deficient mice have increased spleen sizes along with elevated numbers of $CD45^+$ cells, mostly mediated by a significant increase in follicular type I B cells. Although the overall number of $CD45^+$ cells that can be isolated from lymph nodes of Hv1-deficient mice is not different from that of wild type mice, the frequencies of different subsets are shifted. In this way, a significant increase in B cells but a reduced frequency of T cells is observed along with increased T cell activation. Of note, also the frequency of pDCs is strikingly elevated in the lymph nodes but not spleens of Hv1-deficient mice despite showing no change in the expression of costimulatory molecules. Therefore, the collected data demonstrates that the immune phenotype if Hv1-deficient mice is significantly altered at the steady state thereby confirming and extending published data.

4 Discussion

Plasmacytoid dendritic cells express *HVCN1/Hvcn1* and its expression is possibly regulated by the transcription factor E2-2

As a starting point for the presented project the expression of the voltage-gated proton channel Hv1 was assessed in several populations of immune cells. *HVCN1/Hvcn1* is expressed in all immune cells analyzed in this project and, consistent with published data, its expression is highest in B cells[207]. Moreover, the data also shows low expression of Hv1 in $CD4^+$ and $CD8^+$ T cells around the detection limit. Of note, Hv1 expression in T cells is still under debate[228]. On the one hand, proton currents in T lymphocytes as well as altered superoxide anion production in Hv1-deficient T cells could be recorded indicating that Hv1 is functionally expressed in these cells[211,229]. On the contrary, data on the detectability of Hv1 protein by western blot analysis is contradictory[207,211]. Here, *HVCN1/Hvcn1* expression was only assessed on the RNA level. Although it is an obvious prerequisite for the presence of Hv1 protein in T cells, it is also possible that the *HVCN1/Hvcn1* gene is only transcribed, but subsequent translation of the mRNA does not actually occur.

Most importantly, however, the analysis of Hv1 expression also shows intermediate levels of *HVCN1* mRNA in human pDCs as well as relatively high expression of *Hvcn1* in mouse pDCs when compared to other DC-subsets. Of note, no published data on Hv1 expression in pDCs or its function in this cell type exists to date. To verify Hv1 expression on the protein level, nevertheless, western blot analysis and immunocytochemical staining will need to be performed. The latter method is particularly interesting, since it will also provide data on where Hv1 localizes in pDCs. Considering its localization to the phagosomal membrane in other immune cells as well as the functional impairment of endosomal pH and signaling in its absence in pDCs as described in this thesis, it may be speculated that Hv1 in pDCs also localizes to intracellular compartments including endosomes as will be discussed in more detail below.

Evaluation of published data from ChIP-Seq analysis[212] shows that the master transcription factor of pDC development and function E2-2 binds to the *HVCN1* gene making it a likely regulator of the expression of Hv1 in pDCs. Lentiviral shRNA-encoding expression constructs were successfully cloned as part of the presented project to establish a system to prove whether knockdown of E2-2 *in vitro* indeed results in reduced expression of Hv1. Since lentiviral infection of GEN2.2 pDCs using these plasmids was efficient, the next step will be to assess how efficient the shRNAs, which have already been published to knockdown E2-2 with reasonable efficiency when encoded by another vector backbone[213], will reduce E2-2 on the mRNA and protein level in the system used here. Knockdown of E2-2 in pDCs will

inevitably cause these cells to lose their characteristic phenotype turning them into cDC-like cells over time. To exclude that a possible reduction in Hv1 expression by pDCs after E2-2 knockdown does not derive from a mere loss of the pDC-like phenotype and likely alterations in the expression of additional transcription factors it will be important to monitor Hv1 expression as early as possible after shRNA induction and in parallel control for the expression of other pDC characteristic genes. Therefore, in the vector system used here the shRNA expression is only induced after the addition of tetracycline allowing to carefully monitor E2-2 and Hv1 expression over time.

Expression of Hv1 in pDCs is required for proper endosomal acidification and activation after stimulation via TLR9

The expression of *Hvcn1/HVCN1* in pDCs raises the question what function Hv1 serves in this cell type. In phagocytes like neutrophils and macrophages it is well established that Hv1 localizes to the phagosomal membrane where it is needed for sustained NOX activity and phagosomal ROS production[189]. Phagocytosis is a specialized type of endocytosis characterized by the uptake of relatively large particles including cellular debris or whole pathogens[230]. Although pDCs are indeed capable of phagocytosis, it is not particularly relevant for their activation or effector functions. Instead, pDCs are mainly activated after uptake of pathogen-derived nucleic acids. Being small molecules, uptake of oligonucleotides is mediated by distinct endocytic processes, namely receptor-mediated endocytosis or, if present at high concentrations, pinocytosis[231,232]. Despite certain differences, these processes and their downstream events share similarities with phagocytosis and phagosome maturation.

Uptake of extracellular molecules by endocytosis is followed by fusion of early endocytic vesicles with early endosomes that localize to the peripheral cytoplasm. At this stage, cargo accumulates in the early endosomes while some proteins are recycling back to the plasma membrane via recycling endosomes. After a short period of time the endosome starts to mature, a process by which early endosomes convert into late endosome which in turn fuse with lysosomes in order to deliver their content for degradation[233]. A lot remains unknown about the different steps required for proper early to late endosome conversion, but it has been repeatedly shown that the exchange of the Ras-related protein Rab5 to Rab7 is one essential step in this process[234]. In addition, endosome maturation is accompanied by morphological changes, acquisition of hydrolases, but also changes in luminal ion concentrations and, most importantly, endosomal pH[233]. Indeed, while the luminal pH in early endosomes is only lightly acidified with values between 6.8 and 5.9, the pH in endosomes is estimated to be between 6.0 and 4.9[235]. A low endosomal pH is needed for sustained function of endosomal hydrolases, but also ensures membrane trafficking, particularly the

release of ligands inside the endosome, and possibly also an efficient detachment of late from early endosomes[233]. Acidification is mediated by an energy consuming proton pump, the V-ATPase. The regulation of endosomal pH is therefore mostly governed by the regulation of the local V-ATPase concentration, the presence of different isoforms and the efficiency of the coupling of ATP hydrolysis to proton transport[236] as well as, since the V-ATPase is formed by different complexes, its assembly and disassembly[237]. In addition, it has also been shown that V-ATPase activity is susceptible to redox modulation by the formation of disulfide bonds between cysteines in its active center[238–241].

CpG oligonucleotides are frequently used for the activation of pDCs and are detected by TLR9 in early and late endosomes depending on whether they form aggregates as is the case for oligonucleotides type A or remain monomeric as oligonucleotides type B, respectively[72]. Interestingly, stimulation of pDCs with CpG oligonucleotides type A, but not type B, enhances the expression of *Hvcn1* on the RNA level. In addition, also the upregulation of *Cybb* expression is only significant when CpG-A oligonucleotides rather than CpG-B oligonucleotides are used as the stimulating agent. This observation might not only add further evidence to a functional link between NOX2 and Hv1 in pDCs, but also implies that these proteins might especially be required in a situation in which pDCs need to ensure proper function and signaling from early endosomes while their presence is less important for the homeostasis of late endosomes.

In phagosomes, NOX activity has been hypothesized to indirectly affect acidification as observed in Hv1-deficient neutrophils and macrophages[193,242]. In the light of this observation, a possible involvement of Hv1 in the regulation of endosomal pH in pDCs was tested. Indeed, the endosomal pH recorded in pDCs in the absence of Hv1 expression was significantly higher than in wild type cells indicating that Hv1 expression is required to ensure normal acidification of the endosome. At the same time, the general ability of pDCs to endocytose oligonucleotides was not found to be altered in the absence of Hv1. In principle, Hv1 expression could affect endosomal pH both by direct or indirect mechanisms. Since protons entering phagosomes via Hv1 in other immune cells are assumed not to contribute to phagosomal acidification as they are rapidly consumed by ROS production, it is unlikely that Hv1-mediated proton flux is a principal direct mediator of endosomal acidification in pDCs. With respect to previous publications as already mentioned above it may, however, be speculated that the absence of Hv1 impairs endosomal NOX activity and that this either directly or secondary to reduced local ROS concentrations alters V-ATPase recruitment and function in the endosomal membrane.

The altered endosomal pH in Hv1-deficient pDCs suggested that endosomal TLR9-mediated activation might be impaired in these cells which was consequently tested *in vitro*. Strikingly, pDC activation as indicated by secretion of IFNα after stimulation with CpG-A as well as CpG-B induced secretion of IL-6 and TNFα and upregulation of CD40 were significantly reduced in the absence of Hv1. One possible explanation for this observation is an impairment of TLR9 cleavage due to insufficient acidification of the endosomal pH. As a safety mechanism to prevent unspecific signaling of potentially missorted TLRs from the cell surface, TLR9 needs to be cleaved in the endosome to become fully functional[243,244]. TLR9 cleavage occurs in two consecutive steps: First, parts of the TLR9 ectodomain are removed by either asparagine endopeptidase (AEP) or cathepsins. To become fully functional, TLR9 is afterwards trimmed at its N-terminus by cathepsins[245]. Full length TLR9 is able to bind its ligand although with lower affinity, but it is only the truncated C-terminal form that can initiate signaling[246]. AEP and cathepsins are only activated at the physiologically low endosomal pH and block of endosomal acidification by inhibiting V-ATPase causes accumulation of full length receptors in the endolysosomes[246]. It is therefore possible that the altered endosomal pH in the absence of Hv1 hinders TLR9 cleavage which would explain the reduced pDC activation observed after stimulation of TLR9 in Hv1-deficient pDCs. In this case, it should be possible to demonstrate the existence of uncleaved TLR9 by western blot analysis. Nevertheless, low endosomal pH has also been shown to strongly promote the release of various ligands from their receptors after receptor-mediated endocytosis. Although it has to date not been investigated whether this also applies to oligonucleotides and their only partly defined endocytic receptors this might be another possible explanation for the observed results. Accordingly, retention of CpG oligonucleotides bound to their receptors after receptor-mediated endocytosis could in principle prevent their binding to TLR9 in Hv1-deficient endosomes, resulting in reduced TLR9-signalling and pDC activation. Finally, it has also been published that binding of CpG oligonucleotides to TLR9 itself is pH-dependent and impaired in the absence of acidification[60].

In conclusion, the data collected in this part of the thesis strongly suggests an involvement of Hv1 in the regulation of endosomal pH and function in pDCs. To add final proof to this hypothesis it would be necessary to definitely localize Hv1 expression in pDCs to endosomes as already mentioned earlier. Although Hv1 expression was only upregulated after stimulation with CpG oligonucleotides type A targeting TLR9 in early endosomes, both the pH as well as the activation after TLR9 ligation were impaired from early and late endosomes of Hv1-deficient cells. It would thus be particularly interesting whether Hv1 preferentially localizes to one or the other endosomal compartment which could be achieved by costaining for markers of endosome maturation like Rab5 and Rab7. Apart from this, one might

consider stimulating an alternative endosome-independent activation pathway in wild type and Hv1-deficient pDCs which involves signaling via the cytoplasmic retinoic acid-inducible gene I (RIG-I). Physiologically, this pathway is initiated after viral infection of pDCs and it can thus be experimentally induced by administration of, for example, yellow fever live vaccine to pDC cultures[247]. If Hv1 deficiency was only to impair endosomal function, pDC activation of Hv1-deficient cells should not be affected in this experimental setup.

Of note, similar to pDCs, CpG-C oligonucleotides also activate B cells by binding to endosomal TLR9[219,220]. It was hence tested whether absence of Hv1 does not only impair TLR9-mediated activation of pDCs, but also of B cells, thus being a more general phenomenon affecting different immune subsets. Therefore, $CD19^+$ B cells were stimulated with CpG-C oligonucleotides and, in parallel, LPS which induces IL-10 secretion after binding to TLR4 on the plasma membrane[221,222]. Of note, IL-10 production was significantly diminished after stimulation with CpG oligonucleotides and in a tendency also after stimulation with LPS. First of all, this suggests that endosomal signaling via TLR9 could also be impaired in B cells, illustrating that Hv1 might have a more general role in endosomal function also in cells other than pDCs. Nevertheless, the tendency towards decreased IL-10 production after LPS stimulation might also imply a more generalized deficiency of Hv1-deficient B cells for IL-10 production irrespective of the pathway by which it is induced. Importantly, not all B cells are equally capable of secreting IL-10, a function that is rather confined to certain subpopulations of regulatory B cells like $CD1d^{hi}$ $CD5^+$ B10 cells[221]. As the frequency of different B cell subsets was found to be altered in Hv1-deficient mice at the steady state, as discussed further on, it is possible that the frequency of regulatory B cells including B10 cells among all $CD19^+$ cells is lower in Hv1-deficient than in wild type mice. Since bulk $CD19^+$ B cells that comprise many different B cell subsets were used in this experiment, a reduced frequency of B10 cells among $CD19^+$ B cells in Hv1-deficient mice could also be contributing to the observed results.

EAE is exacerbated in Hv1-deficient mice.

Dysregulation of pDCs is a common feature of different autoimmune diseases. Similar to basically all other populations of immune cells, pDCs have in general been shown to be able to promote inflammation, but on the other hand also to contribute to anti-inflammatory processes depending on the circumstances of their activation[33]. Consistently, activation of pDCs in the context of autoimmunity is thought to promote disease progression in some conditions, but limit disease in others[248]. In the context of MS and its mouse model EAE, activation of pDCs and type I IFN secretion are assumed to be beneficial. Notably, administration of type I IFN is a common treatment for patients with MS and its efficiency has been repeatedly proven in clinical trials[133,139]. Furthermore, IFN secretion as well as antigen-

presentation by pDCs in EAE have both been shown to lower disease severity[145,149]. The precise mechanisms underlying these observations are, however, only insufficiently understood.

On the background of the observed reduced activation of Hv1-deficient pDCs in *in vitro* experiments, the disease susceptibility of Hv1-deficient mice during EAE was assessed. In fact, Hv1-knockout mice have a significantly exacerbated course of EAE with higher disease scores and increased weight loss. No difference was, however, observed in the onset of symptoms. To test whether the increased disease severity in Hv1-deficient mice was paralleled by an altered infiltration of immune cells, the number and frequency of CNS infiltrating cells was analyzed during acute and chronic disease by FACS analysis. In acute EAE, initial results show that the number of CNS-infiltrating cells had a tendency to be higher in Hv1-deficient animals even if disease severity was similar to wild type controls. This indicates that in Hv1-deficient animals there is a generally increased recruitment of peripheral immune cells to the CNS. Importantly, increased CNS infiltration of immune cells during EAE does not always reflect the actual disease severity, but may also forecast an upcoming disease exacerbation. Hence, although wild type and Hv1-deficient mice that were chosen for this experiment were assigned with a similar range of disease scores at the day of the experiment, the increased CNS infiltration observed in Hv1-deficient mice could already indicate more pronounced disease with ongoing EAE. Having a closer look at individual immune cell populations, $CD4^+$ T cells and myeloid cells were found at significantly higher numbers in the CNS of Hv1-deficient mice. The latter population was not further subdivided into distinct subsets, but comprises macrophages and DCs including pDCs. The significantly increased number of $CD4^+$ T cells could be a likely explanation for increased disease activity in knockout mice since these cells are particularly known to drive pathology in EAE. The frequencies or counts of infiltrating B cells, on the contrary, which were altered in the periphery of healthy Hv1-deficient mice, were not significantly changed among CNS-infiltrating cells. In chronic EAE, the number of CNS-infiltrating cells in Hv1-deficient mice was not different compared to wild type animals nor could any difference in the frequency of particular immune cell populations be observed. In fact, EAE pathology becomes less immune cell dependent with ongoing disease so that symptoms in chronic EAE already largely derive from ongoing neurodegeneration which might be a possible explanation for this observation.

In conclusion, EAE is indeed aggravated in Hv1-deficient mice compared to wild type mice and associated with a trend towards increased immune cell infiltration during its acute phase. When interpreting this result, it needs to be kept in mind that the mouse model used here is a complete knockout so that Hv1 expression is absent in all immune cells. Being a complex

disease model it is therefore difficult to dissect how individual immune cell populations including pDCs contribute to the observed increased EAE severity. To test, however, whether decreased secretion of IFNα, which would be in accordance with the obtained *in vitro* data, was at least a possible contributor to the observed increased severity of EAE in Hv1-deficient mice, the expression of different IFN response genes was measured in CNS-infiltrating T cells at the end of EAE. Cells respond to the presence of type I IFN by upregulation of IFN response genes and the method used here therefore provides an indirect but frequently used readout of IFNα concentrations. However, no difference with regard to the expression of IFN response genes could be detected by RT-PCR meaning that the level of type I IFN encountered by T cells from wild type and Hv1-deficient mice was similar. Importantly, additional experiments showed that Hv1-deficient T cells are equally responsive to stimulation with IFNα as demonstrated by similar upregulation of IFN response genes compared to wild type controls after stimulation with recombinant IFNα *in vitro*. It can thus be ruled out that the ability of Hv1-deficient cells to respond to type I IFN is *per se* altered which might have confounded the result of this experiment.

The time course of the IFN response during EAE is currently unclear and it is therefore possible that the ameliorating effect of IFNα is largest at early time points of disease, but becoming less important when inflammation ceases during later stages of EAE. This would be one possible explanation for why no differences in the IFN response could be detected in the setting chosen here which otherwise argues against a dysregulated IFN response by pDCs in Hv1-deficient mice in this disease model. It would thus be desirable to assess in future experiments at which time point in EAE the secretion of IFN is actually initiated and for how long it is maintained. Moreover, it has been reported that apart from type I IFN secretion, antigen-presentation by pDCs may serve an anti-inflammatory function in EAE[149]. Hence, it would also be interesting to test whether antigen presentation by pDCs is altered in the absence of Hv1 during EAE. Again, however, the circumstances in which pDCs present antigen in this disease model are not resolved. In order to understand how and whether Hv1-deficiency in pDCs contributes to increased EAE pathology, one would thus need to establish the time course of pDC activation and their different effector functions in more detail before comparing it to that of Hv1-deficient mice at selected, relevant time points. This would certainly require the analysis of pDCs isolated from a large cohort of mice at several different time points, starting just one or two days after immunization and further including samples just before and at the onset of symptoms, in acute disease as well as in early and late chronic EAE.

As mentioned above, the downstream mechanisms underlying the ameliorating effect of type I IFN in MS and EAE are not completely understood. In this context it is interesting to

consider a recent publication by Menon and colleagues which shows that IFNα secretion by pDCs enhances secretion of the anti-inflammatory cytokine IL-10 by CpG-stimulated B cells in co-cultures of cells isolated from healthy human donors[96]. Considering that IL-10 secretion by regulatory B cells is known to limit self-directed immune activation in EAE, in particular during the early phases of disease[249,250], this could be one additional mechanism by which type I IFN could exert its beneficial effect during MS and EAE. Since IFN secretion is impaired in Hv1-deficient pDCs, experiments were performed using murine pDCs and BCs that were co-cultured at different ratios and stimulated with CpG oligonucleotides type C. First of all, the data shows significantly enhanced IL-10 secretion by mouse B cells when these are co-cultured with mouse pDCs thereby confirming the published human data in a murine model. IL-10 secretion was, however, only different in the presence of pDCs with the highest pDC to B cell ratio used. Notably, no differences could be observed when comparing the effect of wild type and Hv1-deficient pDCs. It thus appears that absence of Hv1 expression does not impair these cells in their ability to promote IL-10 secretion by B cells. Although secretion of type I IFN was shown to be the most important factor acting on IL-10-producing B cells, the authors did not exclude the existence of additional mechanisms contributing to the observed interaction. It is thus possible that additional effector mechanisms in Hv1-deficient pDCs might compensate for a putative reduced IFN secretion by these cells in the chosen experimental setup.

Altogether, one conclusion that can, nevertheless, be drawn from the observed disease aggravation in EAE in Hv1-deficient mice irrespective of the underlying mechanisms or cell types involved, is that Hv1 expression in general is important for the maintenance of immune homeostasis and tolerance against self. This supports several other yet incompletely understood findings which implicate Hv1 and the functionally related NOX complex in autoimmunity: Apart from the putative presence of a lupus-like phenotype in Hv1-deficient mice as discussed in more detail below, chronic granulomatous disease (CGD), an immunodeficiency caused by mutations in the genes encoding NOX subunits[251], has paradoxically been associated with increased incidence of autoimmunity[252]. In the majority of cases, CGD is caused by mutations in the X-chromosomal *CYBB* gene which in humans encodes the gp91phox subunit of NOX[251,253] and patients commonly present with recurrent severe infections and granuloma formation[254,255]. Nevertheless, increased incidence of autoimmune pathology including lupus-like symptoms or inflammatory bowel disease has been observed among CGD patients and female heterozygous carriers of the mutation[252]. Providing yet another example, microarray data recently identified a correlation of Hv1 with disease activity in patients with Crohn's disease[256]. No underlying mechanism or the involvement of a particular immune cell populations have been identified to date to account

for any of these observations, but at least on the background of the *in vitro* data presented here one might consider also to investigate the role of pDCs in these contexts.

The immune phenotype of Hv1-deficient mice is altered at the steady state.

It has recently been published that increased immune cell numbers and activation along with lupus-like pathology have been observed in Hv1-deficient mice from a certain age on[228], an observation for which, however, no underlying mechanisms have been described nor has it been confirmed by others since. Still and particularly in the context of this thesis, it is interesting to consider that Hv1-deficiency might already by itself induce autoimmunity in otherwise healthy mice. In addition, any difference in immune cell frequencies or activation might predispose Hv1-deficient mice to develop aggravated disease in induced models of autoimmunity and could thus provide an explanation for the increased symptoms observed in knockout animals during EAE. Among all immune populations analyzed, it was also looked for possible differences with regard to pDC frequencies and expression of costimulatory molecules which is of particular interest in the context of this thesis.

Indeed, Hv1-deficient mice had increased spleen sizes as well as higher numbers of $CD45^+$ immune cells in spleen, but not in inguinal lymph nodes. This effect was more pronounced in female compared to male mice which is in accordance with published data and a generally higher tendency for the development of autoimmunity among female compared to male mice in different disease models. In addition, increased spleen sizes were already observed among mice at the age of 12 weeks which is around the age at which animals were used for functional experiments. According to the data published by Sasaki and colleagues, significant differences in spleen weight were only observed at the age of 6 months. Of note, the Hv1-deficient mouse model used in this project which was established by a different working group albeit using the same method[189]. This disparity may thus be a consequence of differences in the Hv1-deficient mouse line used, but could also result from probable differences in animal housing conditions. In general, splenomegaly can occur in the context of immune system activation, for example, during infection and neoplastic disease, and is sometimes also observed during different autoimmune conditions, including SLE[257].

Along with the overall increased number of immune cells in spleens of Hv1-deficient mice, the frequency of follicular type I B cells was found to be significantly increased in the spleen of these animals. Already being present in the spleen at generally high frequencies, it is reasonable to assume that the increase in follicular type I B cells thereby essentially contributed to the overall increase in $CD45^+$ splenocytes. No further changes in frequency were observed with regard to all other splenic immune cells apart from cDCs which were only found in decreased frequencies. Similar to what was observed in the spleen, an increase in

the frequency of $CD19^+$ B cells, but also a significantly decreased frequency of $CD4^+$ and $CD8^+$ T cells was observed in the inguinal lymph nodes of Hv1-deficient mice. Since the total number of $CD45^+$ cells in the inguinal lymph nodes was similar between wild type and knockout animals this can be assumed to translate into higher absolute numbers of B cells. Interestingly, CD44 expression was higher among $CD4^+$ T cells indicating increased activation of these cells. Particularly interesting in the context of this thesis, the frequency of pDCs was nearly doubled in the inguinal lymph nodes. Moreover, not only the frequency, but also the expression of the costimulatory molecule CD86 was elevated among migratory DCs in lymph nodes of Hv1-deficient mice. This reflects increased activation and antigen presentation by these cells and could therefore provide a causative link to the increased activation of $CD4^+$ T cells in Hv1-deficient animals.

When attempting to explain the observed differences one needs to consider that crosstalk between different innate and adaptive immune subsets within the immune system does not only influence immune cell activation, but also regulates the development, survival and proliferation of different immune cells at the steady state. Since the mouse model used in this project is a global knockout and Hv1-deficiency in nearly all immune cells is associated with their functional impairment, every attempt to explain how a general Hv1-deficiency might account for the observed differences in immune cell frequencies at a mechanistic level requires proof from more specific Hv1-deficient mouse models. Still, a possible B cell intrinsic explanation for the increased follicular B cell frequencies shall be mentioned. It is known that B cell receptor signaling regulates the differentiation of B cells, also with regard to the differentiation of distinct B cell subsets. Considering the established impairment of BCR signaling in Hv1-deficient mice, it appears possible that the increased frequency of follicular B cells observed in Hv1-deficiency might thus be a consequence of reduced BCR signaling. Results published in this context are, however, contradictory, with publications showing decreased BCR signaling to contribute to either higher or lower frequencies of follicular B cells in different models[258,259]. It is in addition interesting to note that according to openly accessible data provided by the Immunological Genome Project Immgen[260], Hv1 expression in follicular B cells is highest among all B cell subpopulations.

In the light of the defective activation of pDCs shown in *in vitro* experiments, the hugely increased frequency of pDCs in inguinal lymph nodes could be the result of a compensatory expansion of these cells. Since pDC frequencies are not increased in the spleen it is, however, unlikely that the increase in pDCs in the lymph nodes is due to an increased development of these cells in the bone marrow. Altered recruitment to the lymph nodes might, however, provide a possible explanation. In this regard it would be interesting to study the expression of CCR7, a chemokine receptor mediating homing of pDCs to the lymph

nodes[261], in Hv1-deficient pDCs. In any case, if considered as being mainly driven by pDC intrinsic mechanisms rather than from interaction with other cells, the altered frequency of pDCs may offer yet another hint towards a strong functional implementation of Hv1 in this cell type. Notably, the expression of costimulatory molecules is not altered in pDCs from spleen and LN in the steady state. Considering the reduced capacity of Hv1-deficient pDCs for activation *in vitro*, an increased expression of costimulatory molecules in Hv1-deficient mice at the steady state would, however, also have been unexpected.

Irrespective of any causative mechanisms, the question emerges whether the observed differences may predispose to a loss of tolerance against self or even indicate ongoing autoimmune pathology. Although the development of lupus-like pathology in Hv1-deficient mice was not investigated in more detail in this project, some key findings published by Sasaki and colleagues, that is increased spleen size and T cell activation, could also be reproduced here. Notably, T cell activation, as indicated by the increased expression levels of CD44 on T cells along with the increased frequency and CD86 expression of migratory DCs in inguinal lymph nodes of Hv1-deficient mice points towards an increased activation of the immune system which is unusual at the steady state and could be part of an autoimmune response. Still, it is unclear what causes the increased T cell activation in this mouse model as well as whether ongoing inflammation in any tissue can be detected. Considering, on the contrary, that most immune cells are functionally impaired in the absence of Hv1 expression, it is difficult to judge how, particularly in the case of follicular B cells and pDCs, an immune cell population that is less able to elucidate proper effector functions, but is increased in number, will affect the development of immune responses.

Concluding remark

Data presented in this thesis evidences the expression of the voltage-gated proton channel Hv1 in pDCs and it was one main aim of the project to analyze the function of this ion channel in this cell type. *In vitro* data strongly suggests a role for Hv1 in endosomal function and signaling since its absence does not only alter endosomal pH, but also impair pDC activation after stimulation via endosomal TLR9. In addition, Hv1-deficiency results in aggravated EAE, the mouse model of MS, and is associated with an altered immune phenotype at the steady state. These findings underline the importance of the proton channel in the control of immune homeostasis and immune responses. Although the precise contribution of pDCs to these observations could not be clarified, data collected in this thesis suggests that these cells are an interesting candidate population for future experiments.

Summary

Dysregulation of plasmacytoid dendritic cells (pDC) has been implicated in the pathogenesis of different autoimmune diseases including multiple sclerosis. The main effector function of pDCs is the secretion of type I interferon (IFN) which essentially contributes to the defense against viral infection. Alternatively, pDCs may also acquire a different activation state which is characterized by the secretion of distinct proinflammatory cytokines and the presentation of antigen. In both cases activation requires the recognition of CpG oligonucleotides by endosomal TLR9, while the nature of pDC activation, that is type I IFN secretion or antigen-presentation, depends on whether TLR9 binds its ligand in early or late endosomes, respectively. Precise regulation of endosomal function is consequently required to ensure sufficient pDC activation during the defense against pathogens, but at the same time prevent inappropriate pDC activation to maintain immune homeostasis at the steady state.

Data presented in this thesis shows for the first time that pDCs express the voltage-gated proton channel Hv1 which is known to be involved in phagosomal function in other immune cells. Of note, stimulation of pDCs via TLR9 in early, but not late endosomes enhances expression of Hv1. In addition, endosomal acidification is impaired in pDCs of Hv1-deficient mice and this is accompanied by reduced secretion of IFNα as well as decreased upregulation of the costimulatory molecule CD40 and secretion of proinflammatory cytokines after stimulation of TLR9 in early and late endosomes, respectively. These findings strongly suggest that Hv1 is essential for normal endosomal function and signaling in this cell type.
Moreover, Hv1-deficient mice show an exacerbated disease course of experimental autoimmune encephalomyelitis (EAE), the mouse model of multiple sclerosis, which might be attributed to an impaired type I interferon response *in vivo*. Providing an additional possible explanation for the aggravated disease severity, the immune phenotype of Hv1-deficient mice is altered at the steady state and characterized by increased T cell activation, an altered B cell compartment and highly elevated frequencies of pDCs in lymph nodes. These results further underline the importance of Hv1 proton channels in the control of immune homeostasis and activation and establish pDCs as a promising candidate population for future research.

Zusammenfasssung

Eine Fehlregulation der Aktivierung und Effektorfunktionen plasmazytoider dendritischen Zellen (PDZ) wurde wiederholt mit der Pathogenese verschiedener Autoimmunerkrankungen wie der Multiplen Sklerose in Verbindung gebracht. Die wichtigste Effektorfunktion von PDZs ist die Sekretion von Typ I Interferonen (IFN), welche wesentlich zur Abwehr viraler Infektionen beiträgt. PDZ können jedoch auch einen alternativen Aktivierungsstatus annehmen, der durch die Sekretion anderer proinflammatorischer Zytokine and Antigenpräsentation gekennzeichnet ist. Die Aktivierung folgt in beiden Fällen auf das Erkennen von CpG-Oligonukleotiden durch TLR9 in Endosomen, wobei die Art der PDZ-Aktivierung, also Sekretion von Typ I IFN oder Antigenpräsentation, davon abhängt, ob TLR9 seinen Liganden in frühen oder späten Endosomen bindet. Eine präzise Regulation der endosomalen Funktion ist daher notwendig, um eine ausreichende Aktivierung von PDZ während der Bekämpfung von Pathogenen zu gewährleisten, aber gleichzeitig eine unerwünschte Aktivierung von PDZ zu verhindern und so zur Aufrechterhaltung der Immunhomöostase beizutragen.

Die in dieser Arbeit präsentierten Daten zeigen zum ersten Mal, dass PDZ den spannungsabhängigen Protonenkanal Hv1 exprimieren, von dem bekannt ist, dass er in anderen Immunzellen für die normale Funktion von Phagosomen benötigt wird. Stimulation von PDZ über TLR9 in frühen, aber nicht in späten Endosomen, erhöht dabei die Expression von Hv1. Darüber hinaus ist die Ansäuerung von Endosomen in PDZ in der Abwesenheit von Hv1 verringert, begleitet von einer verminderten Sekretion von IFNα sowie einer geringeren Expression des kostimulatorischen Moleküls CD40 und der Sekretion proinflammatorischer Zytokine nach TLR9-Stimulation in frühen beziehungsweise späten Endosomen. Diese Ergebnisse weisen stark darauf hin, dass Hv1 in PDZ für eine normale endosomale Funktion und Signalweiterleitung benötigt werden.

Ferner haben Hv1-defiziente Mäuse einen verstärkten Krankheitsverlauf während der experimentellen autoimmunen Enzephalomyelitis (EAE), dem Mausmodell der Multiplen Sklerose, was durch eine eingeschränkte Sekretion von Typ I IFN *in vivo* vermittelt sein könnte. Als eine weitere mögliche Erklärung zeigen Hv1-defiziente Mäuse einen veränderten Immunphänotyp, der durch verstärkte Aktivierung von T-Zellen, einer veränderten B-Zellfrequenz sowie einer erhöhten Frequenz von PDZ in Lymphknoten charakterisiert ist. Diese Daten unterstreichen weiter die Bedeutung von Hv1 Protonenkanälen für die Kontrolle von Immunhomöostase und -aktivierung und etablieren PDZ in diesem Zusammenhang als eine vielversprechende Immunzellpopulation für zukünftige Experimente.

Literature

1. Charcot JM. Histologie de la sclérose en plaques. *Gaz. des Hop.* **41,** 554–555 (1868).
2. Noseworthy, J. H., Lucchinetti, C., Rodriguez, M. & Weinshenker, B. G. Multiple sclerosis. *N. Engl. J. Med.* **343,** 938–52 (2000).
3. Federation, M. S. I. *Atlas of MS 2013*. (2013).
4. Dendrou, C. A., Fugger, L. & Friese, M. A. Immunopathology of multiple sclerosis. *Nat. Rev. Immunol.* **15,** 545–558 (2015).
5. Munger, K. *et al.* Vitamin D intake and incidence of multiple sclerosis.
6. Handel, A. E. *et al.* An updated meta-analysis of risk of multiple sclerosis following infectious mononucleosis. *PLoS One* **5,** 1–5 (2010).
7. Almohmeed, Y. H., Avenell, A., Aucott, L. & Vickers, M. A. Systematic Review and Meta-Analysis of the Sero-Epidemiological Association between Epstein Barr Virus and Multiple Sclerosis. *PLoS One* **8,** (2013).
8. Moutsianas, L. *et al.* Class II HLA interactions modulate genetic risk for multiple sclerosis. *Nat. Genet.* **47,** 1107–13 (2015).
9. International Multiple Sclerosis Genetics Consortium *et al.* Genetic risk and a primary role for cell-mediated immune mechanisms in multiple sclerosis. *Nature* **476,** 214–9 (2011).
10. Boyman, O. & Sprent, J. The role of interleukin-2 during homeostasis and activation of the immune system. *Nat. Rev. Immunol.* **12,** 180 (2012).
11. Gregory, S. G. *et al.* Interleukin 7 receptor alpha chain (IL7R) shows allelic and functional association with multiple sclerosis. *Nat. Genet.* **39,** 1083–91 (2007).
12. Baxter, A. G. The origin and application of experimental autoimmune encephalomyelitis. *Nat. Rev. Immunol.* **7,** 904–12 (2007).
13. Münz, C., Lünemann, J. D., Getts, M. T. & Miller, S. D. Antiviral immune responses: triggers of or triggered by autoimmunity? *Nat. Rev. Immunol.* **9,** 246–58 (2009).
14. Olson, J. K., Ercolini, a M. & Miller, S. D. A virus-induced molecular mimicry model of multiple sclerosis. *Curr. Top. Microbiol. Immunol.* **296,** 39–53 (2005).
15. Hellings, N. *et al.* T-cell reactivity to multiple myelin antigens in multiple sclerosis patients and healthy controls. *J. Neurosci. Res.* **63,** 290–302 (2001).
16. Goverman, J. Autoimmune T cell responses in the central nervous system. *Nat. Rev. Immunol.* **9,** 393–407 (2009).
17. Yamasaki, R. *et al.* Differential roles of microglia and monocytes in the inflamed central nervous system. *J. Exp. Med.* **211,** 1533–49 (2014).
18. Schattling, B., Eggert, B. & Friese, M. A. Acquired channelopathies as contributors to development and progression of multiple sclerosis. *Exp. Neurol.* **262,** 28–36 (2014).

19. Friese, M. A., Schattling, B. & Fugger, L. Mechanisms of neurodegeneration and axonal dysfunction in multiple sclerosis. *Nat. Rev. Neurol.* **10,** 225–238 (2014).
20. Fletcher, J. M., Lalor, S. J., Sweeney, C. M., Tubridy, N. & Mills, K. H. G. T cells in multiple sclerosis and experimental autoimmune encephalomyelitis. *Clin. Exp. Immunol.* **162,** 1–11 (2010).
21. Booss, J., Esiri, M. M., Tourtellotte, W. W. & Mason, D. Y. Immunohistological analysis of T lymphocyte subsets in the central nervous system in chronic progressive multiple sclerosis. *J. Neurol. Sci.* **62,** 219–32 (1983).
22. Kuhlmann, T., Lingfeld, G., Bitsch, A., Schuchardt, J. & Brück, W. Acute axonal damage in multiple sclerosis is most extensive in early disease stages and decreases over time. *Brain* **125,** 2202–12 (2002).
23. Korn, T. *et al.* Myelin-specific regulatory T cells accumulate in the CNS but fail to control autoimmune inflammation. *Nat. Med.* **13,** 423–431 (2007).
24. Stern, J. N. H. *et al.* B cells populating the multiple sclerosis brain mature in the draining cervical lymph nodes. *Sci. Transl. Med.* **6,** 248ra107 (2014).
25. Link, H. & Huang, Y.-M. Oligoclonal bands in multiple sclerosis cerebrospinal fluid: An update on methodology and clinical usefulness. *J. Neuroimmunol.* **180,** 17–28 (2006).
26. Piddlesden, S. J., Lassmann, H., Zimprich, F., Morgan, B. P. & Linington, C. The demyelinating potential of antibodies to myelin oligodendrocyte glycoprotein is related to their ability to fix complement. *Am. J. Pathol.* **143,** 555–64 (1993).
27. Pashenkov, M. *et al.* Two subsets of dendritic cells are present in human cerebrospinal fluid. *Brain* **124,** 480–92 (2001).
28. Lande, R. *et al.* Plasmacytoid dendritic cells in multiple sclerosis: intracerebral recruitment and impaired maturation in response to interferon-beta. *J. Neuropathol. Exp. Neurol.* **67,** 388–401 (2008).
29. Siegal, F. P. *et al.* The nature of the principal type 1 interferon-producing cells in human blood. *Science* **284,** 1835–7 (1999).
30. Asselin-Paturel, C. *et al.* Mouse type I IFN-producing cells are immature APCs with plasmacytoid morphology. *Nat. Immunol.* **2,** 1144–1150 (2001).
31. Nakano, H., Yanagita, M. & Gunn, M. D. CD11c(+)B220(+)Gr-1(+) cells in mouse lymph nodes and spleen display characteristics of plasmacytoid dendritic cells. *J. Exp. Med.* **194,** 1171–8 (2001).
32. Cella, M. *et al.* Plasmacytoid monocytes migrate to inflamed lymph nodes and produce large amounts of type I interferon. *Nat. Med.* **5,** 919–23 (1999).
33. Colonna, M., Trinchieri, G. & Liu, Y. J. Plasmacytoid dendritic cells in immunity. *Nat. Immunol.* **5,** 1219–1226 (2004).
34. Reizis, B., Bunin, A., Ghosh, H. S., Lewis, K. L. & Sisirak, V. Plasmacytoid dendritic

cells: recent progress and open questions. *Annu. Rev. Immunol.* **29,** 163–83 (2011).
35. Banchereau, J. & Steinman, R. M. Dendritic cells and the control of immunity. *Nature* **392,** 245–52 (1998).
36. Villadangos, J. A. & Young, L. Antigen-Presentation Properties of Plasmacytoid Dendritic Cells. *Immunity* **29,** 352–361 (2008).
37. Onai, N. *et al.* Identification of clonogenic common Flt3+M-CSFR+ plasmacytoid and conventional dendritic cell progenitors in mouse bone marrow. *Nat. Immunol.* **8,** 1207–1216 (2007).
38. Karsunky, H., Merad, M., Cozzio, A., Weissman, I. L. & Manz, M. G. Flt3 Ligand Regulates Dendritic Cell Development from Flt3 $^{+}$ Lymphoid and Myeloid-committed Progenitors to Flt3 $^{+}$ Dendritic Cells In Vivo. *J. Exp. Med.* **198,** 305–313 (2003).
39. Naik, S. H., Corcoran, L. M. & Wu, L. Development of murine plasmacytoid dendritic cell subsets. *Immunol. Cell Biol.* **83,** 563–570 (2005).
40. McKenna, H. J. *et al.* Mice lacking flt3 ligand have deficient hematopoiesis affecting hematopoietic progenitor cells, dendritic cells, and natural killer cells. *Blood* **95,** 3489–97 (2000).
41. Onai, N. *et al.* A Clonogenic Progenitor with Prominent Plasmacytoid Dendritic Cell Developmental Potential. *Immunity* **38,** 943–957 (2013).
42. Naik, S. H. *et al.* Diverse and heritable lineage imprinting of early haematopoietic progenitors. *Nature* **496,** 229–232 (2013).
43. Cisse, B. *et al.* Transcription factor E2-2 is an essential and specific regulator of plasmacytoid dendritic cell development. *Cell* **135,** 37–48 (2008).
44. Lazorchak, A., Jones, M. E. & Zhuang, Y. New insights into E-protein function in lymphocyte development. *Trends Immunol.* **26,** 334–338 (2005).
45. Spits, H., Couwenberg, F., Bakker, A. Q., Weijer, K. & Uittenbogaart, C. H. Id2 and Id3 inhibit development of CD34(+) stem cells into predendritic cell (pre-DC)2 but not into pre-DC1. Evidence for a lymphoid origin of pre-DC2. *J Exp Med* **192,** 1775–1784 (2000).
46. Sawai, C. M. *et al.* Transcription factor Runx2 controls the development and migration of plasmacytoid dendritic cells. *J. Exp. Med.* **210,** 2151–2159 (2013).
47. Sasaki, I. *et al.* Spi-B is critical for plasmacytoid dendritic cell function and development. *Blood* **120,** 4733–43 (2012).
48. Omatsu, Y. *et al.* Development of murine plasmacytoid dendritic cells defined by increased expression of an inhibitory NK receptor, Ly49Q. *J. Immunol.* **174,** 6657–62 (2005).
49. Kamogawa-Schifter, Y. *et al.* Ly49Q defines 2 pDC subsets in mice. *Blood* **105,** 2787–92 (2005).

50. Cella, M. *et al.* Plasmacytoid monocytes migrate to inflamed lymph nodes and produce large amounts of type I interferon. *Nat. Med.* **5,** 919–923 (1999).
51. Yoneyama, H. *et al.* Evidence for recruitment of plasmacytoid dendritic cell precursors to inflamed lymph nodes through high endothelial venules. *Int. Immunol.* **16,** 915–28 (2004).
52. Bauer, M. *et al.* Bacterial CpG-DNA Triggers Activation and Maturation of Human CD11c-, CD123+ Dendritic Cells. *J. Immunol.* **166,** 5000–5007 (2001).
53. Svensson, H., Cederblad, B., Lindahl, M. & Alm, G. Stimulation of Natural Interferon-α/β-Producing Cells by Staphylococcus aureus. *J. Interf. Cytokine Res.* **16,** 7–16 (1996).
54. Gregorio, J. *et al.* Plasmacytoid dendritic cells sense skin injury and promote wound healing through type I interferons. *J. Exp. Med.* **207,** 2921–30 (2010).
55. Iwasaki, A. Antiviral immune responses in the genital tract: clues for vaccines. *Nat. Rev. Immunol.* **10,** 699–711 (2010).
56. Diebold, S. S., Kaisho, T., Hemmi, H., Akira, S. & Sousa, C. R. e. Innate Antiviral Responses by Means of TLR7-Mediated Recognition of Single-Stranded RNA TL - 303. *Science (80-.).* **303 VN - ,** 1529–1531 (2004).
57. Lund, J., Sato, A., Akira, S., Medzhitov, R. & Iwasaki, A. Toll-like receptor 9-mediated recognition of Herpes simplex virus-2 by plasmacytoid dendritic cells. *J. Exp. Med.* **198,** 513–20 (2003).
58. Lund, J. M. *et al.* Recognition of single-stranded RNA viruses by Toll-like receptor 7. *Proc. Natl. Acad. Sci. U. S. A.* **101,** 5598–603 (2004).
59. Heil, F. *et al.* Species-specific recognition of single-stranded RNA via toll-like receptor 7 and 8. *Science* **303,** 1526–9 (2004).
60. Rutz, M. *et al.* Toll-like receptor 9 binds single-stranded CpG-DNA in a sequence- and pH-dependent manner. *Eur. J. Immunol.* **34,** 2541–50 (2004).
61. Dreux, M. *et al.* Short-range exosomal transfer of viral RNA from infected cells to plasmacytoid dendritic cells triggers innate immunity. *Cell Host Microbe* **12,** 558–570 (2012).
62. Wieland, S. F. *et al.* Human plasmacytoid dendritic cells sense lymphocytic choriomeningitis virus-infected cells in vitro. *J Virol* **88,** 752–757 (2014).
63. Latz, E. *et al.* Ligand-induced conformational changes allosterically activate Toll-like receptor 9. *Nat. Immunol.* **8,** 772–779 (2007).
64. Yang, K. *et al.* Human TLR-7-, -8-, and -9-mediated induction of IFN-α/β and -λ Is IRAK-4 dependent and redundant for protective immunity to viruses. *Immunity* **23,** 465–478 (2005).
65. Suzuki, N., Suzuki, S. & Yeh, W. C. IRAK-4 as the central TIR signaling mediator in

innate immunity. *Trends Immunol.* **23,** 503–506 (2002).

66. Gohda, J., Matsumura, T. & Inoue, J. Cutting edge: TNFR-associated factor (TRAF) 6 is essential for MyD88-dependent pathway but not toll/IL-1 receptor domain-containing adaptor-inducing IFN-beta (TRIF)-dependent pathway in TLR signaling. *J. Immunol.* **173,** 2913–2917 (2004).
67. Häcker, H. *et al.* Specificity in Toll-like receptor signalling through distinct effector functions of TRAF3 and TRAF6. *Nature* **439,** 204–207 (2006).
68. Kawai, T. *et al.* Interferon-α induction through Toll-like receptors involves a direct interaction of IRF7 with MyD88 and TRAF6. *Nat. Immunol.* **5,** 1061–1068 (2004).
69. Jefferies, C. A. *et al.* Bruton's tyrosine kinase is a Toll/interleukin-1 receptor domain-binding protein that participates in nuclear factor kappaB activation by Toll-like receptor 4. *J. Biol. Chem.* **278,** 26258–64 (2003).
70. Wang, J., Lau, K.-Y., Jung, J., Ravindran, P. & Barrat, F. J. Bruton's tyrosine kinase regulates TLR9 but not TLR7 signaling in human plasmacytoid dendritic cells. *Eur. J. Immunol.* **44,** 1130–6 (2014).
71. Kerkmann, M. *et al.* Activation with CpG-A and CpG-B Oligonucleotides Reveals Two Distinct Regulatory Pathways of Type I IFN Synthesis in Human Plasmacytoid Dendritic Cells. *J. Immunol.* **170,** 4465–4474 (2003).
72. Gilliet, M., Cao, W. & Liu, Y.-J. Plasmacytoid dendritic cells: sensing nucleic acids in viral infection and autoimmune diseases. *Nat. Rev. Immunol.* **8,** 594–606 (2008).
73. Honda, K. *et al.* IRF-7 is the master regulator of type-I interferon-dependent immune responses. *Nature* **434,** 772–777 (2005).
74. Guiducci, C. *et al.* Properties regulating the nature of the plasmacytoid dendritic cell response to Toll-like receptor 9 activation. *J. Exp. Med.* **203,** 1999–2008 (2006).
75. Krug, A. *et al.* Identification of CpG oligonucleotide sequences with high induction of IFN-alpha/beta in plasmacytoid dendritic cells. *Eur. J. Immunol.* **31,** 2154–63 (2001).
76. Pestka, S., Krause, C. D. & Walter, M. R. Interferons, interferon-like cytokines, and their receptors. *Immunol. Rev.* **202,** 8–32 (2004).
77. Schneider, W. M., Chevillotte, M. D. & Rice, C. M. Interferon-stimulated genes: a complex web of host defenses. *Annu. Rev. Immunol.* **32,** 513–45 (2014).
78. Choi, U. Y., Kang, J.-S., Hwang, Y. S. & Kim, Y.-J. Oligoadenylate synthase-like (OASL) proteins: dual functions and associations with diseases. *Exp. Mol. Med.* **47,** e144 (2015).
79. Haller, O. & Kochs, G. Interferon-induced mx proteins: dynamin-like GTPases with antiviral activity. *Traffic* **3,** 710–7 (2002).
80. Gautier, G. *et al.* A type I interferon autocrine-paracrine loop is involved in Toll-like receptor-induced interleukin-12p70 secretion by dendritic cells. *J. Exp. Med.* **201,**

1435–1446 (2005).

81. Dalod, M. *et al.* Interferon alpha/beta and interleukin 12 responses to viral infections: pathways regulating dendritic cell cytokine expression in vivo. *J. Exp. Med.* **195,** 517–28 (2002).
82. Cousens, L. P., Orange, J. S., Su, H. C. & Biron, C. A. Interferon-alpha/beta inhibition of interleukin 12 and interferon-gamma production in vitro and endogenously during viral infection. *Immunology* **94,** 634–639 (1997).
83. Montoya, M. *et al.* Type I interferons produced by dendritic cells promote their phenotypic and functional activation. *Blood* **99,** 3263–3271 (2002).
84. Ito, T. *et al.* Plasmacytoid dendritic cells prime IL-10-producing T regulatory cells by inducible costimulator ligand. *J. Exp. Med.* **204,** 105–15 (2007).
85. Le Bon, a. *et al.* Cutting Edge: Enhancement of Antibody Responses Through Direct Stimulation of B and T Cells by Type I IFN. *J. Immunol.* **176,** 2074–2078 (2006).
86. Spadaro, F. *et al.* IFN-α enhances cross-presentation in human dendritic cells by modulating antigen survival, endocytic routing, and processing. *Blood* **119,** 1407–17 (2012).
87. Parlato, S. *et al.* Expression of CCR-7, MIP-3??, and Th-1 chemokines in type I IFN-induced monocyte-derived dendritic cells: Importance for the rapid acquisition of potent migratory and functional activities. *Blood* **98,** 3022–3029 (2001).
88. Rouzaut, A. *et al.* Dendritic cells adhere to and transmigrate across lymphatic endothelium in response to IFN-α. *Eur. J. Immunol.* **40,** 3054–3063 (2010).
89. Hwang, I. *et al.* Activation Mechanisms of Natural Killer Cells during Influenza Virus Infection. *PLoS One* **7,** (2012).
90. Martinez, J., Huang, X. & Yang, Y. Direct action of type I IFN on NK cells is required for their activation in response to vaccinia viral infection in vivo. *J. Immunol.* **180,** 1592–1597 (2008).
91. Havenar-Daughton, C., Kolumam, G. A. & Murali-Krishna, K. Cutting Edge: The direct action of type I IFN on CD4 T cells is critical for sustaining clonal expansion in response to a viral but not a bacterial infection. *J. Immunol.* **176,** 3315–3319 (2006).
92. Kaser, a, Nagata, S. & Tilg, H. Interferon alpha augments activation-induced T cell death by upregulation of Fas (CD95/APO-1) and Fas ligand expression. *Cytokine* **11,** 736–743 (1999).
93. Petricoin, E. I. *et al.* Antiproliferative action of interferon-a requires components of T-cell receptor signalling. *Nature* **390,** 629–632 (1997).
94. Braun, D., Caramalho, I. & Demengeot, J. IFN-alpha/beta enhances BCR-dependent B cell responses. *Int. Immunol.* **14,** 411–419 (2002).
95. Le Bon, A. *et al.* Type I interferons potently enhance humoral immunity and can

promote isotype switching by stimulating dendritic cells in vivo. *Immunity* **14,** 461–470 (2001).

96. Menon, M., Blair, P. A., Isenberg, D. A. & Mauri, C. A Regulatory Feedback between Plasmacytoid Dendritic Cells and Regulatory B Cells Is Aberrant in Systemic Lupus Erythematosus. *Immunity* **44,** 683–697 (2016).
97. Izaguirre, A. *et al.* Comparative analysis of IRF and IFN-alpha expression in human plasmacytoid and monocyte-derived dendritic cells. *J. Leukoc. Biol.* **74,** 1125–38 (2003).
98. Honda, K. & Taniguchi, T. IRFs: master regulators of signalling by Toll-like receptors and cytosolic pattern-recognition receptors. *Nat. Rev. Immunol.* **6,** 644–658 (2006).
99. Wilson, E. B. *et al.* Blockade of chronic type I interferon signaling to control persistent LCMV infection. *Science* **340,** 202–7 (2013).
100. Teijaro, J. R. *et al.* Persistent LCMV infection is controlled by blockade of type I interferon signaling. *Science* **340,** 207–11 (2013).
101. Grouard, G. *et al.* The enigmatic plasmacytoid T cells develop into dendritic cells with interleukin (IL)-3 and CD40-ligand. *J. Exp. Med.* **185,** 1101–11 (1997).
102. Kadowaki, N., Antonenko, S., Lau, J. Y. & Liu, Y. J. Natural interferon alpha/beta-producing cells link innate and adaptive immunity. *J. Exp. Med.* **192,** 219–26 (2000).
103. Ochando, J. C. *et al.* Alloantigen-presenting plasmacytoid dendritic cells mediate tolerance to vascularized grafts. doi:10.1038/ni1333
104. Hoeffel, G. *et al.* Antigen Crosspresentation by Human Plasmacytoid Dendritic Cells. *Immunity* (2007).
105. Salio, M., Palmowski, M. J., Atzberger, A., Hermans, I. F. & Cerundolo, V. CpG-matured murine plasmacytoid dendritic cells are capable of in vivo priming of functional CD8 T cell responses to endogenous but not exogenous antigens. *J. Exp. Med.* **199,** 567–79 (2004).
106. Schlecht, G. *et al.* Murine plasmacytoid dendritic cells induce effector/memory CD8+ T-cell responses in vivo after viral stimulation. *Blood* **104,** 1808–15 (2004).
107. Fonteneau, J.-F. *et al.* Activation of influenza virus-specific CD4+ and CD8+ T cells: a new role for plasmacytoid dendritic cells in adaptive immunity. *Blood* **101,** 3520–6 (2003).
108. Mouriès, J. *et al.* Plasmacytoid dendritic cells efficiently cross-prime naive T cells in vivo after TLR activation. *Blood* **112,** 3713–22 (2008).
109. LeibundGut-Landmann, S., Waldburger, J.-M., Reis e Sousa, C., Acha-Orbea, H. & Reith, W. MHC class II expression is differentially regulated in plasmacytoid and conventional dendritic cells. *Nat. Immunol.* **5,** 899–908 (2004).
110. Pascale, F. *et al.* Plasmacytoid dendritic cells migrate in afferent skin lymph. *J.*

Immunol. **180,** 5963–72 (2008).

111. Goubier, A. *et al.* Plasmacytoid Dendritic Cells Mediate Oral Tolerance. *Immunity* **29,** 464–475 (2008).
112. Wei, S. *et al.* Plasmacytoid dendritic cells induce CD8+ regulatory T cells in human ovarian carcinoma. *Cancer Res.* **65,** 5020–5026 (2005).
113. Abe, M., Wang, Z., De Creus, A. & Thomson, A. W. Plasmacytoid dendritic cell precursors induce allogeneic T-cell hyporesponsiveness and prolong heart graft survival. *Am. J. Transplant.* **5,** 1808–1819 (2005).
114. Hadeiba, H. *et al.* CCR9 expression defines tolerogenic plasmacytoid dendritic cells able to suppress acute graft-versus-host disease. *Nat. Immunol.* **9,** 1253–60 (2008).
115. Dasgupta, S., Erturk-Hasdemir, D., Ochoa-Reparaz, J., Reinecker, H. C. & Kasper, D. L. Plasmacytoid dendritic cells mediate anti-inflammatory responses to a gut commensal molecule via both innate and adaptive mechanisms. *Cell Host Microbe* **15,** 413–423 (2014).
116. Nestle, F. O. *et al.* Plasmacytoid predendritic cells initiate psoriasis through interferon-alpha production. *J. Exp. Med.* **202,** 135–43 (2005).
117. Allen, J. S. *et al.* Plasmacytoid Dendritic Cells Are Proportionally Expanded at Diagnosis of Type 1 Diabetes and Enhance Islet Autoantigen Presentation to T-Cells Through Immune Complex Capture. *Diabetes* **58,** 113–x (2009).
118. Saxena, V., Ondr, J. K., Magnusen, A. F., Munn, D. H. & Katz, J. D. The Countervailing Actions of Myeloid and Plasmacytoid Dendritic Cells Control Autoimmune Diabetes in the Nonobese Diabetic Mouse. *J. Immunol.* **179,** 5041–5053 (2007).
119. Tsokos, G. C. Systemic Lupus Erythematosus. *N. Engl. J. Med.* **365,** 2110–2121 (2011).
120. Fuchs, T. A. *et al.* Novel cell death program leads to neutrophil extracellular traps. *J. Cell Biol.* **176,** 231–241 (2007).
121. Steinberg, B. E. & Grinstein, S. Unconventional roles of the NADPH oxidase: signaling, ion homeostasis, and cell death. *Sci. STKE* **2007,** pe11 (2007).
122. Napirei, M. *et al.* Features of systemic lupus erythematosus in Dnase1-deficient mice. *Nat Genet* **25,** 177–181 (2000).
123. Hakkim, A. *et al.* Impairment of neutrophil extracellular trap degradation is associated with lupus nephritis. *Proc. Natl. Acad. Sci. U. S. A.* **107,** 9813–8 (2010).
124. Lande, R. *et al.* Neutrophils Activate Plasmacytoid Dendritic Cells by Releasing Self-DNA Peptide Complexes in Systemic Lupus Erythematosus. *Sci. Transl. Med.* **3,** 73ra19–73ra19 (2011).
125. Garcia-Romo, G. S. *et al.* Netting neutrophils are major inducers of type I IFN

production in pediatric systemic lupus erythematosus. *Sci. Transl. Med.* **3,** 73ra20 (2011).

126. Baechler, E. C. *et al.* Interferon-inducible gene expression signature in peripheral blood cells of patients with severe lupus. 0–5 (2002).
127. Bennett, L. *et al.* Interferon and granulopoiesis signatures in systemic lupus erythematosus blood. *J. Exp. Med.* **197,** 711–23 (2003).
128. Rowland, S. L. *et al.* Early, transient depletion of plasmacytoid dendritic cells ameliorates autoimmunity in a lupus model. *J. Exp. Med.* **211,** 1977–91 (2014).
129. Sisirak, V. *et al.* Genetic evidence for the role of plasmacytoid dendritic cells in systemic lupus erythematosus. *J. Exp. Med.* **211,** 1969–76 (2014).
130. Stasiolek, M. *et al.* Impaired maturation and altered regulatory function of plasmacytoid dendritic cells in multiple sclerosis. *Brain* **129,** 1293–305 (2006).
131. Feng, X. *et al.* Type I interferon signature is high in lupus and neuromyelitis optica but low in multiple sclerosis. *J. Neurol. Sci.* **313,** 48–53 (2012).
132. Paty, D. W. & Li, D. K. Interferon beta-1b is effective in relapsing-remitting multiple sclerosis. II. MRI analysis results of a multicenter, randomized, double-blind, placebo-controlled trial. UBC MS/MRI Study Group and the IFNB Multiple Sclerosis Study Group. *Neurology* **43,** 662–7 (1993).
133. Jacobs, L. D. *et al.* Intramuscular interferon beta-1a for disease progression in relapsing multiple sclerosis. The Multiple Sclerosis Collaborative Research Group (MSCRG). *Ann. Neurol.* **39,** 285–94 (1996).
134. Randomised double-blind placebo-controlled study of interferon beta-1a in relapsing/remitting multiple sclerosis. PRISMS (Prevention of Relapses and Disability by Interferon beta-1a Subcutaneously in Multiple Sclerosis) Study Group. *Lancet (London, England)* **352,** 1498–504 (1998).
135. Placebo-controlled multicentre randomised trial of interferon beta-1b in treatment of secondary progressive multiple sclerosis. European Study Group on interferon beta-1b in secondary progressive MS. *Lancet (London, England)* **352,** 1491–7 (1998).
136. Jacobs, L. D. *et al.* Intramuscular interferon beta-1a therapy initiated during a first demyelinating event in multiple sclerosis. CHAMPS Study Group. *N. Engl. J. Med.* **343,** 898–904 (2000).
137. Comi, G. *et al.* Effect of early interferon treatment on conversion to definite multiple sclerosis: a randomised study. *Lancet (London, England)* **357,** 1576–82 (2001).
138. Antonetti, F., Finocchiaro, O., Mascia, M., Terlizzese, M. G. & Jaber, A. A comparison of the biologic activity of two recombinant IFN-beta preparations used in the treatment of relapsing-remitting multiple sclerosis. *J. Interferon Cytokine Res.* **22,** 1181–4 (2002).

139. PRISMS Study Group and the University of British Columbia MS/MRI Analysis Group. PRISMS-4: Long-term efficacy of interferon-beta-1a in relapsing MS. *Neurology* **56,** 1628–36 (2001).
140. Bertolotto, A., Deisenhammer, F., Gallo, P. & Sölberg Sørensen, P. Immunogenicity of interferon beta: differences among products. *J. Neurol.* II15–II24 (2004). doi:10.1007/s00415-004-1204-7
141. Korporal, M. *et al.* Interferon beta-induced restoration of regulatory T-cell function in multiple sclerosis is prompted by an increase in newly generated naive regulatory T cells. *Arch. Neurol.* **65,** 1434–9 (2008).
142. Noronha, A., Toscas, A. & Jensen, M. A. Interferon beta decreases T cell activation and interferon gamma production in multiple sclerosis. *J. Neuroimmunol.* **46,** 145–53 (1993).
143. Galboiz, Y., Shapiro, S., Lahat, N., Rawashdeh, H. & Miller, A. Matrix metalloproteinases and their tissue inhibitors as markers of disease subtype and response to interferon-beta therapy in relapsing and secondary-progressive multiple sclerosis patients. *Ann. Neurol.* **50,** 443–51 (2001).
144. Derkow, K. *et al.* Multiple sclerosis: modulation of toll-like receptor (TLR) expression by interferon-β includes upregulation of TLR7 in plasmacytoid dendritic cells. *PLoS One* **8,** e70626 (2013).
145. Prinz, M. *et al.* Distinct and nonredundant in vivo functions of IFNAR on myeloid cells limit autoimmunity in the central nervous system. *Immunity* **28,** 675–86 (2008).
146. Guo, B., Chang, E. Y. & Cheng, G. The type I IFN induction pathway constrains Th17-mediated autoimmune inflammation in mice. *J. Clin. Invest.* **118,** 1680–90 (2008).
147. Stumhofer, J. S. *et al.* Interleukin 27 negatively regulates the development of interleukin 17-producing T helper cells during chronic inflammation of the central nervous system. *Nat. Immunol.* **7,** 937–45 (2006).
148. Schubert, R. D. *et al.* IFN-β treatment requires B cells for efficacy in neuroautoimmunity. *J. Immunol.* **194,** 2110–6 (2015).
149. Irla, M. *et al.* MHC class II-restricted antigen presentation by plasmacytoid dendritic cells inhibits T cell-mediated autoimmunity. *J. Exp. Med.* **207,** 1891–905 (2010).
150. Duraes, F. V. *et al.* pDC therapy induces recovery from EAE by recruiting endogenous pDC to sites of CNS inflammation. *J. Autoimmun.* **67,** 8–18 (2016).
151. Thomas, R. C. & Meech, R. W. Hydrogen ion currents and intracellular pH in depolarized voltage-clamped snail neurones. *Nature* **299,** 826–8 (1982).
152. Byerly, L., Meech, R. & Moody, W. Rapidly activating hydrogen ion currents in perfused neurones of the snail, Lymnaea stagnalis. *J. Physiol.* **351,** 199–216 (1984).
153. Meech, R. W. & Thomas, R. C. Voltage-dependent intracellular pH in Helix aspersa

neurones. *J. Physiol.* **390,** 433–52 (1987).
154. Ramsey, I. S., Moran, M. M., Chong, J. A. & Clapham, D. E. A voltage-gated proton-selective channel lacking the pore domain. *Nature* **440,** 1213–6 (2006).
155. Sasaki, M. A Voltage Sensor – Domain Protein Is a Voltage-Gated Proton Channel. *Science* **589,** (2006).
156. Doyle, D. A. *et al.* The structure of the potassium channel: molecular basis of K+ conduction and selectivity. *Science* **280,** 69–77 (1998).
157. Catterall, W. A. From Ionic Currents to Molecular Review Mechanisms: The Structure and Function of Voltage-Gated Sodium Channels. *Neuron* **26,** 13–25 (2000).
158. Starace, D. M. & Bezanilla, F. A proton pore in a potassium channel voltage sensor reveals a focused electric field. *Nature* **427,** 548–553 (2004).
159. Gardiner, G. J. *et al.* A role for NADPH oxidase in antigen presentation. *Front. Immunol.* **4,** 1–6 (2013).
160. Capasso, M. Regulation of immune responses by proton channels. *Immunology* **143,** 131–7 (2014).
161. Hondares, E. *et al.* Enhanced activation of an amino-terminally truncated isoform of the voltage-gated proton channel HVCN1 enriched in malignant B cells. *Proc. Natl. Acad. Sci. U. S. A.* **111,** 18078–83 (2014).
162. Morgan, D. *et al.* Sustained activation of proton channels and NADPH oxidase in human eosinophils and murine granulocytes requires PKC but not cPLA2 alpha activity. *J. Physiol.* **579,** 327–44 (2007).
163. Musset, B. *et al.* Identification of Thr29 as a critical phosphorylation site that activates the human proton channel Hvcn1 in leukocytes. *J. Biol. Chem.* **285,** 5117–5121 (2010).
164. Bánfi, B. *et al.* A novel H(+) conductance in eosinophils: unique characteristics and absence in chronic granulomatous disease. *J. Exp. Med.* **190,** 183–94 (1999).
165. Li, S. J. *et al.* The Role and Structure of the Carboxyl-terminal Domain of the Human Voltage-gated Proton Channel Hv1. *J. Biol. Chem.* **285,** 12047–12054 (2010).
166. Fujiwara, Y. *et al.* The cytoplasmic coiled-coil mediates cooperative gating temperature sensitivity in the voltage-gated H+ channel Hv1. *Nat. Commun.* **3,** 816 (2012).
167. Tombola, F., Ulbrich, M. H. & Isacoff, E. Y. The Voltage-Gated Proton Channel Hv1 Has Two Pores, Each Controlled by One Voltage Sensor. *Neuron* **58,** 546–556 (2008).
168. Musset, B. *et al.* Zinc inhibition of monomeric and dimeric proton channels suggests cooperative gating. *J. Physiol.* **588,** 1435–49 (2010).
169. Koch, H. P. *et al.* Multimeric nature of voltage-gated proton channels. *Proc. Natl. Acad. Sci. U. S. A.* **105,** 9111–9116 (2008).

170. Gonzalez, C., Koch, H. P., Drum, B. M. & Larsson, H. P. Strong cooperativity between subunits in voltage-gated proton channels. *Nat. Struct. Mol. Biol.* **17,** 51–6 (2010).
171. Lee, S.-Y., Letts, J. A. & Mackinnon, R. Dimeric subunit stoichiometry of the human voltage-dependent proton channel Hv1. *Proc. Natl. Acad. Sci. U. S. A.* **105,** 7692–5 (2008).
172. Tombola, F., Ulbrich, M. H., Kohout, S. C. & Isacoff, E. Y. The opening of the two pores of the Hv1 voltage-gated proton channel is tuned by cooperativity. *Nat. Struct. Mol. Biol.* **17,** 44–50 (2010).
173. Villalba-Galea, C. A. Hv1 proton channel opening is preceded by a voltage-independent transition. *Biophys. J.* **107,** 1564–1572 (2014).
174. Gonzalez, C., Rebolledo, S., Perez, M. E. & Larsson, H. P. Molecular mechanism of voltage sensing in voltage-gated proton channels. *J. Gen. Physiol.* **141,** 275–85 (2013).
175. Qiu, F. *et al.* Subunit interactions during cooperative opening of voltage-gated proton channels. *Neuron* **77,** 288–98 (2013).
176. Mony, L., Berger, T. K. & Isacoff, E. Y. A specialized molecular motion opens the Hv1 voltage-gated proton channel. *Nat. Struct. Mol. Biol.* **22,** 283–290 (2015).
177. Decoursey, T. E. The voltage-gated proton channel: A riddle, wrapped in a mystery, inside an enigma. *Biochemistry* **54,** 3250–3268 (2015).
178. Berger, T. K. & Isacoff, E. Y. The pore of the voltage-gated proton channel. *Neuron* **72,** 991–1000 (2011).
179. Kulleperuma, K. *et al.* Construction and validation of a homology model of the human voltage-gated proton channel hHV1. *J. Gen. Physiol.* **141,** 445–65 (2013).
180. Morgan, D. *et al.* Peregrination of the selectivity filter delineates the pore of the human voltage-gated proton channel hHV1. *J. Gen. Physiol.* **142,** 625–40 (2013).
181. Dudev, T. *et al.* Selectivity Mechanism of the Voltage-gated Proton Channel, HV1. *Sci. Rep.* **5,** 10320 (2015).
182. Wood, M. L. *et al.* Water wires in atomistic models of the Hv1 proton channel. *Biochim. Biophys. Acta - Biomembr.* **1818,** 286–293 (2012).
183. Kuno, M., Kawawaki, J. & Nakamura, F. A highly temperature-sensitive proton current in mouse bone marrow-derived mast cells. *J. Gen. Physiol.* **109,** 731–740 (1997).
184. Ramsey, I. S. *et al.* An aqueous H+ permeation pathway in the voltage-gated proton channel Hv1. *Nat. Struct. Mol. Biol.* **17,** 869–875 (2010).
185. Musset, B. *et al.* Aspartate 112 is the selectivity filter of the human voltage-gated proton channel. *Nature* **480,** 273–7 (2011).
186. Cherny, V. V & DeCoursey, T. E. pH-dependent inhibition of voltage-gated H(+) currents in rat alveolar epithelial cells by Zn(2+) and other divalent cations. *J. Gen.*

Physiol. **114,** 819–38 (1999).

187. Decoursey, T. E. & Cherny, V. V. Temperature Dependence of Voltage-gated H 2 Currents in Human Neutrophils, Rat Alveolar Epithelial Cells, and Mammalian Phagocytes. *J. Gen. Physiol* **112,** 503–522 (1998).
188. Smith, S. M. E. *et al.* Voltage-gated proton channel in a dinoflagellate. *Proc. Natl. Acad. Sci. U. S. A.* **108,** 18162–7 (2011).
189. Ramsey, I. S., Ruchti, E., Kaczmarek, J. S. & Clapham, D. E. Hv1 proton channels are required for high-level NADPH oxidase-dependent superoxide production during the phagocyte respiratory burst. *Proc. Natl. Acad. Sci. U. S. A.* **106,** 7642–7647 (2009).
190. Okochi, Y., Sasaki, M., Iwasaki, H. & Okamura, Y. Voltage-gated proton channel is expressed on phagosomes. *Biochem. Biophys. Res. Commun.* **382,** 274–279 (2009).
191. El Chemaly, A. *et al.* VSOP/Hv1 proton channels sustain calcium entry, neutrophil migration, and superoxide production by limiting cell depolarization and acidification. *J. Exp. Med.* **207,** 129–39 (2010).
192. Szteyn, K., Yang, W., Schmid, E., Lang, F. & Shumilina, E. Lipopolysaccharide-sensitive H+ current in dendritic cells. *AJP Cell Physiol.* **303,** C204–C212 (2012).
193. El Chemaly, A., Nunes, P., Jimaja, W., Castelbou, C. & Demaurex, N. Hv1 proton channels differentially regulate the pH of neutrophil and macrophage phagosomes by sustaining the production of phagosomal ROS that inhibit the delivery of vacuolar ATPases. *J. Leukoc. Biol.* (2014).
194. Wu, L. J. *et al.* The voltage-gated proton channel Hv1 enhances brain damage from ischemic stroke. *Nat Neurosci* **15,** 565–573 (2012).
195. Segal, A. W. & Jones, O. T. Novel cytochrome b system in phagocytic vacuoles of human granulocytes. *Nature* **276,** 515–7 (1978).
196. Cross, A. R. & Segal, A. W. The NADPH oxidase of professional phagocytes--prototype of the NOX electron transport chain systems. *Biochim. Biophys. Acta* **1657,** 1–22 (2004).
197. DeCoursey, T. E., Morgan, D. & Cherny, V. V. The voltage dependence of NADPH oxidase reveals why phagocytes need proton channels. *Nature* **422,** 531–4 (2003).
198. Morgan, D., Cherny, V. V, Murphy, R., Katz, B. Z. & DeCoursey, T. E. The pH dependence of NADPH oxidase in human eosinophils. *J. Physiol.* **569,** 419–31 (2005).
199. Zhu, X., Mose, E. & Zimmermann, N. Proton channel HVCN1 is required for effector functions of mouse eosinophils. *BMC Immunol.* **14,** 24 (2013).
200. Canton, J., Khezri, R., Glogauer, M. & Grinstein, S. Contrasting phagosome pH regulation and maturation in human M1 and M2 macrophages. *Mol. Biol. Cell* **25,** 3330–41 (2014).
201. Savina, A. *et al.* NOX2 Controls Phagosomal pH to Regulate Antigen Processing

during Crosspresentation by Dendritic Cells. *Cell* **126,** 205–218 (2005).
202. Barrett, A. Leukocyte elastase. *Methods Enzymol.* **80,** 581–588 (1981).
203. Belaaouaj, A. *et al.* Mice lacking neutrophil elastase reveal impaired host defense against gram negative bacterial sepsis. *Nat. Med.* **4,** 615–618 (1998).
204. Forgac, M. Vacuolar ATPases: rotary proton pumps in physiology and pathophysiology. *Nat. Rev. Mol. Cell Biol.* **8,** 917–929 (2007).
205. Jankowski, A., Scott, C. C. & Grinstein, S. Determinants of the phagosomal pH in neutrophils. *J. Biol. Chem.* **277,** 6059–66 (2002).
206. El Chemaly, A. *et al.* VSOP/Hv1 proton channels sustain calcium entry, neutrophil migration, and superoxide production by limiting cell depolarization and acidification. *J. Exp. Med.* **207,** 129–39 (2010).
207. Capasso, M. *et al.* HVCN1 modulates BCR signal strength via regulation of BCR-dependent generation of reactive oxygen species. *Nat. Immunol.* **11,** 265–72 (2010).
208. Okochi, Y. *et al.* The voltage-gated proton channel Hv1/VSOP inhibits neutrophil granule release. *J. Leukoc. Biol.* **99,** 7–19 (2016).
209. Cherny, V. V, Thomas, L. L. & DeCoursey, T. E. Voltage-gated proton currents in human basophils. *Biol. Membr.* **18,** 458–465 (2001).
210. Musset, B. *et al.* A pH-stabilizing role of voltage-gated proton channels in IgE-mediated activation of human basophils. *Proc. Natl. Acad. Sci. U. S. A.* **105,** 11020–5 (2008).
211. Sasaki, M. *et al.* Autoimmune disorder phenotypes in Hvcn1-deficient mice. *Biochem. J.* **450,** 295–301 (2013).
212. Ghosh, H. S. *et al.* ETO family protein Mtg16 regulates the balance of dendritic cell subsets by repressing Id2. *J. Exp. Med.* **211,** 1623–35 (2014).
213. Cheng, M. *et al.* Characterization of species-specific genes regulated by E2-2 in human plasmacytoid dendritic cells. *Sci Rep* **5,** 10752 (2015).
214. Sigl, R., Ploner, C., Shivalingaiah, G., Kofler, R. & Geley, S. Development of a multipurpose GATEWAY-based lentiviral tetracycline-regulated conditional RNAi system (GLTR). *PLoS One* **9,** e97764 (2014).
215. Rybicka, J. M., Balce, D. R., Chaudhuri, S., Allan, E. R. O. & Yates, R. M. Phagosomal proteolysis in dendritic cells is modulated by NADPH oxidase in a pH-independent manner. *EMBO J.* **31,** 932–44 (2012).
216. Honda, K. *et al.* Spatiotemporal regulation of MyD88–IRF-7 signalling for robust type-I interferon induction. *Nature* **434,** 1035–1040 (2005).
217. Sato, M. *et al.* Positive feedback regulation of type I IFN genes by the IFN-inducible transcription factor IRF-7. *FEBS Lett.* **441,** 106–110 (1998).
218. Hornung, V. *et al.* Quantitative expression of toll-like receptor 1-10 mRNA in cellular

subsets of human peripheral blood mononuclear cells and sensitivity to CpG oligodeoxynucleotides. *J. Immunol.* **168,** 4531–7 (2002).

219. Hartmann, G. *et al.* Rational design of new CpG oligonucleotides that combine B cell activation with high IFN-alpha induction in plasmacytoid dendritic cells. *Eur. J. Immunol.* **33,** 1633–41 (2003).
220. Lampropoulou, V. *et al.* TLR-Activated B Cells Suppress T Cell-Mediated Autoimmunity. *J. Immunol.* **180,** 4763–4773 (2008).
221. Yanaba, K. *et al.* A Regulatory B Cell Subset with a Unique CD1dhiCD5+ Phenotype Controls T Cell-Dependent Inflammatory Responses. *Immunity* **28,** 639–650 (2008).
222. Poltorak, A. *et al.* Defective LPS signaling in C3H/HeJ and C57BL/10ScCr mice: mutations in Tlr4 gene. *Science* **282,** 2085–8 (1998).
223. Matsushita, T., Yanaba, K., Bouaziz, J.-D., Fujimoto, M. & Tedder, T. F. Regulatory B cells inhibit EAE initiation in mice while other B cells promote disease progression. *J. Clin. Invest.* **118,** 3420–3430 (2008).
224. Loder, B. F. *et al.* B Cell Development in the Spleen Takes Place in Discrete Steps and Is Determined by the Quality of B Cell Receptor–Derived Signals. *J. Exp. Med.* **190,** 75–90 (1999).
225. Pillai, S., Cariappa, A. & Moran, S. T. Marginal zone B cells. *Annu. Rev. Immunol.* **23,** 161–196 (2005).
226. Naradikian, M. S., Scholz, J. L., Oropallo, M. A. & Cancro, M. P. *Understanding B Cell Biology*. (Springer Basel, 2014).
227. Cariappa, A. *et al.* The Recirculating B Cell Pool Contains Two Functionally Distinct, Long-Lived, Posttransitional, Follicular B Cell Populations. *J. Immunol.* **179,** 2270–2281 (2007).
228. Sasaki, M. *et al.* Autoimmune disorder phenotypes in Hvcn1-deficient mice. *Biochem. J.* **450,** 295–301 (2013).
229. Schilling, T., Gratopp, A., DeCoursey, T. E. & Eder, C. Voltage-activated proton currents in human lymphocytes. *J. Physiol.* **545,** 93–105 (2002).
230. Flannagan, R. S., Jaumouillé, V. & Grinstein, S. The Cell Biology of Phagocytosis. *Annu. Rev. Pathol. Mech. Dis.* **7,** 61–98 (2012).
231. Yakubov, L. A. *et al.* Mechanism of oligonucleotide uptake by cells: involvement of specific receptors? *Proc. Natl. Acad. Sci. U. S. A.* **86,** 6454–8 (1989).
232. Beltinger, C. *et al.* Binding, uptake, and intracellular trafficking of phosphorothioate-modified oligodeoxynucleotides. *J. Clin. Invest.* **95,** 1814–23 (1995).
233. Huotari, J. & Helenius, A. Endosome maturation. *EMBO J.* **30,** 3481–500 (2011).
234. Rink, J. *et al.* Rab Conversion as a Mechanism of Progression from Early to Late Endosomes. *Cell* **122,** 735–749 (2005).

235. Maxfield, F. R. & Yamashiro, D. J. Endosome acidification and the pathways of receptor-mediated endocytosis. *Adv. Exp. Med. Biol.* **225,** 189–98 (1987).
236. Kawasaki-Nishi, S., Nishi, T. & Forgac, M. Yeast V-ATPase complexes containing different isoforms of the 100-kDa a-subunit differ in coupling efficiency and in vivo dissociation. *J. Biol. Chem.* **276,** 17941–8 (2001).
237. Lafourcade, C., Sobo, K., Kieffer-Jaquinod, S., Garin, J. & van der Goot, F. G. Regulation of the V-ATPase along the endocytic pathway occurs through reversible subunit association and membrane localization. *PLoS One* **3,** e2758 (2008).
238. Hager, A. & Lanz, C. Essential sulfhydryl groups in the catalytic center of the tonoplast H+-ATPase from coleoptiles ofZea mays L. as demonstrated by the biotin-streptavidin-peroxidase system. *Planta* **180,** 116–122 (1989).
239. Feng, Y. & Forgac, M. A novel mechanism for regulation of vacuolar acidification. *J. Biol. Chem.* **267,** 19769–72 (1992).
240. Seidel, T. *et al.* Regulation of the V-type ATPase by redox modulation. *Biochem. J* **448,** 243–251 (2012).
241. Oluwatosin, Y. E. & Kane, P. M. Mutations in the CYS4 Gene Provide Evidence for Regulation of the Yeast Vacuolar H+-ATPase by Oxidation and Reduction in Vivo. *J. Biol. Chem.* **272,** 28149–28157 (1997).
242. Nunes, P., Chemaly, A. El, Jimaja, W., Castelbou, C. & Demaurex, N. The Hv1 voltage-gated proton channel regulates the pH of neutrophil but not macrophage phagosomes. *FASEB J.* **27,** 913.44–913.44 (2013).
243. Fukui, R. *et al.* Unc93B1 restricts systemic lethal inflammation by orchestrating toll-like receptor 7 and 9 trafficking. *Immunity* **35,** 69–81 (2011).
244. Barton, G. M., Kagan, J. C. & Medzhitov, R. Intracellular localization of Toll-like receptor 9 prevents recognition of self DNA but facilitates access to viral DNA. *Nat. Immunol.* **7,** 49–56 (2006).
245. Ewald, S. E. *et al.* Nucleic acid recognition by Toll-like receptors is coupled to stepwise processing by cathepsins and asparagine endopeptidase. *J. Exp. Med.* **208,** 643–651 (2011).
246. Ewald, S. E. *et al.* The ectodomain of Toll-like receptor 9 is cleaved to generate a functional receptor. *Nature* **456,** 658–62 (2008).
247. Bruni, D. *et al.* Viral entry route determines how human plasmacytoid dendritic cells produce type I interferons. *Sci. Signal.* **8,** ra25 (2015).
248. Swiecki, M. & Colonna, M. Unraveling the functions of plasmacytoid dendritic cells during viral infections, autoimmunity, and tolerance. *Immunol. Rev.* **234,** 142–62 (2010).
249. Fillatreau, S., Sweenie, C. H., McGeachy, M. J., Gray, D. & Anderton, S. M. B cells

regulate autoimmunity by provision of IL-10. *Nat. Immunol.* **3,** 944–950 (2002).

250. Matsushita, T. *et al.* Regulatory B cells inhibit EAE initiation in mice while other B cells promote disease progression. *J. Clin. Invest.* **118,** 229–245 (2008).
251. Segal, A. W. *et al.* Absence of Cytochrome b -245 in Chronic Granulomatous Disease. *N. Engl. J. Med.* **308,** 245–251 (1983).
252. Ravin, S. S. De. Chronic Granulomatous Disease as a Risk Factor for Autoimmune Disease. *J. Allergy Clin Immunol* **122,** 1097–1103 (2008).
253. Roos, D. The Genetic Basis of Chronic Granulomatous Disease. *Immunol. Rev.* **138,** 121–157 (1994).
254. Janeway, C.A., Craig J, Davidson M, Downry W, Gitlin D, S. J. Hypergammaglobulinemia associated with severe, recurrent and non-specific infection. *Am J Dis Child* **88,** 388–392 (1954).
255. Berendes, H., Bridges, R. A. & Good, R. A. A fatal granulomatosus of childhood: the clinical study of a new syndrome. *Minn. Med.* **40,** 309–12 (1957).
256. Haglund, S., Almer, S., Peterson, C. & Söderman, J. Gene expression and thiopurine metabolite profiling in inflammatory bowel disease - novel clues to drug targets and disease mechanisms? *PLoS One* **8,** e56989 (2013).
257. Harris, A. *et al.* Splenic volume in systemic lupus erythematosus. *Lupus* **18,** 1119–1120 (2009).
258. Cariappa, A. *et al.* The follicular versus marginal zone B lymphocyte cell fate decision is regulated by Aiolos, Btk, and CD21. *Immunity* **14,** 603–615 (2001).
259. Wen, L. *et al.* Evidence of marginal-zone B cell- positive selection in spleen. *Immunity* **23,** 297–308 (2005).
260. Heng, T. S. P. *et al.* The Immunological Genome Project: networks of gene expression in immune cells. *Nat. Immunol.* **9,** 1091–1094 (2008).
261. Seth, S. *et al.* CCR7 Essentially Contributes to the Homing of Plasmacytoid Dendritic Cells to Lymph Nodes under Steady-State As Well As Inflammatory Conditions. *J. Immunol.* **186,** 3364–3372 (2011).

Abbreviations

AEP	asparagine endopeptidase
ANOVA	analysis of variance
Arg	arginine
BCR	B cell receptor
BM	bone marrow
BTK	Bruton's tyrosine kinase
BV	Brilliant Violet
C57BL/6	C 57 black 6
CCR7	C-C chemokine receptor 7
CD	cluster of differentiation
cDC	classical dendritic cell
cDNA	complementary DNA
CFA	complete Freund's adjuvant
CGD	chronic granulomatous disease
ChIP	chromatin immunoprecipitation
CSF	cerebrospinal fluid
CNS	central nervous system
CO_2	carbon dioxide
DAPI	4',6-diamidino-2-phenylindole
DMSO	Dimethyl sulfoxide
DNA	deoxyribonucleic acid
DNase I	deoxyribonuclease I
dNTP	deoxynucleotide triphosphate
EAE	experimental autoimmune encephalomyelitis
EBV	Epstein Barr virus
EDTA	ethylenediamine tetraacetic acid
ELISA	enzyme-linked immunosorbent assay
FACS	fluorescence-activated cell sorting
FCS	fetal calf serum
FSC	forward scatter
Flt3	FMS-related tyrosine kinase 3
Flt3L	FMS-related tyrosine kinase 3 ligand
GFP	green fluorescent protein
HLA	human leukocyte antigen
Hv1	voltage-gated proton channel 1

IFN	interferon
IFNAR	interferon alpha receptor
IL	interleukin
IRAK	interleukin 1 receptor associated kinase
Irf	interferon regulatory factor
ISG	interferon stimulated gene
LPS	lipopolysaccharide
MACS	magnetic-acitivated cell sorting
MEM	minimal essential medium
MFI	mean fluorescence intensity
MHCII	major histocompatibilty complex class II
MOG	myelin oligodendrocyte glycoprotein
MOI	multiplicity of infections
MRI	magnet resonance imaging
mRNA	messenger RNA
MS	multiple sclerosis
MyD88	myeloid-differentiation primary response gene 88
mV	millivolt
MZ	marginal zone
Mx1	myxovirus resistance 1
NET	neutrophil extracellular trap
NADPH	nicotinamide adenine dinucleotide phosphate
NFκB	nuclear factor kappa-light-chain-enhancer of activated B cells
NK cell	natural killer cell
NOX	NADPH oxidase
OAS3	2’-5’-oligoadenylate sythetase 3
OG	Oregon Green
PBS	phosphate buffered saline
PBMC	peripheral blood mononuclear cell
PCR	polymerase chain reaction
PFA	paraformaldehyde
PTX	pertussis toxin
pDC	plasmacytoid dendritic cell
PS	polystyrene
p-value	probability value
Rab	Ras-related protin
RNA	ribonucleic acid

ROS	reactive oxygen species
RPMI	Roswell Park Memorial Institute medium
RRMS	relapsing-remitting multiple sclerosis
RT-PCR	real time PCR
scr	scrambled
SEM	standard error of the mean
shRNA	small hairpin RNA
SLE	systemic lupus erythematosus
SPMS	secondary progressive MS
SSC	side scatter
STAT	signal transducers and activators of transcription
TBP	Tata-box binding protein
Thr	threonine
TLR	toll-like receptor
TNFα	tumor necrosis factor alpha
TRAF6	TNF receptor associated factor 6
V-ATPase	vacuolar-type proton ATPase
VSOP	voltage-sensor only protein

Acknowledgements

First of all, I would like to thank Prof. Manuel Friese for giving me the opportunity to work on this exciting project at the INIMS, valuable support and insightful discussion of data.

In addition, I would like to thank Prof. Christian Lohr for evaluation of this thesis.

Moreover, I am grateful to all members of my ZMNH PhD program thesis committee, namely Dr. Sabine Fleischer, Dr. Irm Hermanns-Borgmeyer, Prof. Thomas Jacobs and Prof. Friedrich Nolte, for sharing their scientific experience and letting me benefit from their critical questions.

I would also like to thank all my current and former colleagues at the INIMS for all kinds of support and pleasant working days in the lab. In particular, I would like to address special thanks to Simone Bauer, Sabine Wehrmann and Michael Moles for excellent technical assistance. Furthermore, I am grateful to Dr. Benjamin Schattling for import of the Hv1-deficient mouse line and initiation of this project as well as to Dr. Jan-Broder Engler for help with the analysis of the ChIP dataset.

In addition to providing technical help, I would also like to thank Michael Moles for proofreading of this thesis.

Finally, I am truly thankful to my family and friends for their endless support, encouragement and trust which guided me through even the most troubling times. You have a big part to this!